Cosmological Tests of Gravity

by

Ali Narimani

B.Sc., Mechanical Engineering, Isfahan University of Technology, 2007
B.Sc., Physics, Isfahan University of Technology, 2008
M.Sc., Mechanical Engineering, Isfahan University of Technology, 2009
M.Sc., Astronomy, The University of British Columbia, 2011

A THESIS SUBMITTED IN PARTIAL FULFILLMENT OF
THE REQUIREMENTS FOR THE DEGREE OF

DOCTOR OF PHILOSOPHY

in

The Faculty of Graduate and Postdoctoral Studies

(Physics)

UNIVERSITY OF BRITISH COLUMBIA

(Vancouver)

August 2016

Abstract

General Relativity (GR) has long been acclaimed for its elegance and simplicity, and has successfully passed many stringent observational tests since it was introduced a century ago. However, there are two regimes in which the theory has yet to be fully challenged. One of them is in the neighbourhood of very strong gravitational fields, and the other is the behaviour of gravity on cosmological scales. While strong field gravity has challenged theorists because of the desire to find consistency between GR and quantum mechanics, cosmology has motivated extensions to GR via the empirical discoveries of dark matter and dark energy.

In this thesis, we study a diverse range of modifications to GR and confront them with observational data. We discuss how a generic theory of modified gravity can be parameterized for studies within cosmology, and we introduce a general parameterization that is simpler than those that have been previously considered. This parameterization is then applied to investigate a specific theory, known as "gravitational aether". The gravitational aether theory was created to solve one of the theoretical inconsistencies that exists between GR and quantum mechanics, namely the fact that vacuum fluctuations appear not to gravitate. Cosmology is unique in testing this theory, and we find that the gravitational aether solution is excluded when all of the available cosmological data are combined. Nevertheless, a generalization of this theory provides a consistent way to describe the strength of coupling between pressure and gravity, and we present the most accurate measurements of this coupling parameter.

In addition, we discuss the constraints that can be placed on modified gravity models using the latest data from cosmic microwave background (CMB) anisotropies, combined with

several other probes of large-scale structure. Currently the most accurate CMB anisotropy measurements come from the *Planck* 2015 CMB power spectra, which we use, along with other cosmological data sets, to perform an extensive study of modified theories of gravity. We find that GR remains the simplest model that can explain all of the data. We end with a discussion of the prospects for future experiments that can improve our understanding of gravity.

Preface

Three chapters of this dissertation are based on previously published work. My contributions to each work are explained below.

- Chapter 3 is based on a published paper in Physical Review D titled "Minimal parameterizations for modified gravity". I performed the numerical calculations, made the plots, and wrote a first draft of the paper. Douglas Scott provided crucial guidance and significant improvement to the text. We received helpful feedbacks from James Zibin.

- Chapter 4 is based on a published paper in Journal of Cosmology and Asroparticle Physics. The analytical and numerical calculations, statistical analyses, and plots were made by me. I received guidance and feedback from Niayesh Afshordi, and Douglas Scott. I wrote the first draft of the paper which was edited by Douglas Scott and Niayesh Afshordi. Niayesh also added important parts to the conclusion chapter.

- Chapter 5 is a reformatted version of published work in Astronomy and Astrophysics. The original paper was among the 2015 primary publication and data release of the *Planck* collaboration. The numerical calculations, plots, and first draft of the included sections were all done by me. I received feedback from Martin Kunz and Valeria Pettorini in our weekly teleconferences, and the text was edited by the *Planck* editorial board.

Table of Contents

List of Tables

List of Figures

Glossary

CMB Cosmic Microwave Background

BAO Baryon Acoustic Oscillations

WMAP Wilkinson Microwave Anisotropy Probe

ACT Atacama Cosmology Telescope

SPT South Pole Telescope

PPN Parameterized Post-Newtonian

PPF Parameterized Post-Friedmann

CAMB Code for Anisotropies in the Microwave Background

EFT Effective Field Theory

Acknowledgements

There are a few people I should thank, without whom aiming for a PhD, and writing this thesis would have been impossible. First, I want to thank my eighth-grade science teacher, Reza Khalifeh-Mahmoodi, for all the things he did for me (from inviting my parents to school for a private conversation, to his one-on-one lessons that enabled me pass the entrance exams of the best high schools in my home-town). His encouragement and belief in me was so influential that I sometimes think I could have been somewhere else doing something totally different without his presence in my life.

Next, I should thank my Bachelor's and Masters degree advisers and supervisors in Iran, Mansour Haghighat, Mojtaba Mahzoon, Behrouz Mirza, and Saeed Ziaei-Rad.

The biggest thank you goes to my Masters and PhD supervisor, Douglas Scott. I cannot thank him enough for his persistent effort in guiding me through my research projects, connecting me with other researchers in the field, and creating the opportunity for me to become a *Planck* member. I benefited multiples of times from his generous travel supports, and his endless patience in reading and editing my reports, paper drafts, and, of course, this thesis.

I want to thank Niayesh Afshordi for offering me one of his research projects and paying for my visit and stay in Perimeter Institute. We had a fruitful collaboration that resulted in a paper in JCAP, and is the basis for a whole chapter of this thesis.

I would also like to thank Lloyd Knox for offering me a travel support to UC-Davis. I learnt a lot from his expertise during my visit, and our weekly telecons with him, Marius Millea, Silvia Galli, Martin White, and Douglas Scott.

My office mate, Anna Hughes, helped me in translating the two poems at the beginning

of the Introduction, and the end of the Conclusion chapters. Thanks Anna for all your help, and all the political-social thought provoking discussions.

I would want to sincerely thank my beloved parents and sisters. Thank you so much for giving me the freedom to choose my path independently, and being supportive of all the decisions I have made for my life.

This thank-you-list misses a significant member without the love of my life, Mina. Thanks darling for all your care, love, and support during these my best five years of life.

Chapter 1

Introduction

اگر عشق اوفتد در سینهٔ سنگ — به معشوقی زند در گوهری چنگ

که مغناطیس اگر عاشق نبودی — بدان شوق آهنی را چون ربودی

وگر عشقی نبودی در گذرگاه — نبودی کهربا جوینده کاه

بسی سنگ و بسی گوهر بجایند — نه آهن را نه کِه را می ربایند

هر آن جوهر که هستند از عدد بیش — همه دارند میل مرکز خویش

طبایع جز کشش کاری ندانند — حکیمان این کشش را عشق نامند

گر از عشق آسمان آزاد بودی — کجا هرگز زمین آباد بودی

... If love falls in the heart of a stone
It reaches out its hands, like a lover, to embrace a gem
For if magnetism was not in love
Why should it grab an iron so enthusiastically
And, with no love going on
Amber would not always seek for a straw
There are so many stones and gems on the Earth
And they neither absorb iron, nor straw

The essences, that are countless in number
All have a tendency towards a centre
Creatures do not know anything but to absorb each other
And this absorption is called "love" by philosophers

With no love in the heavens
There would be no life on the Earth

from "Khosro and Shirin" by Nezami Ganjavi, Iranian poet, 12th century AD

1.1 Ancient history

The struggle for understanding the sky above us, and the effort to tie all of the seemingly unrelated phenomena around us on Earth, along with what is going on in the skies, into a meaningful and coherent story, has a long history, probably as long as humanity. Among the earliest theories (or stories) accessible to us, are the works of Thales, from the 7th century B.C., communicated to us through other philosophers [6]. Thales's main concern, like other thinkers of his time, was to find the element that is the origin of everything we see on Earth. According to him, Earth is flat and floating on a great ocean, the water of which is the origin of everything. The ocean beneath is not supported by anything, and the world above is limited by a vault, to which the stars are attached. He makes no distinction between the solar system planets and the distant stars.

The real breakthrough, at least among the ancient Greeks, comes with the Pythagorean school, 6th-4th century B.C. They, famously, held the rather eccentric idea that numbers are the origin of everything. Although strange by modern scientific standards, their obsession with numbers led to a better picture of the *'Kosmos'*. They believed that Earth, together with all of the other celestial bodies, has a spherical shape, because a sphere possesses the most perfect shape of all the objects. They were the first to figure out that the harmony in musical sounds is governed by a regular pattern of intervals, and that the planets and the Sun are also going around the Earth in regularity. As for their view of the large-scale Universe, they dissected the Universe into three spherical pieces [6]: the *Heavens*, which included the Earth, was bounded with the sphere of the Moon, and was the home for life and change; the *Kosmos*, which encompassed the Moon, the Sun, and the planets and was the place of regular motion; and the *Olympus*, the sphere of distant fixed stars, which was the place for elements in their pure form. They also had a few odd beliefs, even judged by the standards of their own time, which stemmed from their unusual mathematical principle. They believed that there exists a planet that is not observable for us on Earth, because it is always behind the Sun, and named that planet *antichthon*, or anti-Earth [7]. They added this new planet because the sum of the other bodies in the sky, i.e. the Sun, the Moon, Earth,

the five planets, and the distant stars is nine, which is not a perfect number. Their solution was to add one more planet to complete the system of ten objects.

Pure thinking and mythology occasionally led ancient Greeks to notions that were later adopted by modern physics. The idea of an *"aether"* or pure air (sometimes referred to as quintessence) that gods breathe, first appeared in Greek mythology, and was later introduced to philosophy through the works of Plato and Aristotole [8]. These great philosophers introduced aether as the fifth classical element. These five elements were proposed to interpret the nature of all that exists, and aether was proposed to explain the circular motion of the celestial bodies. Aether came back to modern physics at times when the known constituents of the Universe were not sufficient for explaining the world, e.g. in defining the speed of light with respect to a reference frame, or for what drives the expansion of the Universe (as we will discuss at length later). It is also remarkable that Leukippus and his disciple Demokritus, 5th century B.C., believed that the building blocks of all the material should be indivisible bodies which they called "atoms" [6], an idea that is also more or less equivalent to our modern atomic view.

Following this story further would require a thesis of its own, but it is probably sufficient to mention that things had changed a lot by the beginning of the twentieth century. A series of observations and insights by Brahe, Galileo, and Kepler, had led Newton to his remarkable discovery of Newtonian gravity. Two new planets, other than the ones known since ancient times, had been found, the discoveries of which were a source of admiration and debate in science and philosophy and provided further tests of Newtonian gravity [9]. It was common knowledge among scientists by then that Earth is not at the centre of everything, but is actually going around the Sun. The existence of other galaxies was still just a speculative idea, and the common belief among many was that the Milky Way galaxy is the only structure in the Universe [10]. Earth was not at the centre of everything, but still occupied a special place, since the solar system was thought to be very close to the centre of the Milky Way. Although these discoveries were all effectively tests of the Newtonian ideas of gravity, there was still a fundamental problem that there was no consistent gravitational

theory for describing the whole Universe.

One major difference between twentieth century scientists and ancient Greek philosophers, which is probably more remarkable than their factual discoveries, lies in the world-view of the scientists. The main concern of early 20th century scientists was to explain newly discovered phenomena, based on other known facts and well-tested theories, rather than wrapping them in metaphysical stories or unchangeable rules. This is the key to practising science even today.

We have now come far from those earlier ideas of antiquity, or even the somewhat misguided beliefs about the Universe a century ago. We now know that the Milky Way is only one galaxy among an incredibly large (perhaps infinite) number of them. We can, however, only access a subset of these galaxies, the ones that are inside the "observable Universe". We also know that the Universe is full of a "*dark energy*" that forms approximately 70% of the energy content, and causes an ever increasing expansion rate for the Universe. Of the remaining 30%, in terms of energy budget, most is in a substance dubbed "*dark matter*", for it can be neither touched nor seen, even though it is responsible for the formation of galaxies and large-scale structures in the Universe, among other things. All that can be observed, touched, or felt with our senses consists of about $1/6$ of the matter, a 5% fraction of the whole Universe, that is in the form of atoms or regular matter. Among all of these structures and substances of the Universe, the solar system holds no special place, since it is in an unremarkable part of the disk of a fairy normal galaxy, which is one of billions of galaxies in the observable Universe.

Even though it may appear that we have invented a new set of "mystical" ideas for explaining the newly discovered cosmological phenomena, there is a big difference between these set of modern ideas, and those of antiquity. The real merit of these ideas is in their capability to explain a very diverse range of empirical phenomena with high precision while being amenable to tests using further observations, *and*, maybe most importantly, to guide us to a whole new set of questions and directions for understanding the physical world.

The main goal of this thesis is to explore one of these directions, namely the theoretical

space of "modified theories of gravity" and to test their predictions using cosmological data. Modified theories of gravity alter Einstein's gravity in order to either find an explanation for one of the two dark entities in the Universe, or to solve some of the theoretical difficulties that face the theory when it is combined with quantum mechanics. Such ideas will be constrained by performing tests on the behaviour of gravity on the largest scales that we can probe. We will explain Einstein's gravity and the standard model of cosmology in the rest of this chapter, and introduce modifications to this theory, as well as discussing the relevance of cosmology for testing those modified theories in the following chapter. Note that we use units in which the speed of light is unity, $c = 1$, throughout this thesis.

1.2 Modern cosmology

The birth of modern cosmology was made possible only after the introduction of general relativity (GR) by Einstein in 1915 [11]. GR links the structure of space-time with its energy contents through the field equations,

$$G_{\mu\nu} + \Lambda g_{\mu\nu} = 8\pi G\, T_{\mu\nu}\,. \tag{1.1}$$

The left-hand side of this equation is a specific nonlinear second-order differential equation for the space-time metric, $g_{\mu\nu}$, while the right-hand side holds the energy momentum tensor of the constituents of that space-time, $T_{\mu\nu}$ (times a constant). Here, G is Newton's gravitational constant and Λ, or the cosmological constant, is a free parameter of the theory, whose non-zero value is also the best currently available candidate for dark energy. The $\{\mu, \nu\}$ indices run from zero to three, representing time and the three spatial coordinates.

Even though the Universe looks very lumpy and anisotropic on very small scales, (e.g. Earth has a very high density compared to the space between the planets) it becomes more and more homogeneous and isotropic as we go to larger and larger scales, e.g. hundreds of millions of light years, compared to the solar system scales that are hundreds of light hours at most.

Isotropy and homogeneity of the Universe on its largest scales was once a mere assumption, called the "cosmological principle", but it now has roots in cosmological observables (e.g. see [12]). The assumption of homogeneity and isotropy dictates the form of the energy-momentum tensor and the metric [13]. The energy-momentum tensor will only contain perfect fluids, and the metric is the Friedman-Robertson-Walker (FRW) metric,

$$\mathrm{d}s^2 = g_{\mu\nu}\,\mathrm{d}x^\mu\,\mathrm{d}x^\nu = -\mathrm{d}t^2 + a^2(t)\left(\frac{\mathrm{d}r^2}{1-k\,r^2} + r^2\mathrm{d}\Omega^2\right). \tag{1.2}$$

Here, k is a parameter that determines the curvature of the Universe, with positive k values corresponding to spherical geometry, negative to hyperbolic, and $k = 0$ to a flat Universe. We set $k = 0$ in the rest of this thesis, since this is what the most recent data points to [2]. The quantity $a(t)$, with $a = 1/(1+z)$ (z being the observed redshift), is a free function called the "scale factor" that simply scales all lengths at different times.

The FRW metric [14, 15] is the basis of big bang cosmology, leaving us to determine k and $a(t)$ through observations. The only dynamical element of this metric is the scale factor, whose evolution is governed by Eq. (1.1). The evolution equations were first derived by Friedmann in 1922 [16] and are

$$\begin{aligned} H^2 &= \frac{8\pi G\rho + \Lambda}{3}, \\ \frac{\ddot{a}}{a} &= -\frac{4\pi G}{3}(\rho + 3\,p) + \frac{\Lambda}{3}. \end{aligned} \tag{1.3}$$

Here, $H \equiv \dot{a}/a$ is called the Hubble constant, with a dot meaning a derivative with respect to the coordinate time, t. The quantities ρ and p are the total density and pressure of all the fluids in the energy momentum tensor and Λ is again the cosmological constant.

ΛCDM model

In order to fully specify the theory, one has to define the fluids in the energy-momentum tensor. Based on the currently accepted model, the energy momentum tensor contains five different types of substance: baryons, photons, neutrinos, cold dark matter, and dark energy

[17, 18]. The most fundamental difference between these different types of fluids lies in their equation of state, $p = w\rho$, where p stands for pressure, ρ is the density of the fluid and w is the equation of state parameter.

All of the particles that are formed from electrons, protons, and neutrons are grouped under "baryons" with an equation of state where $w = 0$ (actually not quite zero, but the thermal pressure is negligible in density units). While photons and massless neutrinos share the same equation of state, $w = 1/3$, massive neutrinos start from this state at early times, but gradually move towards $w = 0$ as the Universe evolves. Dark matter has the unique property that it either has a very weak, or entirely vanishing interaction through any force other than gravity with any particle (including itself), and therefore $w = 0$. The cosmological constant, on the other hand, has a constant density and pressure, with $p = -\rho$, and therefore $w = -1$. As was mentioned before, the cosmological constant, Λ, is the best (i.e. simplest) mathematical model of dark energy as of today, although possibilities with $w \neq 0$ and non-constant $w(a)$ are also consistent [19].

This "standard" model, ΛCDM, is named after its two strange components, Λ for dark energy, and CDM for cold dark matter. The model is fully specified through its six parameters: $\{\Omega_b h^2, \Omega_{DM} h^2, H_0, \tau, A_s, n_s\}$. The first two parameters of the list are proportional to the energy density of baryons and cold dark matter,

$$\Omega_x h^2 \equiv \frac{8\pi G \rho_x}{3 * (100)^2}. \tag{1.4}$$

Here, x stands for either baryons (b), or CDM (DM). τ is the optical depth of the Universe, the probability that a given photon scatters before reaching the observer. $\{A_s, n_s\}$ are the initial condition parameters, and determine the current lumpiness of the Universe on different scales. As we shall see, this six-parameter model fits a wide range of data extremely well.

1.3 Evidence for hot big bang cosmology

There are three classical pieces of evidence for the hot big bang model, which we now describe in turn.

1.3.1 Expansion of the Universe

Eq. (1.3) states that, in contrast to the generally held belief of the early 20th century, the Universe cannot be static but is instead expanding. This expansion was discovered by Edwin Hubble in 1929 [20] (the story of this discovery is complicated, Kragh and Smith [21] present a rather long discussion of who should be credited for this discovery). The Hubble constant, defined in the previous section, measures the expansion rate of the Universe at the present time. The current estimate of this parameter from the local Universe, measured from Cepheid data [22] (including reassessment of uncertainties [23]) is

$$H_0 = (70.6 \pm 3.3)\,\mathrm{km\,s^{-1}\,Mpc^{-1}}. \tag{1.5}$$

Adding a '0' subscript is a standard notation for referring to the present time.

Further observations determined that the expansion is accelerating [18], giving constraints on the behaviour of $a(t)$. But the basic idea of an expanding Universe has been examined and confirmed by a huge set of observations over the last decades [24]. This also tells us that the Universe has a finite age in the big bang model, with the best current estimate being $t_0 = 13.813 \pm 0.038$ Gyr[2].

1.3.2 Big bang nucleosynthesis

Using Eq. (1.3), along with an equation of state for each of the fluids, it is clear that the Universe should have been in a hot and dense state during the earliest stages of its evolution. This temperature was so high that the protons and neutrons could not bind together to form any of the elements in the periodic table. The high density and hot temperature of the Universe at early times meant very frequent collisions between particles, keeping them in

equilibrium with each other, until the collision rate became comparable to the expansion rate of the Universe. This was when the out-of-equilibrium process of the formation of heavier elements began. Alpher et. al. [25] calculated the ratio of hydrogen to helium atoms based on the big bang theory in 1948. Their predictions were later confirmed by a continuous set of observations [26], extending to the present day. This explains why, on average, the Universe consists of about 25% helium (by mass) and 75% hydrogen, with about one part in 10^5 of the hydrogen in the form of deuterium [27].

1.3.3 Relic radiation

As the Universe expanded, its temperature cooled adiabatically and the first neutral atoms started to form a few hundred thousand years after the big bang. As these atoms formed, the collision rate between photons and baryons dropped significantly and the photons started their "free streaming" phase. This epoch is called "recombination", even though it was the first time that electrons and protons combined together and formed neutral atoms. The prediction that the remnant of the early radiation should now be detectable on Earth according to the first estimates, by Alpher et. al in 1948 [25] (although the story is again complicated, see the book by Peebles et al. [28]), and particularly its discovery in 1964 by Penzias and Wilson [29] had a major impact on the general acceptance of the hot big bang theory. This relic radiation has a blackbody spectrum, its temperature is the best currently measured number in cosmology [30], $T_{0,\mathrm{CMB}} = (2.7255 \pm 0.0006)\mathrm{K}$, and it is usually referred to as the "Cosmic Microwave Background" or CMB. It is a "cosmic" background, since it is received as a very nearly isotropic radiation field that cannot be attributed to any individual star, galaxy, or other localized structure. Although almost isotropic, as we shall show, small amplitude variations in the CMB are a critical observable that is used to precisely pin down our cosmological model, as well as to constrain theories of modified gravity.

Although we have described the three main pieces of evidence used to support the hot big bang model, there have been a huge number of additional observations that back up this picture, including studies of objects at high redshift, clustering of galaxies, and clouds

along the line of sight to distant objects [31].

1.4 Perturbations in the Universe

Though generally successful, the classical big bang theory had a few problems or missing ingredients. One of the most important shortcomings was the lack of a clear recipe for making galaxies and all the other structures we see in the Universe. It also potentially suffered from a singularity at the bang moment, $t = 0$ and no *explanation* for the expansion. Additionally there were issues with explaining flatness, near-isotropy of the CMB sky and lack of magnetic monopoles. These problems were solved by the addition to the theory of an early era of exponential expansion. Based on this new picture, the Universe is presumed to be dominated by the potential energy of a scalar field during an "inflationary" era [32, 33]. The quantum fluctuations of this scalar field provide the initial perturbations in the Universe, which then grow through gravitational instabilities and form the structures, such as galaxies and galaxy clusters, which we see today. We will complete this chapter by describing the basics of the theory at the perturbation level, and some of the most relevant observations that are used to test the theory.

1.5 Metric perturbations

Even though the FRW metric (which describes a homogeneous and isotropic Universe) can successfully explain a good number of observations, the existence of galaxy clusters and voids show that the Universe is far from being homogeneous and isotropic on all scales. The general idea for explaining the structures in the Universe is to assume that they are formed from minuscule perturbations in the density field of the fluids. These early perturbations act like seeds of structure formation. The regions that are a little overdense will expand more slowly, and hence the effect of gravity is to make them increasingly more dense compared to the expanding background. This positive feedback loop continues until the formation of very first stars and structures in the Universe. Since the deviations from homogeneity are

believed to be relatively small at early times (on all scales), it is reasonable to adopt linear perturbation theory for studying their evolution. We lay out the foundations of cosmological perturbation theory in this section, and will explain the observational tests that follow from its use in the following section.

In order to perturb the gravitational fields in GR, we need to consider metric perturbations. The first order background metric was written based on the observed symmetries of our Universe, i.e. homogeneity and isotropy. We now break these symmetries by adding some general perturbation to the background metric:

$$\mathbf{g}_{\mu\nu} = g_{\mu\nu} + h_{\mu\nu}, \qquad h_{\mu\nu} \ll 1. \tag{1.6}$$

For the rest of this chapter, a bold quantity will mean a tensor that contains both the background and perturbation terms. In words, Eq. (1.6) means that $g_{\mu\nu}$, which was a good tool for measuring the distance in a fully isotropic space-time, is slightly modified to $\mathbf{g}_{\mu\nu}$. The quantity $\mathbf{g}_{\mu\nu}$ will take us one step closer to reality, because it is capable of describing phenomena beyond perfect homogeneity, and will allow us to address observables that relate to inhomogeneity and anisotropy.

1.5.1 Classification of metric perturbations

Let us use the symmetries of the background metric to classify the metric perturbations defined in Eq. (1.6). Consider the following transformation of the space-time coordinates:

$$\begin{cases} t \ \rightarrow t' = t; \\ x^i \rightarrow x'^i = \Delta^i(x^j). \end{cases} \tag{1.7}$$

Here 'i' runs from one to three and Δ^i is a function consisting of either a (constant) rotation or displacement.[1] Following the general rule of coordinate transformation for tensors we

[1] The rotation or the displacement transformations are not infinitesimal in general.

find that the space-time metric transforms as

$$\begin{aligned}\mathbf{g}'_{\mu\nu} \;=\; g'_{\mu\nu} + h'_{\mu\nu} \;&=\; \frac{\partial x^\alpha}{\partial x'^\mu}\frac{\partial x^\beta}{\partial x'^\nu}\mathbf{g}_{\alpha\beta} \\ &=\; \frac{\partial x^\alpha}{\partial x'^\mu}\frac{\partial x^\beta}{\partial x'^\nu}(g_{\alpha\beta} + h_{\alpha\beta}) \\ &=\; g_{\mu\nu} + \frac{\partial x^\alpha}{\partial x'^\mu}\frac{\partial x^\beta}{\partial x'^\nu}h_{\alpha\beta}. \end{aligned} \tag{1.8}$$

The last line follows because the background metric is invariant under the coordinate transformations defined in Eq. (1.7), i.e. under rotations and displacements. The zeroth-order equation then simply reads $g'_{\mu\nu} = g_{\mu\nu}$, and the first-order terms give

$$\begin{cases} h'_{00} = h_{00}, \\ h'_{0i} = \dfrac{\partial x^a}{\partial x'^i}h_{0a}, \\ h'_{ij} = \dfrac{\partial x^a}{\partial x'^i}\dfrac{\partial x^b}{\partial x'^j}h_{ab}. \end{cases} \tag{1.9}$$

Therefore, h_{00} transforms like a scalar, h_{0i} like a spatial vector, and h_{ij} like a tensor. A spatial vector can be further decomposed into a scalar and a vector, while a tensor, like h_{ij}, can be decomposed into two scalars, a divergenceless vector and a traceless divergenceless tensor:

$$\begin{aligned} &h_{00} \equiv -A, \\ &h_{0i} \equiv a(t)\,(\partial_i B + E_i), \quad \partial_i E_i = 0, \\ &h_{ij} \equiv a^2(t)\,(C\delta_{ij} + \partial_i\partial_j D + \partial_i F_j + \partial_j F_i + J_{ij}),\ \{\partial_i F_i = 0,\ J_{ii} = 0,\ \partial_i J_{ij} = 0\} \end{aligned} \tag{1.10}$$

Hence, under the transformations defined in Eq. (1.7), the set $\{A, B, C, D\}$ behaves like scalars, $\{E_i, F_i\}$ transform like vectors, and J_{ij} like a tensor. The metric perturbation thus has four degrees of freedom in scalars, four in vectors,[2] and two in tensors,[3] a total of 10 degrees of freedom (like one would expect from a four by four symmetric tensor).

[2] There are two three-dimensional vectors, each of which have one constraint (they are divergenceless).

[3] J_{ij} is a 3×3 symmetric tensor, which means six degrees of freedom. However, there are also four constraints on the components of this tensor, defined in Eq. (1.10).

Under a completely general (infinitesimal) coordinate transformation,

$$\begin{cases} t \ \to t' = t + \alpha(x^\mu), \quad \alpha \ll 1, \\ x^i \to x'^i = x^i + \delta^{ij}\partial_j\beta(x^\mu) + \xi^i(x^\mu), \quad \partial_i\xi^i = 0, \quad \{\beta, \xi^i\} \ll 1, \end{cases} \tag{1.11}$$

the perturbed metric transforms as

$$\begin{aligned} \mathbf{g}'_{\mu\nu} \ = \ g'_{\mu\nu} + h'_{\mu\nu} \ &= \ \frac{\partial x^\alpha}{\partial x'^\mu}\frac{\partial x^\beta}{\partial x'^\nu}g_{\alpha\beta} + \frac{\partial x^\alpha}{\partial x'^\mu}\frac{\partial x^\beta}{\partial x'^\nu}h_{\alpha\beta} \\ &= \ \frac{\partial x^\alpha}{\partial x'^\mu}\frac{\partial x^\beta}{\partial x'^\nu}g_{\alpha\beta} + h_{\mu\nu}. \end{aligned} \tag{1.12}$$

Here the last line follows because we only keep terms up to first-order. Although one can still classify the terms into perturbation and background, it is not obvious how to separate a *real* perturbation, i.e. deviations from a homogeneous isotropic background, from a fictitious space-time dependency that is merely due to a minuscule coordinate transformation. To make some progress, one can define the components of the perturbed metric in any coordinate system as

$$\begin{aligned} \mathbf{g}_{00} \ &\equiv \ -1 - A, \\ \mathbf{g}_{0i} \ &\equiv \ a(t)(\partial_i B + E_i), \\ \mathbf{g}_{ij} \ &\equiv \ a^2(t)(1 + C\delta_{ij} + \partial_i\partial_j D + \partial_i F_j + \partial_j F_i + J_{ij}), \end{aligned} \tag{1.13}$$

and take any space-time dependency (besides the $a(t)$) as a perturbation. Our previous sets of scalars, vectors, and tensors do not behave as they should under these general coordinate transformations. However, one can prove that for first-order perturbations, the scalars, vectors and tensors evolve independently under Einstein's equations, Eq. (1.1), thanks to the rotational symmetry of the background space-time (see [34] for a nice short proof of this).

To summarize, the perturbed metric defined in Eq. (1.13), is the sum of the background metric defined in Eq. (1.2) and the perturbation defined in Eq. (1.10). Under a general

coordinate transformation, the perturbed metric transforms as

$$\begin{aligned}\mathbf{g}'_{\mu\nu} &= g'_{\mu\nu} + h'_{\mu\nu} \\ &= \frac{\partial x^{\alpha}}{\partial x'^{\mu}}\frac{\partial x^{\beta}}{\partial x'^{\nu}}\mathbf{g}_{\alpha\beta} \\ &= g_{\mu\nu} + \Delta h_{\mu\nu} + h_{\mu\nu}. \end{aligned} \tag{1.14}$$

Here: $g'_{\mu\nu}$ and $g_{\mu\nu}$ are equal to each other and are both equal to the metric defined in Eq. (1.2); $h'_{\mu\nu}$ and $h_{\mu\nu}$ have the same general structure defined in Eq. (1.10), and are related to each other, since $h'_{\mu\nu} = h_{\mu\nu} + \Delta h_{\mu\nu}$; and $\Delta h_{\mu\nu}$ holds the change caused by the coordinate transformation and at first-order is completely defined via the general coordinate transformation parameters $\{\alpha, \beta, \xi^i\}$. After a coordinate transformation, the metric perturbations transform as

$$\begin{aligned} A' &= A - 2\dot{\alpha}, \\ B' &= B + \frac{\alpha}{a} - a\dot{\beta}, \\ C' &= C + 2H\alpha, \\ D' &= D - 2\beta, \\ E'_i &= E_i + 2\,a\,\dot{\xi}_i, \\ F'_i &= F_i - \xi_i, \\ J'_{ij} &= J_{ij}. \end{aligned} \tag{1.15}$$

1.5.2 Choosing a gauge

Since all of the coordinate systems follow the same field equations in GR (in contrast to Newtonian mechanics, where only inertial frames follow Newton's second law), any arbitrary choice of the $\{\alpha, \beta, \xi^i\}$ functions will generate a new legitimate set of metric variables at the perturbation level. Fixing the parameters of the coordinate system are usually referred to in the literature as "fixing the gauge" [35, 36]. In particular, starting from a general non-

zero set of metric variables, one can use Eq. (1.15) and choose a set of $\{\alpha, \beta, \xi^i\}$ functions that can set two of the scalars and one of the vectors to zero in the transformed coordinate system. This is in fact not a choice but a necessity, since the Einstein equations provide two independent equations for each of the scalar, vector, and tensor components, while the metric perturbation has ten independent components (as was explained earlier). One should therefore use this freedom of choosing a coordinate system to eliminate the four extra degrees of freedom. Among the two widely used gauges for scalar-perturbations in cosmology, one of them sets $\{B, D\}$ to zero (known as the Newtonian gauge) while the other one chooses $\{C, D\}$ as its non-zero metric fields (synchronous gauge). These two metrics are explained further in Chapter 3.

1.5.3 Matter fluctuations

The fluids at the background level were completely specified with two numbers (at any given time), their density and pressure. In this homogeneous picture, the particles of a fluid moved with the same speed (called the "Hubble flow"), and there was therefore no shear stress between the particles. This picture is significantly enhanced at the perturbation level by adding spatial and temporal deviations to the pressure and density field of the fluids, allowing deviations from the Hubble flow, and non-zero shear stress.

The perturbations of the energy momentum tensor from a homogeneous background can be decomposed into scalar, vector, and tensor perturbations in a similar way as for the metric perturbations. The scalar part of the energy momentum tensor can then be defined as [37]

$$\begin{aligned} \mathbf{T}^0{}_0 &= -\bar{\rho}(1+\delta\rho), \\ \mathbf{T}^0{}_i &= (\bar{\rho}+\bar{p})\partial_i V, \\ \mathbf{T}^i{}_j &= \delta_{ij}(\bar{p}+\delta p) + (\partial_i\partial_j - \frac{1}{3}\delta_{ij}\nabla^2)\sigma. \end{aligned} \tag{1.16}$$

Here, a bar means a background quantity, ρ and p stand for the density and pressure of the

fluids, respectively, V is the amplitude of velocity perturbations, and σ is the source for anisotropic shear stress.

After this point, one can use Einstein's equations, along with a set of initial conditions, to solve the differential equations of the matter and metric perturbations. This is done in many standard texts e.g. in Ref. [37] for the two widely used coordinate systems in cosmology.

1.6 Qualitative understanding of the perturbation equations

The perturbation equations form a system of coupled first-order ordinary differential equations. The number of these coupled equations varies depending on the approximations that are used and typically grows to as many as a hundred in numerical integrators. Approximate analytical solutions of these equations have been extensively studied (e.g. in Hu and Sugiyama [38] or Dodelson [39]), and exact numerical solutions are available in public codes such as CAMB [40]. In this section, we provide a qualitative description of these equations and their solution.

The general picture to have in mind is an expanding Universe that embodies different fluids, and is affected by each of these fluids in turn. The first one that dominates the Universe by density (and is therefore the most important for gravity) is radiation. As the Universe evolves, radiation gives its place to matter domination, which is then substituted by dark energy at recent times.

The differential equations describe the effect of two rival forces on the perturbations during the times that radiation plays a significant role. One is gravity, which is effective on all causal scales (with the limit typically known as the "Hubble scale"), and the other one is pressure, which is only important on scales smaller than the sound horizon. Hubble scale is roughly equal to the speed of light multiplied by the age of the Universe, and the sound horizon is determined from the speed of sound in the fluid. Since the sound speed is always smaller than the speed of light (e.g. is equal to $(1/\sqrt{3})$ for radiation), the sound horizon is always smaller than the Hubble scale. These two scales determine the effective forces for

different scales at every moment in time.

At early times when radiation is the dominant fluid, the temperatures are so high that electrons do not efficiently bind with the hydrogen or helium nuclei and all the atoms are effectively ionized. The photons are thus tightly coupled with electrons (which are in turn coupled with the rest of the baryons) through electromagnetic forces, and the fluctuations in one fluid are also reflected in the other. On scales smaller than the sound horizon, the two opposing gravity and pressure forces induce a harmonic oscillatory motion in the perturbations of the density fields, while the perturbations on larger scales (but smaller than the Hubble scale) grow slightly due to gravity. The largest scale perturbations are not affected at all by either pressure or gravity. As the Universe evolves and adiabatically cools, it becomes favourable for electrons to abandon photons and "recombine" with the positively charged hydrogen and helium atoms. As this happens, the interaction between electrons and photons drops significantly, and the photons start to "free stream" in the Universe, while carrying the oscillatory structure of early times within themselves. A map of the perturbations of the relic (CMB) photons is therefore like a picture of the Universe when it was still young.

Similar to CMB anisotropies, baryon acoustic oscillations (BAO) are the imprints of perturbations on the matter density field [39]. Unlike CMB photons that free-stream from the epoch of recombination to now, baryons have gravitational (and other) interactions with dark matter and themselves, leading to the formation of stars, galaxies, and the other structures in the Universe. The imprints of those early oscillations is visible in the matter power spectrum on the largest scales, where the evolution of perturbations is still linear.

1.7 Observational evidence for big bang cosmology at the perturbation level

As was explained before, small field perturbations in the very early Universe led to anisotropies and inhomogeneities in the fluids. Since the origin of these perturbations is believed to be quantum mechanical in nature, it is impossible to predict their exact form, due the so called

"uncertainty principle". The 1-dimensional analogue of this situation is a particle in an infinite potential well; while it is impossible to predict the exact location of such a particle at a given moment, the average position of an ensemble of similarly prepared particles, and the variance of these particle positions, are determined by the width of the potential well, and the energy state of the particles. These ideas are related to two of the main pieces of observational evidence for the ΛCDM model, which confirm the theory at the perturbation level.

1.7.1 CMB anisotropies

The prediction of small anisotropies in CMB radiation, and their detection by the COBE [41], *WMAP* [3], and *Planck* [42] satellites, is one of the greatest successes of modern cosmology. As well as defining the parameters of the ΛCDM model, CMB anisotropies also play a significant role in testing theories of gravity beyond Einstein's theory, as will be explained in later chapters of this thesis.

The anisotropies in CMB temperature can be simply defined as

$$T(x^i, t) = T_0 + \delta T(x^i, t, \hat{n}). \tag{1.17}$$

Here the coordinates (x^i, t) specify the time and location of the observations, which are typically taken to be today (in a cosmological sense) and on Earth, while $\hat{n}$ specifies the observation direction. Similar to the particle in a 1-dimensional well, it is intrinsically impossible to determine the exact shape of the fluctuations, $\delta T(x^i, t, \hat{n})$. However, one can instead determine the average power-spectrum of these fluctuations, $P \equiv \left\langle \delta T(x^i, t, \hat{n}) \delta T(x'^i, t', \hat{n}') \right\rangle$. It is common to decompose the temperature anisotropies into spherical harmonics, $Y_{\ell m}$,

$$\delta T(x^i, t, \hat{n}) = \sum_{\ell, m} a_{\ell m}(x^i, t)\, Y_{\ell m}(\hat{n}), \quad \text{with } \langle a_{\ell m} \rangle = 0, \tag{1.18}$$

and define the power spectrum as

$$C_\ell \equiv \delta_{\ell\ell'}\delta_{mm'}\,\langle a_{\ell m} a_{\ell' m'}\rangle\,. \tag{1.19}$$

Fig. 1.1 shows the best-fit ΛCDM model prediction, together with data from the *Planck* satellite [2]. The imprints of the early harmonic fluctuations of the density fields are distinctively visible in this figure.

CMB anisotropies have perturbation amplitudes much smaller than one, $\delta T/T \sim 10^{-5}$, and hence the mathematical equations for describing them are linear and straightforward. Because of this, and the fact that measurements have been made in many different multipole modes, the CMB provides the most powerful constraints on the cosmological parameters of the ΛCDM model. Comparison with *Planck* data will form a large part of Chapter 5.

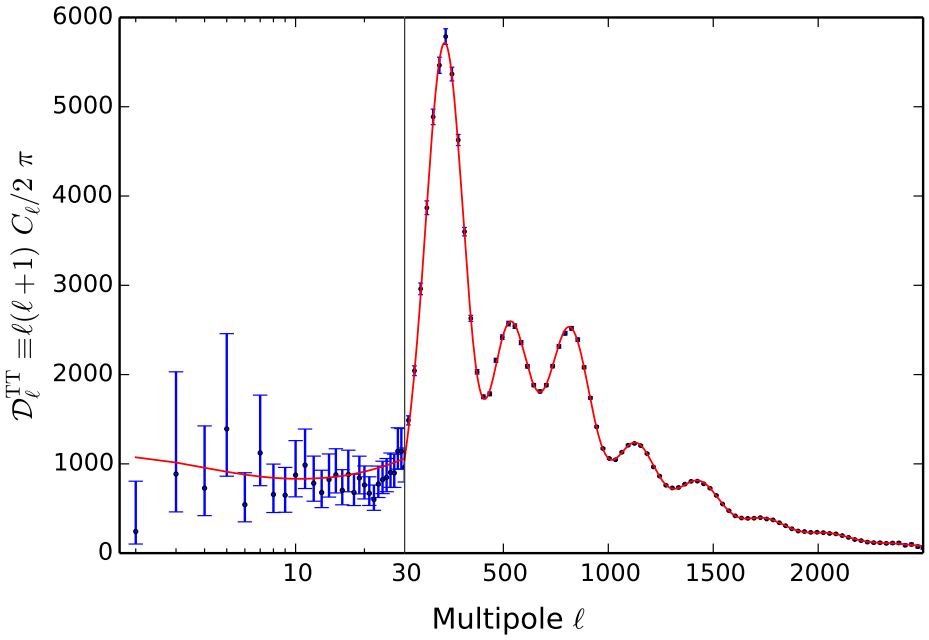

Figure 1.1. Measurements of the CMB temperature anisotropies from the *Planck* satellite [2], and the predictions of the best-fit ΛCDM model (red curve). Error bars show 68% confidence intervals. The low-ℓ range is plotted in a logarithmic axis, with each multipole plotted, while the high-ℓ range os plotted on a linear axis, with points binned together.

1.7.2 Baryon acoustic oscillations and other data sets

The study of BAO signatures is a fairly recent field in modern cosmology. The earliest foundations of the modern ideas about BAO, and their detection were proposed and discussed around 2003 by a number of different researchers [43–46], and their first detection was confirmed in the Sloan Digital Sky Survey, and the 2-degree Field galaxy redshift survey [47, 48] in 2005.

Besides CMB and BAO data sets that have established the ΛCDM model, there are other data sets, such as galaxy weak lensing [49, 50], and redshift space distortions [51], which can provide stringent constraints on modified theories of gravity and will be used in later chapters. Galaxy weak lensing data measures the deflection of light that is emitted from distant galaxies. It is called "weak" since the lensing effects are considerably smaller than in "strong" lensing, and cannot be distinguished by eye. Redshift space distortions, on the other hand, measure the standard deviation of fluctuations in the matter-density field. This is done via apparent distortions that happen in the redshift space. Distance of galaxies are measured through their redshift, but the redshift of a galaxy is caused by both its receding velocity (due to the Hubble flow), and also its "peculiar velocity" (caused by the environment of the galaxy). The redshift space distortions are caused by peculiar velocities, and are good proxies of matter-density fluctuations in the Universe.

These data sets prove to be useful since they test theories at the perturbation level *and* at late times. Since deviations from GR tend to grow over time in many models of modified gravity, the late time probes of structure formation, such as redshift space distortions and galaxy weak lensing, provide very strong constraints on these types of models.

Table 1.1 summarizes the different data sets that are used in cosmology, and their relevance in testing the theory of gravity.

Observation	**Information**
BBN	Background evolution at $a \sim 10^{-10}$
CMB, ($\ell \lesssim 800$)	Background evolution since $z \sim 1100$ and perturbations at $z \sim 1100$
CMB, ($\ell \gtrsim 800$)	Some of the information contained in $\ell \lesssim 800$ plus perturbations at recent times
BAO	Perturbations at the decoupling epoch, and background evolution since decoupling up to $a \sim 1$
WL and RSD	Perturbations at recent times ($a \sim 1$)

Table 1.1. A list of the cosmological observables and their information content. WL and RSD stand for weak lensing and redshift space distorsion data sets, respectively.

1.8 Structure of this thesis

After this brief summary of modern cosmology, the big bang theory, its predictions, and observational evidence, we will continue the thesis by reviewing some common theoretical approaches for modifying GR. In Chapter 2, we will explain the motivations behind modified gravity, and the possible ways that the theory can be modified within the context of the language of Lagrangians. We will then proceed in chapter 3 by introducing a general parameterization scheme that can capture any generic modification of gravity in cosmology. We will use this parameterization to study a specific theory of modified gravity that aims at solving the so called "old cosmological constant problem" in chapter 4. A new effective field theory approach to cosmology is presented in chapter 5, along with tests from the latest observations of CMB anisotropies by the *Planck* satellite, combined with other cosmological data. We conclude the thesis in chapter 6 with some discussion of directions for future study.

Chapter 2

An Introduction to Modified Gravity

General relativity has been extremely successful up to now in describing the behaviour of gravity in experiments, as well as introducing new physical phenomena, and providing quantitative predictions for them. Effects such as gravitational time delay [52], gravitational waves [53], and gravitational lensing were all predicted by Einstein as a consequence of GR field equations. When combined with astrophysics, GR has also established the foundations of fields like cosmology, and the study of compact objects.

Despite all of its successes, however, there are a few regimes where general relativity does not provide a satisfactory answer, even though gravity plays a significant role in them. Specifically, these regimes are the Universe at its earliest times, and a full, proper treatment of black holes, both of which may ultimately require a theory of gravity that is also quantum mechanical by construction. There are also observational phenomena, such as dark energy, where the answer provided by GR is still the best existing solution (in this case a cosmological constant with a very small size), but is not widely accepted, since it is not compatible with the general expectations of quantum mechanics (see Chapter 4 for further discussion on cosmological constant problems).

The answer to all of these problems and shortcomings may one day come from a coherent theory of quantum-gravity. Combining general relativity and quantum mechanics, however, appears to be a prohibitively hard problem. Theories such as string theory or loop quantum gravity claim success in building a quantum theory of gravity, but they both fall short of providing precise quantitative predictions, at least as of today [54, 55].

Part of the problem for building a new theory of gravity is the lack of any clear observational deviations from the predictions of GR. Here is where theories that modify GR can

be at least partially helpful. Instead of an attempt to build a fully coherent and complete theory that resolves the inconsistencies of quantum theory and GR, modified theories of gravity set about to perform a systematic search for observational deviations from GR by proposing specific theoretical extensions for investigating the theory space that lies close to GR itself. Several different ideas have been proposed (see e.g. [56, 57] for reviews). We will introduce some of the main classes of modified gravity in this chapter, and will present cosmological tests for some of these theories in the next three chapters.

2.1 Gravity beyond GR

General relativity is a unique theory with a strikingly simple Lagrangian:

$$\mathcal{L} = \frac{1}{16\,\pi G}\,\sqrt{-g}\,\left(R - 2\,\Lambda\right). \tag{2.1}$$

Here, R is the Ricci scalar and g is the determinant of the metric. More explicitly, Lovelock's theorem [58] states that field equations of GR (Eq. (1.1)) are the only second-order, local differential equations derivable from the Lagrangian $\mathcal{L} = \mathcal{L}(g_{\mu\nu})$, in 4-dimensional free space (i.e. with $T_{\mu\nu} = 0$). This theorem not only puts GR at a special position in the space of theories, but also provides a clear method for classifying modified theories of gravity. According to the theorem, the only possible ways to extend GR are one of (or a combination of) the following:

- extending the degrees of freedom in the Lagrangian and including scalar, vector, or tensor degrees of freedom;
- including higher-order terms in the Lagrangian;
- writing the theory in higher dimensions;
- breaking locality;
- dropping the requirement of obtaining field equations from a Lagrangian at all.

Different proposals that have been discussed in the literature break one or more of these conditions. In this context, we will describe some of the most well-known theories of modified gravity in the rest of this section.

2.1.1 Scalar-Tensor theories

Scalar-Tensor theories were among the very first proposed theories of modified gravity. They evade Lovelock's theorem by adding a new degree of freedom in the form of a scalar field. The simplest version of this idea, known as the "Brans-Dicke theory" [59], was introduced in 1961. The main goal of the Brans-Dicke theory was to incorporate Mach's principle [60] into the theory of relativity.[4] The authors argued that a theory of gravity would follow Mach's principle only if the Newton gravitational constant becomes an environment-dependant variable. They therefore substituted the constant G with a scalar field, and wrote the following Lagrangian density for what is now known as the Brans-Dicke theory:

$$\mathcal{L} = \frac{1}{16\pi}\sqrt{-g}\left(\phi R - \frac{\omega}{\phi}\nabla_\mu\phi\,\nabla^\mu\phi\right) + \mathcal{L}_{\rm m}(g_{\mu\nu}, \Psi). \tag{2.2}$$

Here, ϕ is a scalar field, R is the Ricci scalar, g is the determinant of the metric $g_{\mu\nu}$, $\mathcal{L}_{\rm m}$ is the Lagrangian of the matter fields Ψ, and ω is a free parameter of the theory. GR is a special case of the theory with $\omega \to \infty$ (very large values for ω would suppress the gradient terms in the Lagrangian ($\nabla_\mu\phi$) and would hence correspond to a constant ϕ field, which will make the Lagrangian equivalent to GR). In the paragraph following the first appearance of this Lagrangian, the authors state that "In any sensible theory ω must be of the general order of magnitude of unity". However, the tightest constraints on this parameter now come from the Cassini satellite [61], implying $\omega > 40000$ at (95% confidence limit[5]). This means that if we have such a theory, then the modifications to GR have to be very small.

A more general version of the theory has also been considered in the literature [62, 63]:

[4] The Brans-Dicke paper explains Mach's principle in a few pages. In short, one can state the principle as: "the large-scale structure of the Universe determines the local inertial frame."

[5] Abbreviated to "CL" in the remainder of this thesis.

$$\mathcal{L} = \frac{1}{16\,\pi}\sqrt{-g}\left(\phi\,R - \frac{\omega(\phi)}{\phi}\,\nabla_\mu\phi\,\nabla^\mu\phi + V(\phi)\right) + \mathcal{L}_{\rm m}(g_{\mu\nu},\Psi). \tag{2.3}$$

Here the parameter ω has become a function of the scalar field ϕ. One can apply the conformal transformation $g_{\mu\nu} = \tilde{g}_{\mu\nu}/\phi$ and write this theory in the so-called "Einstein frame", where the scalar field is not coupled to the Ricci scalar [56]

$$\mathcal{L} = \frac{1}{16\,\pi}\sqrt{-\tilde{g}}\left(\tilde{R} - \frac{1}{2}\,\tilde{\nabla}_\mu\psi\,\tilde{\nabla}^\mu\psi + V(\psi)\right) + \mathcal{L}_{\rm m}(g_{\mu\nu},\Psi). \tag{2.4}$$

Here, ϕ and ψ are related to each other according to

$$\frac{\partial\psi}{\partial\chi} = \sqrt{\frac{3+2\,\omega}{4\,\pi}}, \quad \text{with } e^{2\chi} = \phi^{-1}. \tag{2.5}$$

The first term of this new Lagrangian looks very similar to the Einstein-Hilbert action, Eq. (2.1), plus a scalar field, and therefore the field equations for the metric are similar to the field equations of GR. However, one should notice that the matter fields are coupled to the original metric, $g_{\mu\nu}$. This means that the energy momentum tensor is not conserved with respect to the transformed metric, $\tilde{g}_{\mu\nu}$, and test particles do not follow the geodesics of this metric. There has been some debate in the literature on the validity of using the "Einstein frame" and the physical meaning of the solutions in this space (see e.g. [64–66]). This debate is inherently tied to the definition of units, and becomes philosophical at some point (see e.g. [67] for a discussion of the importance of units, and particularly the use of dimensionless quantities in modified gravity studies).

Horndeski [68] has further generalized the scalar-tensor Lagrangian and has written the most general Lagrangian of a local, second-order theory of scalar-tensor gravity in 4-dimensions. This Lagrangian is constructed from the metric-field, a scalar-field, and four completely general functions of the scalar. It is a particularly long Lagrangian and we refer the interested reader to the original paper, or the notationally more modern versions of it in Ref. [69]. The Lagrangian has second-order terms that are coupled with each other, and it is therefore not immediately clear that the resulting field equations will be second order

as well. However, these second-order terms in the Lagrangian are carefully added so that the higher-order terms cancel each other in the field equations. We will come back to this theory in Chapter 5, where we constrain a subclass of Horndeski theories with cosmological data.

2.1.2 $f(R)$ theories

Another approach is to write some $f(R)$ in the Lagrangian in place of R, i.e. $\mathcal{L} = \sqrt{-g}(R + f(R))$.[6] These $f(R)$ theories break another assumption of the Lovelock theorem. They are among the so-called "higher-order" theories, where the equations of motion have more than two derivatives. Lagrangians for these theories are in some sense the most obvious way for extending GR, but then there is still freedom to choose the form of f.

The special case of $f(R) = cR^2$ was proposed as one of the earliest models of inflation [32, 70] and still appears to be consistent with the data [71].

Most higher-order theories of gravity exhibit "ghost-like" degrees of freedom. In the context of modified gravity, a "ghost" refers to degrees of freedom that show up with the wrong sign for the kinetic term in the Lagrangian. As a result, ghosts have the undesired property of increasing their kinetic energy as they climb up the potential. They should also be avoided for quantum mechanical reasons, because of the lack of a well defined ground state. However $f(R)$ theories, despite being "higher-order", are equivalent to a version of the scalar-tensor theory in Eq. (2.3) with no kinetic terms, and are therefore ghost-free theories.

Cosmology proves to be a strong tool for constraining $f(R)$ models, as we will explain in more detail in Chapter 5. Cosmological data provide unique tests because of the time-dependent background metric, and due to the various fluids that dominate the Universe at different epochs. Starting from radiation domination with $R = 0$, the Universe transits into matter domination with an evolving Ricci scalar, and ends with a (close to) cosmological constant dominated state with a constant (but non-zero) value of the Ricci scalar. Each

[6] It is convenient to define the $f(R)$-Lagrangian this way, and separate standard GR from the modification terms in $f(R)$.

of these different eras of cosmology constrain the form of the $f(R)$ function in a unique manner, and dictate that the form of the function has to be very close to that of GR. General deviations from GR are parameterized via the function

$$B = \frac{f_{RR}}{1 + f_R} \frac{H\dot{R}}{\dot{H} - H^2} \tag{2.6}$$

in cosmology. Here, f_R and f_{RR} are the first and second derivatives of $f(R)$, and a dot means a derivative with respect to conformal time, $d\tau = dt/a$. GR corresponds to $B \equiv 0$, and the tightest constraints on the present value of this parameter come from CMB data combined with the matter power spectrum, $B_0 < 0.83 \times 10^{-4}$ (95 % CL). We will explain the cosmological constraints on these theories in more detail in Chapter 5.

Almost all possible ways of escaping from the Lovelock theorem have been examined in the literature. We have only discussed two of the most well-known ideas of modified gravity here, because they have shown some merit in providing an explanation for the inflationary era, and because they will be used later in this thesis. A complete list of even just the names of the different proposed models would not fit this page, so we refer the interested reader to the extensive and comprehensive review of Ref. [56].

2.2 Notes on modified gravity studies, their limitations and uses

In a remarkable contrast to the theories of general and special relativity, which redefine fundamental notions such as mass, energy, space, and time, the modified theories of gravity accept all of these relativistic notions and simply reformulate their interactions. Modified theories of GR are thus like modified versions of Newtonian gravity that use different functions of distance for the gravitational force, without establishing a new paradigm to reformulate physics. They are, therefore, incapable of introducing genuinely new physical effects (like GR did by introducing gravitational waves, gravitational lensing, etc.), and can only modify the quantitative predictions for the set of observables that were already introduced by GR. Perhaps one day we will have a fundamentally different way of extending

GR, with a full theory of quantum gravity, and entirely new phenomena will emerge. But for now the ambitions of those who study "modified gravity" are more modest.

Despite the above-mentioned deficiency, modified gravity deserves some credit for the way it allows us to systematically search for deviations from GR. This is a search that covers a diverse range of scales in distance and energy, and scrutinises GR predictions under many different conditions, as we will see in the following chapters.

When discussing different physical regimes, it is common practice to chart the whole set of physical observables in terms of energy and distance, and put the focus of the search for new physics at the extremes of this chart (e.g. see Fig. 2.1). Even though this same exercise was historically fruitful for the cases of special relativity and quantum mechanics, it does not always hold. As an example, let us look at this type of argument in the light of the well-known story of the precession of Mercury.

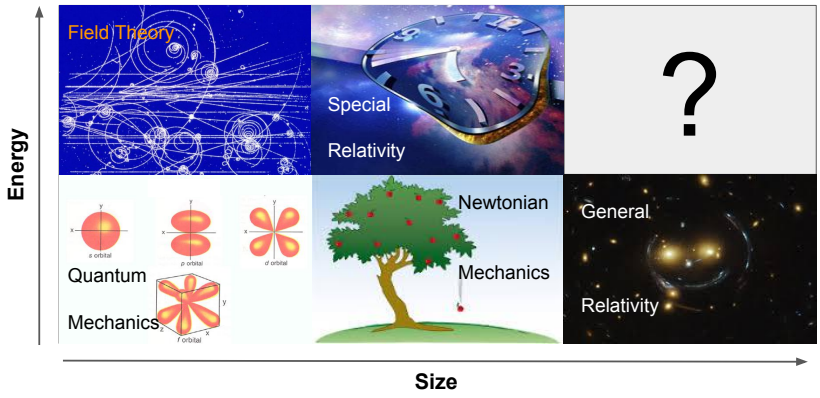

Figure 2.1. A very schematic chart of the different theories in physics, and their realm of relevance. While Newtonian mechanics works well on everyday scales, things change rather drastically on very small/large scales, or high energies.

The excess in precession of Mercury was discovered around 1859 by Leverrier [72]. In terms of distance, Mercury is not special, since Newtonian gravity works well from metre scales on Earth up to tens of AU in the solar system. In terms of gravitational energy,

Mercury also does not hold a special place, since the amount of energy stored in the Jupiter-Sun system is the largest among the planets in the solar system. Mercury's gravitational acceleration is much smaller than values we experience everyday on Earth, and even though the force of gravity between the Sun and Mercury is much stronger than what is achievable here, it is not the strongest among the planets, because Venus, Earth, Jupiter, and Saturn all experience stronger gravitational pulls from the Sun than Mercury. The only thing that is somewhat special for Mercury is the Sun's gravitational potential at its position. It is the deepest among the solar system planets, and certainly deeper than the gravitational potential on the Earth's surface. However, even though the gravitational potential at Mercury is the deepest, releasing a test particle from Mercury's orbit and tracking its trajectory will show very good agreement with Newtonian mechanics. The only thing that made Mercury a unique example for testing gravity was a combination of a relatively strong gravitational potential, a periodic orbital motion in that potential, and observations that spanned a 150-year time interval. But despite all of this, observations of the precession of Mercury were key to establishing the validity of GR, which overthrew Newtonian gravity entirely. Perhaps in a similar sense, modified theories of gravity might be able to discover some deviation from GR in conditions that are not necessarily extreme in terms of distance or energy scales.

In summary, no modified theories of gravity seem to be observationally favoured at the moment, and they appear to lack clear philosophical justification. Nevertheless, a search for observational deviations from the predictions of GR under different conditions is a valuable exercise, and modified theories of gravity provide us with systematic tools for developing such observational tests (as we will see in the next three chapters).

Chapter 3

Minimal Parameterization for Modified Gravity in Cosmology

3.1 Introduction

General Relativity (GR) has been confronted with many theoretical and experimental tests since its birth in 1915. From the gravitational lensing experiments in 1919 [73] up to the extensive studies and tests in the 1960s and 1970s [74–78], the theory has been confirmed observationally and theoretically bolstered in many different respects.

Cosmology has challenged GR with two, yet to be fully understood discoveries: dark matter and dark energy [79, 80]. Along with these two phenomena, the lack of renormalizability in GR [56] and the apparently exponential expansion in the very early Universe [81] are usually taken as signs for the incompleteness of the theory at high energies. Due to these shortcomings in GR the study of modified gravity has become a broad field. Scalar-tensor theories [59, 82], $f(R)$ modifications [83, 84], Horava-Lifshitz theory [85], multidimensional theories of gravity [86, 87], and many other suggestions have been made in the hope of finding, or at least deriving, some hints for, a fully consistent theory that can successfully explain the observations and satisfy the theoretical expectations. (Ref. [56] has an extensive review).

The new data coming from various experiments such as the *WMAP* and *Planck* satellite measurements of the cosmic microwave background (CMB) anisotropies [88], and the WiggleZ [89] or Baryon Oscillation Spectroscopic Survey [90] measurements of the matter power spectrum, provide us with an opportunity to test specific modified theories of grav-

ity. However, since there are many different modified theories, all with their own sets of parameters, there has recently been some effort to come up with a way to describe generic modified theories using only a few parameters, and to try to constrain those parameters with general theoretical arguments and by direct comparison with cosmological data.

The parameterized post-Friedmann (PPF) approach, as described in Ref. [91], is an effective way to parameterize many of the modified theories of gravity. However, it is not really feasible to constrain its more or less dozen additional free functions, even with the power of Markov Chain codes such as CosmoMC [92]; there are just too many degrees of freedom to provide useful constraints in the general case. In this chapter we will describe a somewhat different way to parameterize modified theories of gravity in which we try to retain only a small number of parameters, which we then constrain using *WMAP* 9-year [3] and South Pole Telescope (SPT) data [4].

In the next section we will describe the formulation of this new parameterization, and will show its connection with PPF and other approaches in Sect. 3.3. In Sect. 3.4 we will discuss the results of a numerical analysis using CAMB [40] and CosmoMC, and we will conclude the chapter in Sect. 3.5 with a brief discussion.

3.2 Modified gravity formulation

There are two common strategies for modifying gravity. One can start from the point of view of the Lagrangian or from the equations of motion. The Lagrangian seems like the more obvious path for writing down specific new theories, where one imagines retaining some desired symmetries while breaking some others. We will pursue this further in Chapter 5. The equations of motion, on the other hand, provide an easier way in practice to parameterize a general theory of modified gravity, especially in the case of first-order perturbations in a cosmological context.

The evolution of the cosmological background has been well tested at different redshift slices, specifically at Big Bang nucleosynthesis and at recombination through the CMB anisotropies. It therefore seems reasonable to assume that the background evolution is not

affected by the gravity modification, with the only background level effect being a possible explanation for a fluid behaving like dark energy.

The linearized and modified equations of motion for gravity can be written in the following form in a covariant theory:

$$\delta G_{\mu\nu} = 8\pi G\, \delta T_{\mu\nu} + \delta U_{\mu\nu}. \tag{3.1}$$

Here, $\delta G_{\mu\nu}$ is the perturbed Einstein tensor around a background metric, $\delta T_{\mu\nu}$ is the first order perturbation in the energy-momentum tensor and $\delta U_{\mu\nu}$ is the modification tensor source from any term that is not already embedded in GR.

Since we will be using CAMB for numerical calculations, we will choose the synchronous gauge from now on, and focus only on the spin-0 (scalar) perturbations. This will make it much more straightforward to adapt the relevant perturbed Boltzmann equations. The metric in the synchronous gauge is written as

$$\begin{aligned} ds^2 &= a^2(\tau)\left[-d\tau^2 + (\delta_{ij} + h_{ij})dx^i dx^j\right], \\ h_{ij} &= \int d^3k e^{i\vec{k}.\vec{x}}\{\hat{k}_i\,\hat{k}_j\,h(\vec{k},\tau) + (\hat{k}_i\,\hat{k}_j - \frac{1}{3}\delta_{ij})\,6\,\eta(\vec{k},\tau)\} \quad , \quad \vec{k} = k\hat{k}, \end{aligned} \tag{3.2}$$

where $\vec{k}$ is the wave vector. Putting this metric into Eq. (3.1) results in the following four equations [37]:

$$k^2\eta - \frac{1}{2}\frac{\dot{a}}{a}\dot{h} = -4\pi G\, a^2\delta\rho + k^2\, A(k,\tau); \tag{3.3}$$

$$k\dot{\eta} = 4\pi G\, a^2(\bar{\rho} + \bar{p})\, V + k^2 B(k,\tau); \tag{3.4}$$

$$\ddot{h} + 2\frac{\dot{a}}{a}\dot{h} - 2\,k^2\,\eta = -24\pi G\, a^2(\delta P) + k^2\, C(k,\tau); \tag{3.5}$$

$$\ddot{h} + 6\ddot{\eta} + 2\frac{\dot{a}}{a}(\dot{h} + 6\dot{\eta}) - 2\,k^2\eta = -24\pi G\, a^2(\bar{\rho} + \bar{p})\Sigma + k^2 D(k,\tau). \tag{3.6}$$

Here we have used the following definitions:

$$\begin{aligned}
\delta T^0_0 &= -\delta\rho \quad , \quad a^2\delta U^0_0 = k^2\, A(k,\tau),\\
\delta T^0_i &= (\bar{\rho}+\bar{p})\, V_i \quad , \quad a^2\delta U^0_i = k^2\, B(k,\tau),\\
\delta T^i_i &= 3\,\delta P \quad , \quad a^2\delta U^i_i = k^2\, C(k,\tau),\\
\mathcal{D}_{ij}\delta T^{ij} &= (\bar{\rho}+\bar{p})\Sigma \quad , \quad a^2\mathcal{D}_{ij}\delta U^{ij} = k^2\, D(k,\tau),
\end{aligned} \tag{3.7}$$

with $\bar{\rho}$ and $\bar{p}$ being the background energy density and pressure, respectively, and a dot representing a derivative with respect to τ. The factors of k are chosen to make the modifying functions, $\{A, B, C, D\}$, dimensionless. The quantity $\mathcal{D}_{ij}$ is defined as $\hat{k}_i\hat{k}_j - \frac{1}{3}\delta_{ij}$. The parameterization described here has a very close connection in practice with the PPF method explained in Ref. [91]. The most important differences are that we have grouped a number of separate parameters into a single parameter, and have used the synchronous gauge in Eqs.(3.3) to (3.6).

As was mentioned earlier in Chapter 1, Einstein's equations provide six independent equations. For the case of first order perturbations in cosmology, two of these six equations are for the two spin-2 (tensor) degrees of freedom, two of the equations are for the spin-1 (vector) variables and only two independent equations are left for the spin-0 (scalar) degrees of freedom. This means that Eqs. (3.3) to (3.6) are not independent and one has to impose two consistency relations on this set of four equations. These consistency relations of course come from the energy-momentum conservation equation, $\nabla_\mu(T^\mu{}_\nu + U^\mu{}_\nu) = 0$. Assuming that energy conservation holds independently for the conventional fluids, $\nabla_\mu T^\mu{}_\nu = 0$, (see Ref. [91] for the strengths and weaknesses of such an assumption) one then obtains the following two consistency equations:

$$\frac{2\,\dot{A}}{\mathcal{H}} + 2\,A - \frac{2\,k\,B}{\mathcal{H}} + C = 0\,; \tag{3.8}$$

$$6\,\dot{B} + k\,C + 12\,\mathcal{H}\,B - k\,D = 0\,. \tag{3.9}$$

Here we have defined $\mathcal{H} \equiv \dot{a}/a$ and dropped the arguments of the functions A to D.

Eqs. (3.3) to (3.6), together with Eqs. (3.8) and (3.9), show that two general functions of space and time would be enough to parameterize a wide range of modified theories of gravity. This approach of course does not provide a test for any specific modified theory. However, given the current prejudice that GR *is* the true theory of gravity at low energies (e.g. see Ref. [93] for a discussion), the main question is whether or not cosmological data can distinguish between GR and any other generic theory of modified gravity. Clearly, if we found evidence for deviations from GR, then we would have a parametric way of constraining the space of allowed models, and hence hone in on the correct theory.

3.3 Connection with other methods of parameterization

In this section we show the connection between the $\{\mu, \gamma\}$ parameterization of modified gravity, the PPF parameters and the parameterization introduced in Sect. 3.2.

The parameters defined in Sect. 3.2 are related to the PPF parameters according to

$$A(k,\tau) = A_0\hat{\Phi} + F_0\hat{\Gamma} + \alpha_0\hat{\chi} + \frac{\alpha_1}{k}\dot{\hat{\chi}}, \tag{3.10}$$

$$B(k,\tau) = B_0\hat{\Phi} + I_0\hat{\Gamma} + \beta_0\hat{\chi} + \frac{\beta_1}{k}\dot{\hat{\chi}}, \tag{3.11}$$

$$C(k,\tau) = C_0\hat{\Phi} + \frac{C_1}{k}\dot{\hat{\Phi}} + J_0\hat{\Gamma} + \frac{J_1}{k}\dot{\hat{\Gamma}} + \gamma_0\hat{\chi} + \frac{\gamma_1}{k}\dot{\hat{\chi}} + \frac{\gamma_2}{k^2}\ddot{\hat{\chi}}, \tag{3.12}$$

$$D(k,\tau) = D_0\hat{\Phi} + \frac{D_1}{k}\dot{\hat{\Phi}} + K_0\hat{\Gamma} + \frac{K_1}{k}\dot{\hat{\Gamma}} + \epsilon_0\hat{\chi} + \frac{\epsilon_1}{k}\dot{\hat{\chi}} + \frac{\epsilon_2}{k^2}\ddot{\hat{\chi}}. \tag{3.13}$$

While the authors of Ref. [91] have insisted on the modifications being gauge invariant[7], it is good to keep in mind that there is nothing special about the use of gauge invariant parameters, as is shown in Ref. [94]. The important issue is to track the degrees of freedom in the equations. There are originally four free functions for the spin-0 degrees of freedom in the metric, but the gauge freedom can be used to set two of them to zero. Using only two gauge invariant functions instead of four, means that the gauge freedom has been implicitly used somewhere to omit the redundant variables.

[7] They have slightly modified the tone of their paper in its later versions.

All 22 of the parameters on the right hand side of Eqs. (3.10) to (3.13) are in fact two-dimensional functions of the wave number, k, and time. A hat on a function means that it is a gauge invariant quantity. The symbol $\hat{\chi}$ is the gauge invariant form of any extra degree of freedom that can appear, for example, in a scalar-tensor theory, or in an $f(R)$ theory as a result of a number of conformal transformations (see section D.2 of Ref. [91] for further explanation). $\hat{\Phi}$ and $\hat{\Gamma}$ are related to the synchronous gauge metric perturbations through:

$$\hat{\Phi} = \eta - \frac{\mathcal{H}}{2\,k^2}(\dot{h} + 6\,\dot{\eta}); \tag{3.14}$$

$$\hat{\Psi} = \frac{1}{2\,k^2}(\ddot{h} + 6\,\ddot{\eta} + \mathcal{H}\,(\dot{h} + 6\,\dot{\eta})); \tag{3.15}$$

$$\hat{\Gamma} = \frac{1}{k}(\dot{\hat{\Phi}} + \mathcal{H}\,\hat{\Psi}). \tag{3.16}$$

One needs to add more parameters to the right hand side of Eqs. (3.10) to (3.13) if there is more than one extra degree of freedom, or if the equations of motion of the theory are higher than second order and the theory cannot be conformally transformed into a second order theory. The reason this many parameters were introduced in Ref. [91] is that there is a direct connection between these parameters and the Lagrangians of a number of specific theories, like the Horava-Lifshitz, scalar-tensor or Einstein Aether theories. Therefore, in principle, constraining these parameters is equivalent to constraining the theory space of those Lagrangians.

However, there are a number of issues that may encourage one to consider alternatives to the PPF approach for parameterizing modifications to gravity. First of all, it is practically impossible to run a Markov chain code for 22 two-dimensional functions. One can reduce the number of free functions to perhaps 15 using Eqs. (3.8) and (3.9), but there is still a huge amount of freedom in the problem. The second reason is that the whole power of the PPF method lies in distinguishing among a number of classically modified theories of gravity that are mostly proven to be either theoretically inconsistent, like the Horava-Lifshitz theory [56], or already ruled out observationally, like TeVeS (at least for explaining away dark matter) [95]. While it is certainly important and useful to check the GR predictions with the

new coming data sets, it does not appear reasonable at this stage to stick with the motivation of any specific theory. For the moment it therefore seems prudent to consider an even simpler approach, as we describe here.

There is another popular parameterization in the literature, described fully in Refs. [96–98]. This second parameterization is best described in the conformal Newtonian gauge, via the following metric:

$$ds^2 = a^2(\tau)[-(1+2\,\psi)d\tau^2 + (1-2\,\phi)\delta_{ij}dx^i dx^j]. \tag{3.17}$$

The modifying parameters, $\{\mu, \gamma\}$, are defined through the following:

$$k^2\psi = -\mu(k,a)4\pi G a^2\{\bar{\rho}\Delta + 3(\bar{\rho}+\bar{p})\Sigma\}\,; \tag{3.18}$$

$$k^2[\phi - \gamma(k,a)\psi] = \mu(k,a)12\pi G a^2(\bar{\rho}+\bar{p})\Sigma\,. \tag{3.19}$$

Here $\Delta = \delta\rho + 3\frac{\mathcal{H}}{k}(1+\bar{p}/\bar{\rho})V$, and all of the matter perturbation quantities are in the Newtonian gauge.

In order to see the connection between this method of parameterization and the one described in the previous section through Eqs. (3.3) to (3.6), one needs to use the modified equations of motion in the Newtonian gauge:

$$k^2\phi + 3\mathcal{H}\left(\dot{\phi} + \mathcal{H}\psi\right) = -4\pi G a^2\delta\rho + k^2 A_{\rm N}\,; \tag{3.20}$$

$$k^2\left(\dot{\phi} + \mathcal{H}\psi\right) = 4\pi G a^2(\bar{\rho}+\bar{p})k\,V + k^3 B_{\rm N}\,; \tag{3.21}$$

$$k^2(\phi - \psi) = 12\pi G a^2(\bar{\rho}+\bar{P})\Sigma + k^2 D_{\rm N}\,. \tag{3.22}$$

The parameters $\{A_{\rm N}, B_{\rm N}, D_{\rm N}\}$ are the modifying functions in the Newtonian gauge. These

parameters are related to γ and μ via

$$\alpha \equiv 1 - \mu\,, \tag{3.23}$$

$$\beta \equiv \gamma - 1, \tag{3.24}$$

$$4\pi G a^2 \alpha\,\{\bar{\rho}\Delta + 3(\bar{\rho} + \bar{p})\Sigma\} = k^2\left(A_{\rm N} - 3\frac{\mathcal{H}}{k}B_{\rm N} + D_{\rm N}\right), \tag{3.25}$$

$$\beta\,\psi = 12\,\pi G a^2\,\alpha\Sigma + k^2\,D_{\rm N}, \tag{3.26}$$

where one can choose between using the functions $\{A_{\rm N}, B_{\rm N}, C_{\rm N}, D_{\rm N}\}$, along with two constraint equations similar to the Eqs. (3.8) and (3.9), or using the two parameters γ and μ and trying to remain consistent in the equations of motion.

It is argued in Ref. [99] that the $\{\gamma, \mu\}$ choice is not capable of parameterizing second order theories in the case of an unmodified background and no extra fields. To show this the authors use the fact that, in the absence of extra fields, all of the Greek coefficients in Eqs. (3.10) to (3.13), i.e. $\{\alpha_0, ..., \epsilon_2\}$, have to be zero. Furthermore, they argue that in the case of second order theories, F_0 and I_0 have to be zero, and therefore the constraints of Eqs. (3.8) and (3.9) show that J_0 and K_0 are zero as well. After all of this, one can see that Eq. (3.22) can be written as the following in this special case:

$$k^2(\phi - \psi) = 12\pi G a^2(\bar{\rho} + \bar{P})\Sigma + k^2\left(D_0\phi + \frac{D_1}{k}\dot{\phi}\right). \tag{3.27}$$

Ref. [99] then shows that the absence of a term proportional to the metric derivative will lead to an inconsistency. However, this conclusion is valid only if one assumes that β in Eq. (3.26) is a function of background quantities, which usually is not the case. Otherwise, one can use Eq. (3.26) to define β:

$$\beta \equiv \frac{12\,\pi G a^2\,\alpha\Sigma + k^2(D_0\phi + \frac{D_1}{k}\dot{\phi})}{\psi}, \tag{3.28}$$

leaving no ambiguity or inconsistency.[8]

It is also claimed in Ref. [100] that the $\{\gamma, \mu\}$ parameterization becomes ambiguous on large scales, while none of these shortcomings apply to the PPF method. However, these criticisms do not seem legitimate, since, as was shown in this section, there is a direct connection between $\{\gamma, \mu\}$, and the PPF parameters.[9] For any given set of functions for the PPF method, one can find a corresponding set of functions $\{\gamma, \mu\}$, using Eqs. (3.10) to (3.13) and (3.26), that will produce the exact same result for any observable quantity. One only needs to ensure the use of consistent equations while modifying gravity through codes such as CAMB.

Although we believe that there is no ambiguity in the $\{\gamma, \mu\}$ parameterization, we also believe that our $\{A, B, C, D\}$ parameterization can be implemented much more easily in Boltzmann codes. Furthermore, there is a potential problem for the $\{\gamma, \mu\}$ parameterization on the small scales that enter the horizon during the radiation domination era. The metric perturbation ψ will oscillate around zero a couple of times for these scales and that makes the γ function blind to any modification at those instants of time. This behaviour also has the potential to lead to numerical instabilities.

3.4 Numerical calculation

In this section we will constrain the parameterization described in Sect. 3.2 using the CMB anisotropy power spectra. We will describe the effects of the modifying parameters on the CMB and show the results of numerical calculations from CAMB and CosmoMC.

3.4.1 Effects of A and B on the power spectra

Before showing numerical results, we first describe some of the physical effects of having non-zero values of A or B. So far we have not placed any constraints on these quantities,

[8] Note that this might be troublesome if ψ goes to zero at some moments of time. This can happen for the scales that enter the horizon during radiation domination.

[9] In particular there is nothing wrong with the $\{\gamma, \mu\}$ parameterization on large scales, since ψ is certainly always non-zero.

which are in general functions of both space and time. There are some effects that can be explicitly seen from the equations of motion and energy conservation. For example, a positive A enhances the pressure perturbation and anisotropic stress, while reducing the density perturbation. On the other hand, a positive B will enhance the momentum perturbation and reduce the pressure perturbation and anisotropic stress.

There are also some other effects that need a little more algebra to see, and we now discuss four examples.

Neutrino moments:

The neutrinos' zeroth and second moments, $\{F_{\nu 0}, F_{\nu 2}\}$, are coupled to the modifying gravity terms according to the Boltzmann equations [37] and Eqs. (3.3) to (3.6):

$$\dot{F}_{\nu 0} = -k\,F_{\nu 1} - \frac{2}{3}\dot{h}; \tag{3.29}$$

$$\dot{F}_{\nu 2} = \frac{2}{5}k\,F_{\nu 1} - \frac{3}{5}k\,F_{\nu 3} + \frac{4}{15}(\dot{h} + 6\dot{\eta}). \tag{3.30}$$

Here $\dot{h}$ is modified according to Eq. (3.3), and the term $\dot{h} + 6\dot{\eta}$ is coupled to A and B through Eqs. (3.3) and (3.4):

$$\dot{h} + 6\dot{\eta} = \frac{2\,k^2\,\eta + 8\,\pi G\,a^2\delta\rho}{\mathcal{H}} + 24\,\pi G\,a^2(\bar{\rho} + \bar{p})\frac{V}{k} - \frac{2\,k^2\,A}{\mathcal{H}} + 6\,k\,B. \tag{3.31}$$

Therefore, modified gravity can have a significant effect on the neutrino second moment.

Photon moments:

While the same thing is valid for the photons' second moment after decoupling, the situation is different during the tight coupling regime. The Thomson scattering rate is so high in the tight coupling era that it makes the second moment insensitive to gravity. In other words, the electromagnetic force is so strong that it does not let the photons feel gravity.

ISW effect:

The integrated Sachs-Wolfe (ISW) [101] effect is proportional to $\dot{\phi} + \dot{\psi}$ in the Newtonian

gauge. In the synchronous gauge this is

$$\dot{\phi} + \dot{\psi} = \frac{\ddot{h} + 6\,\ddot{\eta}}{2\,k^2} + \dot{\eta}. \tag{3.32}$$

Here $\dot{\eta}$ is modified according to Eq. (3.4) and, therefore, a subtle change in the function $B(k, \tau)$, can have a considerable influence on the ISW effect. Fig. 3.1 shows the effects of a constant non-zero A and B on the ISW effect. For the case of a constant non-zero B, the ISW effect is always present, since the time derivative of the potential is constantly sourced by this function. This will result in more power on all scales, including the tail of the CMB power spectrum (see Fig. 3.2). Fig. 3.2 shows that if a non-zero B is favoured by CMB data, it will happen in the large ℓs, ($\ell > 1500$), and will be due to its anti-damping behaviour.

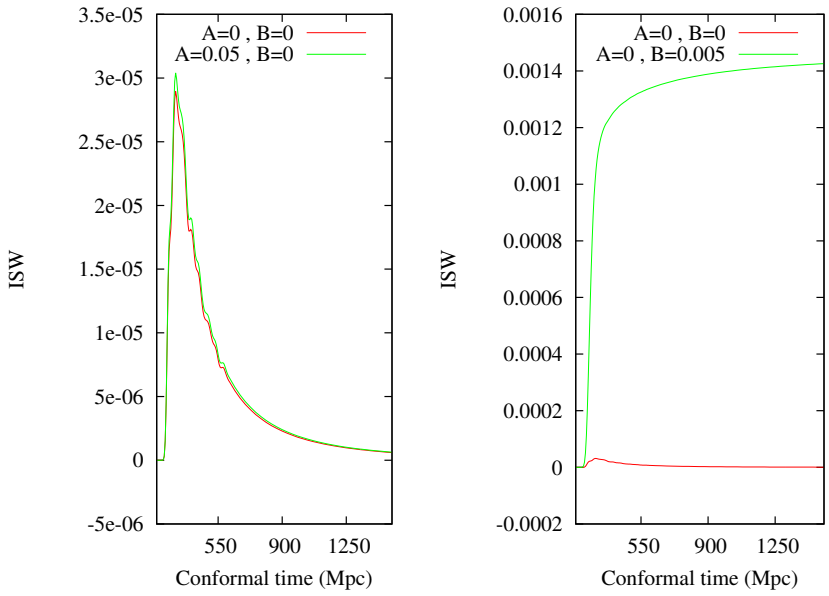

Figure 3.1. Effects of a constant, non-zero A and B on the ISW effect. This plot shows the ISW effect for a specific scale of $k = 0.21\,\mathrm{Mpc}^{-1}$.

Fig. 3.3 shows the CMB power spectra for the case of a constant but non-zero A or B. Note how a constant non-zero B raises the tail of the spectrum up. One might also point to the degeneracy of A and the initial amplitude (usually called A_s) mostly by looking at the

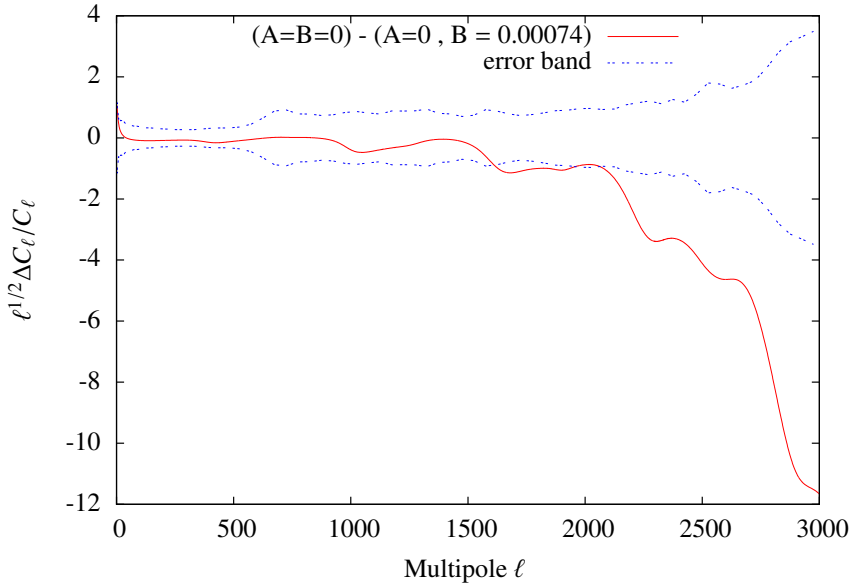

Figure 3.2. Effects of a constant B on the CMB power spectra. The plot shows the difference in power for the case of zero B minus the best fit non-zero B, using *WMAP*9 and SPT12 data, while keeping all the rest of the parameters the same. The error band plotted is based on the reported error on the binned CMB power spectra from the *WMAP*9 [3] and SPT12 [4] groups.

height of the peaks.

Matter overdensity:

The Boltzmann equation for cold dark matter overdensity in the synchronous gauge reads [37]

$$\dot{\delta}_{\rm CDM} \equiv \left(\frac{\delta\rho_{\rm CDM}}{\bar{\rho}_{\rm CDM}}\right)^{\cdot} = -\frac{1}{2}\,\dot{h}. \tag{3.33}$$

Using Eqs. (3.3), (3.4), and the Friedmann equation, $\mathcal{H}^2 = \dfrac{8\pi G a^2}{3}\bar{\rho}$, and assuming a matter-dominated Universe with no baryons, one obtains the following equation for the

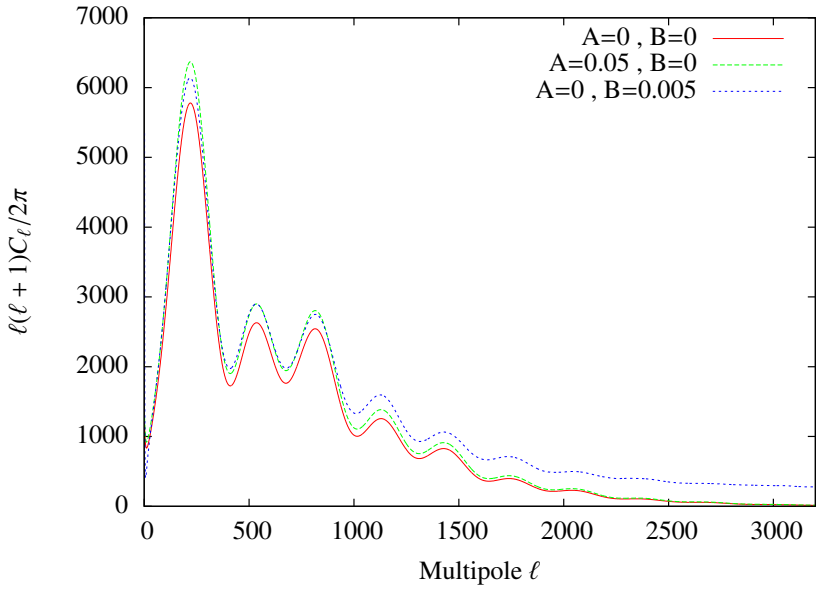

Figure 3.3. Effects of a constant, non-zero A or B on the CMB power spectra. One can see that the two parameters have quite different effects.

cold dark matter overdensity:

$$\mathcal{H}\,\dot{\delta}_{\rm CDM} = -\frac{3\,\mathcal{H}^2}{2}\delta_{\rm CDM} + k^2 A - k^2\eta,$$

$$\text{i.e.} \qquad \ddot{\delta}_{\rm CDM} + \left(\frac{\dot{\mathcal{H}}}{\mathcal{H}} + \frac{3}{2}\mathcal{H}\right)\dot{\delta}_{\rm CDM} + 3\,\dot{\mathcal{H}}\delta_{\rm CDM} = -\frac{k^3}{\mathcal{H}}B + \frac{k^2}{\mathcal{H}}\dot{A}. \tag{3.34}$$

The above equation clearly shows the role of A and B as driving forces for the matter overdensity. The k^3 prefactor makes the first term on the right hand side dominant on small scales and this will therefore have a significant effect on the matter fluctuation amplitude at late times. The matter power spectrum will therefore be expected to put strong constraints on modified gravity models.

3.4.2 Markov chain constraints on A and B

Since $A(k,\tau)$ and $B(k,\tau)$ are free functions, we need to choose some simple cases to investigate. We choose here to focus on the simple cases of A and B being separate constants (i.e.

independent of both scale and time). We do not claim that this is in any sense a preferred choice — we simply have to pick something tractable. With better data one can imagine constraining a larger set of parameters, for example describing A and B as piecewise constants or polynomial functions.

We used CosmoMC to constrain constant A and B, together with the *WMAP*-9 [3] and SPT12 [4] CMB data. The amplitudes of the CMB foregrounds were added as additional parameters and were marginalized over for the case of SPT12. The resulting constraints and distributions are shown in Fig. 3.4. Here we focus entirely on the effects of A and B on the CMB. Hence we turn off the post-processing effects of lensing [102], and ignore constraints from any other astrophysical data-sets.

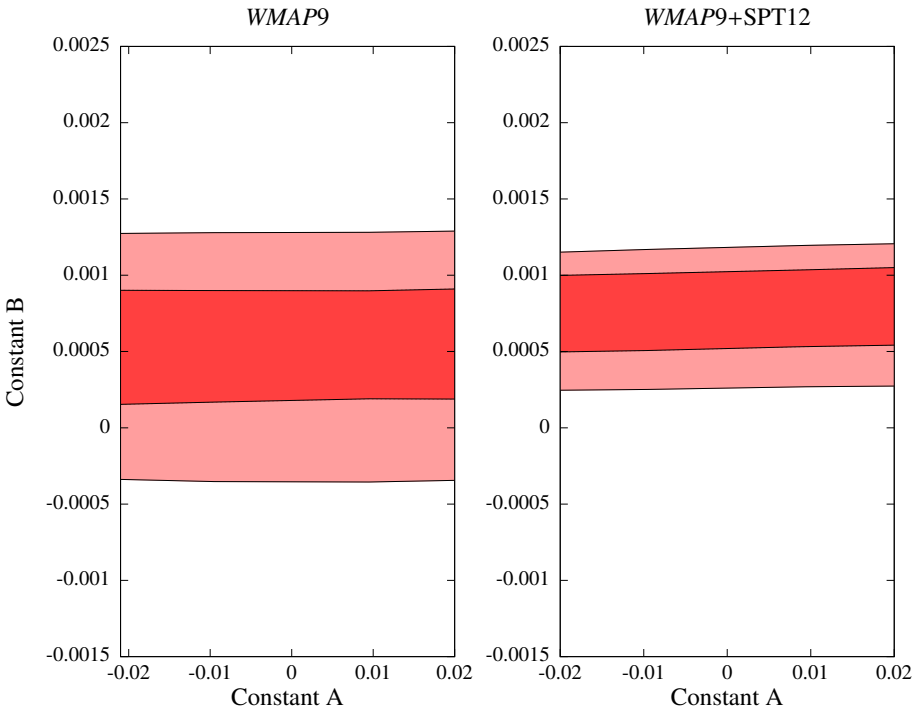

Figure 3.4. 68 and 95 percent contours of the constants A and B using *WMAP*9-year data alone (left) and SPT12 (right) without including lensing effects, and neglecting late time growth effects.

One might conclude from Fig. 3.4 that general relativity is ruled out by nearly 3σ using CMB alone, since a non-zero value of B is preferred. However, adding lensing to the picture will considerably change the results. As was shown in Eq. (3.34), a non-zero B will change the matter power spectrum so drastically that in a universe with non-zero B, lensing will be one of the main secondary effects on the CMB. The results of a Markov chain calculation that includes the effects of lensing (i.e. assuming B was constant not only in the CMB era, but all the way until today) is shown in Fig. 3.5, and are entirely consistent with GR.

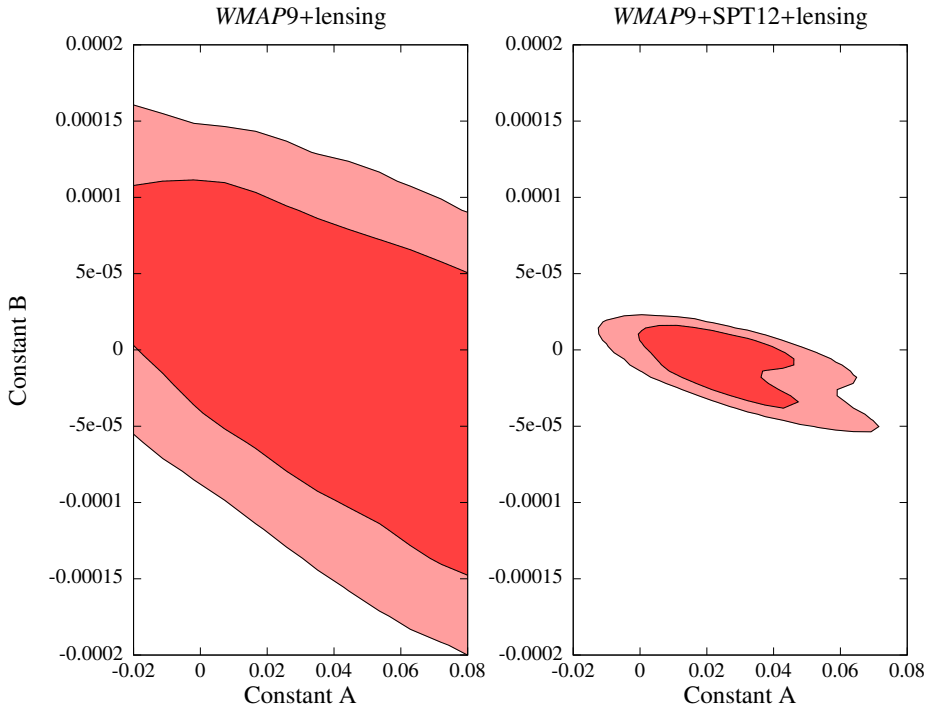

Figure 3.5. 68 and 95 percent contours of the constants A and B using *WMAP*9-year data alone (left) and *WAMP*9 + SPT12 (right), with lensing effects included.

The broad constraint on A is mainly due to a strong (anti-)correlation between A and the initial amplitude of the scalar perturbations. Two-dimensional contour plots of A versus A_s, the initial amplitude of scalar curvature perturbations, are shown in Fig. 3.6.

The mean of the likelihood and 68% confidence interval for the six cosmological pa-

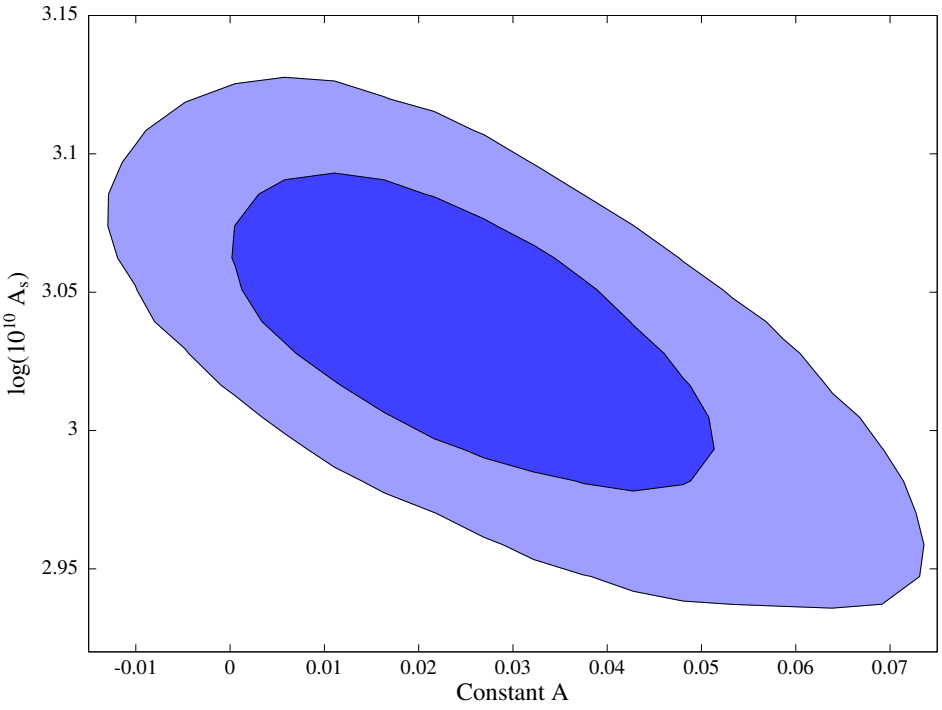

Figure 3.6. The strong anti-correlation between parameter A and the initial amplitude, A_s, makes the constraints on either one of these two parameters weaker.

rameters together with A and B are tabulated in Table 3.1. Note that the simplified case we are considering here treats CMB constraints only. If we really took B as constant for all time, then there would be large effects on the late time growth, affecting the matter power spectrum, and hence tight constraints coming from a relevant observable, such as σ_8 from cluster abundance today.

3.4.3 Alternative powers of k in B

Examining Eq. (3.34) reveals that the only term modifying the matter power spectrum in the case of constant A and B, is $k^3 B/\mathcal{H}$. This term is important for two reasons. Firstly, this is the only term introducing a k dependence in the cold dark matter amplitude at late times and at sufficiently large scales where one can completely ignore the effect of baryons

Parameter	WMAP9	WMAP9+SPT12	WMAP9+SPT12+lensing
$100\,\Omega_b h^2$	2.22 ± 0.05	2.10 ± 0.03	2.22 ± 0.04
$\Omega_{DM} h^2$	0.118 ± 0.005	0.122 ± 0.005	0.115 ± 0.004
$100\,\theta$	1.038 ± 0.002	1.040 ± 0.001	1.042 ± 0.0010
τ	0.086 ± 0.014	0.076 ± 0.012	0.084 ± 0.012
$\log(10^{10} A_s)$	3.1 ± 0.2	3.1 ± 0.2	3.0 ± 0.4
n_s	0.96 ± 0.01	0.93 ± 0.01	0.96 ± 0.01
$100A$	1 ± 10	0.02 ± 10	2.7 ± 1.7
$1000B$	0.44 ± 0.41	0.74 ± 0.24	-0.0097 ± 0.016

Table 3.1. The mean likelihood values together with the 68% confidence interval for the usual six cosmological parameters, together with constant A and B, using CMB constraints only.

on the matter power spectra. Secondly, the k^3 factor enhances this term significantly on small scales in the case of a constant B. Since the amplitude of matter power spectrum (via lensing effects) was the main source of constraints on B, it would seem reasonable to choose $B = \mathcal{H}\, B_0/k$, where B_0 is a dimensionless constant. This should avoid too much power in the matter densities on small scales, and therefore reduce lensing as well. However, this choice will lead to enormous power on the largest scales, as is shown in Fig. 3.7.

In order to match with data, one could choose a form in which B switches from $B = \mathcal{H}\, B_0/k$ to $B = \mathcal{H}\, B_0/k_0$, where k_0 is some small enough transition scale. We discuss this simply as an alternative to the B = constant case. There is clearly scope for exploring a wider class of forms for the functions $A(k, \tau)$ and $B(k, \tau)$.

3.5 Discussion

Since a constant A is essentially degenerate with the initial amplitude of the primordial fluctuations, the CMB alone cannot constrain this parameter. On the other hand, constant B seems to be fairly well constrained by the CMB data. However, if B was an oscillating function of time, changing sign from time to time, its total effect on the CMB power spectra would become weaker and the constraints would be broader. According to Eq. (4.19), a constant B will change η monotonically, while the effect of an oscillating B will partially

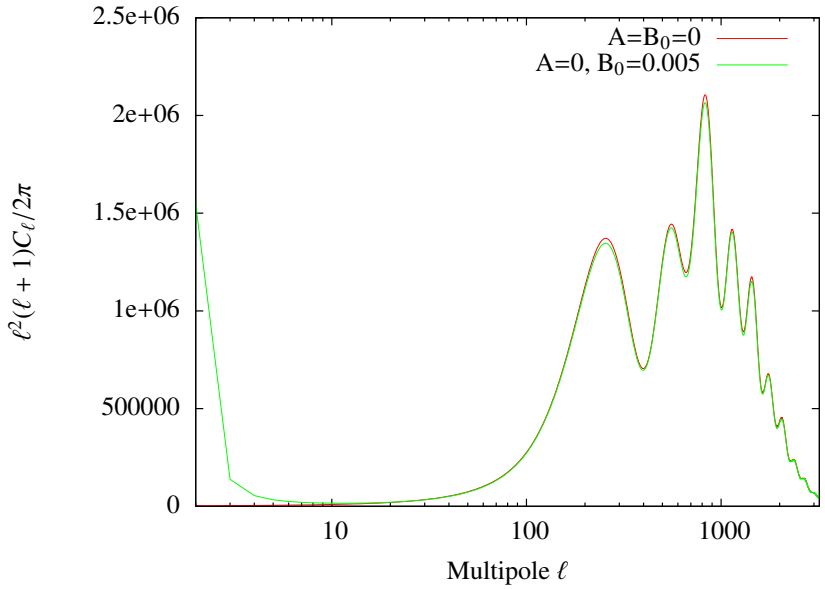

Figure 3.7. Effect of a non-zero B_0 on the CMB power spectra, with the choice $B = \mathcal{H}\,B_0/k$.

cancel some of the time. Together, the results of Sect. 3.4 show that the ISW effect and the growth at relatively recent times (driving the amplitude of matter perturbations) can have huge constraining power for many generic theories of modified gravity. (See Ref. [103] for a recent example). One can consider different positive or negative powers of $(\mathcal{H}/k)$ as part of the dependence of B in order to get around the matter constraints, as was discussed in Sect. 3.4.3.

We have seen that when considering CMB data alone, there seems to be a mild preference for non-zero B. This is essentially because it provides an extra degree of freedom for resolving a mild tension between *WMAP* and SPT. Neveretheless it remains true that a model with B constant for all time would be tightly constrained by observations of the matter power spectrum at redshift zero. We leave for a future study the question of whether there might be any preference for more general forms for $A(k,\tau)$ and $B(k,\tau)$ using a combination of *Planck* CMB data and other astrophysical data-sets.

Chapter 4

How Does Pressure Gravitate? Cosmological Constant Problem Confronts Observational Cosmology

4.1 Introduction

One of the most immediate puzzles of quantum gravity (i.e., applying the rules of quantum mechanics to gravitational physics) is an expectation value for the vacuum energy that is 60–120 orders of magnitude larger than its measured value from cosmological (gravitational) observations. This is known as the (now old) *cosmological constant problem* [104], and has been thwarting our understanding of modern physics for almost a century [105]. The discovery of late-time cosmic acceleration [106, 107], added an extra layer of complexity to the puzzle, showing that the (gravitational) vacuum energy, albeit tiny, is non-vanishing (now dubbed, the *new* cosmological constant problem).

Gravitational Aether (GA) theory is an attempt to find a solution to the *old* cosmological constant problem [108, 109], i.e., the question of why, in lieu of fantastic cancellations, the vacuum quantum fluctuations do not appear to source gravity. The approach is to stop the quantum vacuum from gravitating by modifying our theory of gravity, as we describe below. In this way the (mean density of) quantum fluctuations will have no dynamical effect in astrophysics or cosmology (see [110] for one of the very first steps and [111] for an alternative but related attempt for solving the problem).

Although GA is a very specific proposal for modifying gravity, it may serve as an ex-

ample of more general theories. As we will see below, a generalized version may represent a broader class of theories in which the gravitational effects of pressure (and including anisotropic stress) might be different from those of GR.

It is important to be clear that this theory does not have any solution for the "new" cosmological constant problem, i.e., the empirical existence of a small vacuum energy density which now dominates the energy budget of the Universe, driving the accelerated expansion and making the geometry of space close to flat. Hence in GA theory it is assumed that the vacuum quantum fluctuations (the old problem) and the small but non-zero value of Λ (the new problem) are two separate phenomena that should be explained independently (but see [112]).

The Einstein field equations in the GA theory (in units with $c = 1$, and with metric signature=(−+++)) are modified to

$$(8\pi G_{\rm R})^{-1}(G_{\mu\nu} + \Lambda g_{\mu\nu}) = T_{\mu\nu} - \frac{1}{4}T^{\alpha}_{\alpha}g_{\mu\nu} + T'_{\mu\nu}, \tag{4.1}$$

$$\text{with } T'_{\mu\nu} = p'(u'_{\mu}u'_{\nu} + g_{\mu\nu}). \tag{4.2}$$

Most significantly, the second term on the right hand side of Eq. (4.1), $-\frac{1}{4}T^{\alpha}_{\alpha}g_{\mu\nu}$, solves the old cosmological constant problem by cancelling the effect of vacuum fluctuations in the energy momentum tensor. The third term, $T'_{\mu\nu}$, is then needed to make the field equations consistent, and is dubbed *gravitational aether*.

The form used for $T'_{\mu\nu}$ in Eq. (4.2) is a convenient choice, but is probably not unique, although it is limited by phenomenological and stability constraints [108]. However, p' and u'_{μ}, the pressure and four velocity unit vector of the aether, are constrained through the terms in the energy-momentum tensor by applying the Bianchi identity and the assumption of energy-momentum conservation, i.e.,

$$\nabla^{\mu}T'_{\mu\nu} = \frac{1}{4}\nabla_{\nu}T. \tag{4.3}$$

The only free constant of this theory, as in General Relativity (GR), is $G_{\rm R}$, although, as

we will see, this is not the same as the usual Newtonian gravitational constant, $G_{\rm N}$. In addition, of course, there are parameters describing the constituents in the various tensors, i.e., the cosmological parameters. In cosmology, the energy-momentum tensor, $T_{\mu\nu}$, consists of the conventional fluids, i.e., radiation, baryons, and cold dark matter, plus a contribution due to vacuum fluctuations,

$$T_{\mu\nu} = T^{\rm R}_{\mu\nu} + T^{\rm B}_{\mu\nu} + T^{\rm C}_{\mu\nu} + \rho_{\rm vac} g_{\mu\nu}, \tag{4.4}$$

$$T \equiv T^{\alpha}_{\alpha} = -(\rho^{\rm B} + \rho^{\rm C}) + 4\,\rho_{\rm vac}, \tag{4.5}$$

where neutrinos are included as part of radiation, and their mass is set to zero in this paper.

Equations (4.1) and (4.2) that describe GA are drastic modifications of GR with no additional tunable parameter. Therefore, one may wonder whether GA can survive all the precision tests of gravity that have already been carried out. These tests are often expressed in terms of the parameterized post-Newtonian (PPN) modifications of GR, which are expressed in terms of 10 dimensionless PPN parameters [113]. While these parameters do not capture all possible modifications of GR, they are usually sufficient to capture leading corrections to GR predictions in the post-Newtonian regime (i.e., nearly flat space-time with non-relativistic motions), in lieu of new scales in the gravitational theory. It turns out that only one PPN parameter, ζ_4, which quantifies the anomalous coupling of gravity to pressure has not been significantly constrained empirically, as the existing precision tests only probe gravity in vacuum, or for objects with negligible pressure. Indeed, since only the sourcing of gravity is modified in GA, the vacuum gravity content is identical to GR, and the only PPN parameter that deviates from GR is $\zeta_4 = 1/3$ (as opposed to $\zeta_4 = 0$ in GR) [108, 109].

The idea that ζ_4 could be non-zero runs contrary to the conventional wisdom that relates gravitational coupling to pressure on the one hand, to the couplings to internal and kinetic energies on the other [114], both of which are already significantly constrained by experiments. However, this expectation is based on the assumption that the average gravity of a gas of interacting point particles, is the same as the gravity of a perfect fluid that is obtained

by coarse-graining the particle gas.[10] This connects with the whole issue of the assumption of the continuum approximation for cosmological fluids, where the particle density is low, so that the average distance between particles is a macroscopic scale. Gravity is only well-tested on scales $\gtrsim 0.1\,\mathrm{mm}$ [115], which are larger than the distance between particles in most terrestrial or astrophysical precision tests of gravity. Therefore, there is no guarantee that the same laws of gravity apply to microscopic constituents of the continuous media in which gravity is currently tested. Indeed, GA could only be an effective theory of gravity above some scale $\lambda_c \lesssim 0.1$ mm, implying that sources of energy-momentum on the right hand sides of Eqs. (4.1) or (4.3) should be coarse-grained on scale λ_c.

At first sight, it might appear that the dependence of gravitational coupling on pressure signals a violation of weak and/or strong equivalence principles (WEP and/or SEP). However, WEP is explicitly imposed in GA, as all matter components couple to the same metric. Moreover, SEP is so far only tested for gravity in vacuum (e.g. point masses in the solar system), where GA is equivalent to GR, as aether is not sourced, and thus vanishes (in lieu of non-trivial boundary conditions; see e.g. [112]).

What goes against one's intuition in the case of the GA modification of Einstein gravity, compared to e.g. scalar-tensor theories, is that even in the Newtonian limit, comparable effects come from the change in couplings *and* the gravity of the energy/momentum of the aether. In contrast, the additional fields in the usual modified gravity theories carry little energy/momentum in the Newtonian regime, while they could modify couplings by order unity. If the change in the gravitational mass (due to the dependence of G on the equation of state) is by the same factor as the change in energy/momentum (due to the additional terms on the RHS of Einstein equations), then the ratio of gravitational to inertial mass remains unchanged.

A more intuitive picture might be to consider aether (minus the trace term) as an exotic fluid *bound* to matter, similar to an electron gas for example, within ordinary GR. Like the

[10] This would not be the case in the GA theory, since the aether tracks the motion of individual particles, due to the constraint of Eq. (4.3). Therefore, the nonlinear back-reaction of the motion of the aether would be lost in the coarse-grained perfect fluid.

electron gas, the effect will be to modify the gravitational field source, by the amount of energy/momentum in the exotic fluid. However, unlike the electron gas, the non-gravitational energy/momentum exchange between matter and the exotic fluid is tuned to zero, which ensures WEP, at least at the classical level. Moreover, the action-reaction principle (Newton's 3rd law) for gravitational forces should include the momentum in, and interaction with the exotic fluid.

Another conceptual issue with Eqs (4.1–4.2) is that, at least to our knowledge, they do not follow from an action principle. However, an action principle may not be necessary (or even possible) for a low energy effective theory, such as in the case of Navier-Stokes fluid equations, even if the fundamental theory does follow from an action principle. Given the severity of the cosmological constant problem, it seems reasonable that we might be prepared to relax requirements that are not absolutely necessary for a sensible effective description of nature.

There are two obvious places in the Universe to look for the gravitational effect of relativistic pressure, and thus constrain ζ_4:

1. The first situation involves compact objects, particularly the internal structure of neutron stars [116, 117]. While, in principle, mass and radius measurements of neutron stars can be used to constrain ζ_4, at the moment the constraints are almost completely degenerate with the uncertainty in the nuclear equation of state (not to mention other observational systematics). However, future observations of gravitational wave emission from neutron star mergers (e.g., with Advanced LIGO interferometers) might be able to break this degeneracy [117]. It may also be possible to develop tests that probe near the hot accretion disks of black holes or during the formation of compact objects in supernova explosions.

2. The second situation is the matter-radiation transition in the early Universe. Ref. [118] studied constraints arising from the big bang nucleosynthesis epoch. However, more precise measurements come from various cosmic microwave background (CMB) anisotropy experiments, such as the *Wilkinson Microwave Anisotropy Probe* (*WMAP*)

[119], *Planck* [120], the Atacama Cosmology Telescope (ACT) [121], and the South Pole Telescope (SPT) [5], amongst other cosmological observations. The constraints on GA were studied in detail in Ref. [109], with the data sets available at that time. While GA might arguably ease tension among certain observations, such as the Ly-α forest, primordial Lithium abundance, or earlier ACT data, it was discrepant with others, such as Deuterium abundance, SPT data, or low-redshift measurements of cosmic geometry. The aim of this paper is to carefully revisit these tensions in observational cosmology, in light of the significant advances within the past three years.

With this introduction, in Sect. 4.2, we move on to derive the equations for the cosmological background, as well as linear perturbations, in the GA theory. Similar to Ref. [109], we use the Generalized Gravitational Aether (GGA) framework, which interpolates between GR and GA, to quantify the observational constraints. This framework depends on the ratio of the gravitational constant in the radiation and matter eras, $G_{\rm R}/G_{\rm N} = 1+\zeta_4$, which is $1 + \frac{1}{3} = \frac{4}{3}$ $(1 + 0 = 1)$ for GA (GR). Sect. 4.3 discusses our numerical implementation of the GGA equations, and the resulting constraints from different combinations of cosmological data sets, some of which appear to exclude GA at the 4–5 σ level, while others are equally (in)consistent with GR or GA at about the 3 σ level. Finally, Sect. 4.5 summarizes our results, discusses various open questions, and highlights avenues for future inquiry.

4.2 Equations of motion at the background and perturbative level

Baryons, radiation, and cold dark matter can be considered as perfect fluids with simple equations of state, $p = w\rho$, at the background level. The following p' and u' will solve

Eqs. (4.1–4.3) in this case:

$$p' = \sum_i \frac{(1+w^i)(3\,w^i-1)}{4}\rho^i; \tag{4.6}$$

$$u'_\mu = \sum_i \frac{(1+w^i)(1-3\,w^i)}{2}u^i_\mu. \tag{4.7}$$

Here, "i" stands for either baryons, radiation, cold dark matter, or vacuum fluctuations. Based on Eqs. (4.6) and (4.7), $p' = -(\rho^{\rm B}+\rho^{\rm C})/4$, and $u'_\mu = u^{\rm C}_\mu$ at the background level. Substituting these relations back into Eq. (4.1), the field equations will take the following form in terms of the conventional fluids in $T_{\mu\nu}$:

$$(8\,\pi)^{-1}(G_{\mu\nu}+\Lambda g_{\mu\nu}) = G_{\rm R}\,T^{\rm R}_{\mu\nu} + \frac{3}{4}\,G_{\rm R}\,(T^{\rm B}_{\mu\nu}+T^{\rm C}_{\mu\nu}). \tag{4.8}$$

One of the clearest testable predictions of this theory is that space-time reacts differently to matter and to radiation: a spherical ball full of relativistic matter curves the space-time more than a spherical ball of non-relativistic substance (of the same size and density). Defining $G_{\rm R} \equiv 4\,G_{\rm N}/3$, where $G_{\rm N}$ is the usual Newtonian gravitational constant, and using the FRW metric, $ds^2 = a^2(-d\tau^2 + d\mathbf{x}^2)$, the Friedmann equation in the GA theory will be:

$$\mathcal{H}^2 = \frac{8\pi G_{\rm N} a^2}{3}(\rho + \frac{1}{3}\rho^{\rm R}) \quad , \quad \rho = \rho^{\rm R}+\rho^{\rm B}+\rho^{\rm C}+\rho^{\Lambda}. \tag{4.9}$$

$\mathcal{H}$ is defined as $\dot{a}/a$ here, and a dot represents a derivative with respect to the conformal time, τ.

The Friedmann equation can be used to calculate the predictions of the theory for big bang nucleosynthesis (BBN) (see e.g., Ref. [109]). Although the different effective value of G in the early Universe means that the BBN predictions are different from the standard model, uncertainties in the consistency of the light element abundances suggest that the comparison with data cannot be considered as fatal for the theory. Therefore, one needs to go one step further and calculate the first-order perturbations to determine the predictions for observables such as the CMB anisotropies, or the matter power spectrum.

Before dealing with the perturbations, it is worth noticing that the GA theory can be treated as a special case of a more general framework. We shall call this the Generalized Gravitational Aether (GGA), which has the following field equations:

$$(8\,\pi)^{-1}(G_{\mu\nu} + \Lambda g_{\mu\nu}) = G_{\rm R} T_{\mu\nu} - G_{\rm RN} T^{\alpha}_{\alpha} g_{\mu\nu} + 4\,G_{\rm RN} T'_{\mu\nu}. \tag{4.10}$$

Here $G_{\rm RN} \equiv G_{\rm R} - G_{\rm N} = \zeta_4 G_{\rm N}$ is the difference in gravitational constants between radiation and matter. $G_{\rm R}$ and $G_{\rm N}$ are both free constants and one will recover the gravitational aether by setting $G_{\rm R} = 4G_{\rm N}/3$. General relativity is also a special case of GGA, with $G_{\rm RN} = 0$. The Friedmann equation in GGA will be:

$$\mathcal{H}^2 = \frac{8\pi a^2}{3}(G_{\rm N}\rho + G_{\rm RN}\rho^{\rm R}). \tag{4.11}$$

Using GGA as a framework, we then have a family of models, parameterized by ζ_4, with $\zeta_4 = 0$ corresponding to GR and $\zeta_4 = 1/3$ being GA.

It is fairly straightforward to calculate the perturbation equations in the general (GGA) framework, which will then contain GA and GR as special cases. We will use the cold dark matter gauge (see e.g., Ref. [37]) with the following metric for the first order perturbations:

$$\begin{aligned} ds^2 &= a^2(\tau)\left[-d\tau^2 + (\delta_{ij} + h_{ij})dx^i dx^j\right]; \\ h_{ij} &= \int d^3k e^{i\vec{k}.\vec{x}}\left[\hat{k}_i\hat{k}_j h(\vec{k},\tau) + \left(\hat{k}_i\hat{k}_j - \frac{1}{3}\delta_{ij}\right)6\eta(\vec{k},\tau)\right] \quad , \quad \vec{k} = k\hat{k}. \end{aligned} \tag{4.12}$$

We will also use the following definitions for the perturbation parts of the energy momentum tensor:

$$\delta T^0_0 = -\delta\rho; \tag{4.13}$$

$$\delta T^0_i = (\bar{\rho} + \bar{p})\,V_i; \tag{4.14}$$

$$\delta T^i_i = 3\,\delta p; \tag{4.15}$$

$$\mathcal{D}_{ij}\delta T^{ij} = (\bar{\rho} + \bar{p})\Sigma. \tag{4.16}$$

The barred variables refer to background quantities and $\mathcal{D}_{ij}$ is defined as $\hat{k}_i\hat{k}_j - \frac{1}{3}\delta_{ij}$. Once again, the fluids in $T_{\mu\nu}$ are baryons, cold dark matter, radiation, and vacuum quantum fluctuations. We will follow the conventions of Ref. [109] and define the perturbations in the aether density and four velocity as

$$\delta p' = p' - \left(-\frac{\rho^{\rm M}}{4}\right), \quad \delta u'_\mu = u'_\mu - u^{\rm C}_\mu. \tag{4.17}$$

Here $\rho^{\rm M}$ is the total matter density, i.e., baryons plus cold dark matter, and the quantities $\rho^{\rm M}$ and $u^{\rm C}_\mu$ consist of both their background and perturbation parts. Using the above definitions and the metric defined in Eq. (4.12), we obtain four equations of motion from the GGA field equations:

$$k^2\eta - \frac{1}{2}\mathcal{H}\dot{h} = -4\pi G_{\rm N} a^2\delta\rho + k^2 A(k,\tau); \tag{4.18}$$

$$k\dot{\eta} = 4\pi G_{\rm N} a^2(\bar{\rho}+\bar{p})V + k^2 B(k,\tau); \tag{4.19}$$

$$\ddot{h} + 2\mathcal{H}\dot{h} - 2k^2\eta = -24\pi G_{\rm N} a^2(\delta P) + k^2 C(k,\tau); \tag{4.20}$$

$$\ddot{h} + 6\ddot{\eta} + 2\mathcal{H}(\dot{h}+6\dot{\eta}) - 2k^2\eta = -24\pi G_{\rm N} a^2(\bar{\rho}+\bar{p})\Sigma + k^2 D(k,\tau). \tag{4.21}$$

The four functions, $\{A, B, C, D\}$, are

$$A(k,\tau) = \frac{-4\pi G_{\rm RN} a^2\,\delta\rho^{\rm R}}{k^2}, \tag{4.22}$$

$$B(k,\tau) = \frac{4\pi G_{\rm RN} a^2\,(i\,k^i\delta T^0_i - \bar{\rho}^{\rm M}\,\omega)}{k^3}, \tag{4.23}$$

$$C(k,\tau) = \frac{-8\pi G_{\rm RN} a^2(\delta\rho^{\rm R} + 12\,\delta p')}{k^2}, \tag{4.24}$$

$$D(k,\tau) = \frac{-24\pi G_{\rm RN} a^2\mathcal{D}_{ij}\delta T^{\rm R}_{ij}}{k^2}. \tag{4.25}$$

Here ω is defined as the divergence of the aether four velocity perturbation: $\omega \equiv ik^i\delta u'_i/a$. One can equally use Eqs. (4.18) to (4.21), or use Eq. (4.3) to derive the following two

constraints for the aether parameters:

$$3\,\frac{\mathcal{H}}{a}\,\partial_\tau(a\,\omega) + k^2\,\omega \;=\; k^2\,\frac{\bar{\rho}_0^{\rm B}}{\bar{\rho}_0^{\rm M}}\,\theta^{\rm B}; \tag{4.26}$$

$$\delta p' \;=\; \frac{\bar{\rho}^{\rm M}}{12\,\mathcal{H}}(\omega - \frac{\bar{\rho}_0^{\rm B}}{\bar{\rho}_0^{\rm M}}\,\theta^{\rm B}). \tag{4.27}$$

Here $\bar{\rho}_0^{\rm B}$ and $\bar{\rho}_0^{\rm M}$ are the current background density in baryons and matter, respectively, and $\theta^{\rm B}$ is the divergence of the baryon velocity perturbation: $\theta \equiv ik^i\,V_i^{\rm B}$. At very early times, when $k \ll \mathcal{H}$, one can ignore the right hand side of Eq. (4.26), together with the $k^2\,\omega$ factor on the left hand side. The initial condition for the divergence should therefore be deduced from

$$\dot{\omega} + \mathcal{H}\,\omega = 0\,. \tag{4.28}$$

Any non-zero initial condition on ω will be damped as a^{-1}, and it is therefore reasonable to assume the initial condition $\omega = 0$ at all scales. It is also interesting to notice that, since we are using the cold dark matter gauge, ω will once again be washed out for very large scales, $k \ll \mathcal{H}$, at late times when baryons fall into the potential well of the cold dark matter particles and start co-moving with them.

The physical meaning of the four modifying terms, $\{A, B, C, D\}$, is explained in Ref. [122] for an even more general theory. In short, the second term and the time derivative of the first term will act as driving forces for matter overdensities, while the second term and the time derivative of the fourth term are important in the integrated Sachs-Wolf (ISW) [123] effect.

We will confront the GGA theory with cosmological observations in the next section.

4.3 Cosmological constraints on GGA

We have modified the cosmological codes `CAMB` [40] and `CosmoMC` [92] in order to test the predictions of GGA against cosmological data. Before confronting the theory with data, it is necessary to make sure that the codes are internally consistent and error-free. We will

list a number of consistency checks we have made on CAMB in the next subsection, and then report the constraints on the GGA parameter.

4.3.1 Consistency checks on CAMB

One of the relatively trivial tests on the modified CAMB code is that it should reproduce the C_ℓs of the non-modified code after setting $G_{\rm RN} = 0$. The next obvious thing is a test at the background level. The GA theory is completely degenerate at the background level with a GR model that has one third more radiation (see Eq. (4.9)). In the standard picture each light neutrino species adds 0.23 times as much radiation as the photons. Therefore, the following models should result in exactly the same $a(\tau)$ and $\mathcal{H}(\tau)$ functions: $\mathcal{B}1 := \{G_{\rm RN} = 1/3G_{\rm N}, \mathcal{N}_{\rm eff} = 3.04\}$[11] and $\mathcal{B}2 := \{\text{GR with } \mathcal{N}_{\rm eff} = 5.54\}$, where $\mathcal{N}_{\rm eff}$ is the effective number of light neutrinos.

The effect of GGA at the perturbation level is evident through the four modifying functions $\{A, B, C, D\}$. Using constraint equations such as Eq. (4.3), one can see that the functions $\{C, D\}$ are linear combinations of the first two functions $\{A, B\}$ and their time derivatives. Therefore, the two functions $\{A, B\}$ are sufficient for tracing the perturbative effects of GGA. Between the two, A is purely dependent on radiation at the perturbation level (see Eq. (4.22)). Looking closer at B in Eq. (4.23) we see that

$$k^3 B = \frac{4}{3}\pi G_{\rm RN}\, a^2 \left(3\Delta\omega + 4\,\bar{\rho}^{\nu}\theta^{\nu} + 4\,\bar{\rho}^{\gamma}\theta^{\gamma}\right). \tag{4.29}$$

Here $\Delta\omega$ is defined as $(\bar{\rho}^{\rm B}\,\theta^{\rm B} - \bar{\rho}^{\rm M}\,\omega)$, which is proportional to the time derivative of ω, according to Eq. (4.26), and is therefore smaller than the radiation terms (see Fig. 4.1). θ^{ν} and θ^{γ} are the neutrino and photon first moments, respectively [37].

Putting this together, we find that the GGA effects are almost degenerate with extra radiation, even when we consider perturbations. However, the GGA-$\mathcal{N}_{\rm eff}$ degeneracy does not hold exactly at the perturbation level, since $\delta\rho^{\gamma}/\delta\rho^{\nu}$ and $\theta^{\gamma}/\theta^{\nu}$ are both time- and scale-dependent, contrary to the previous case at the background level, where $\bar{\rho}^{\gamma}/\bar{\rho}^{\nu}$ was a con-

[11] Here $\mathcal{B}$ is for background, and $\mathcal{P}$ will be for perturbations.

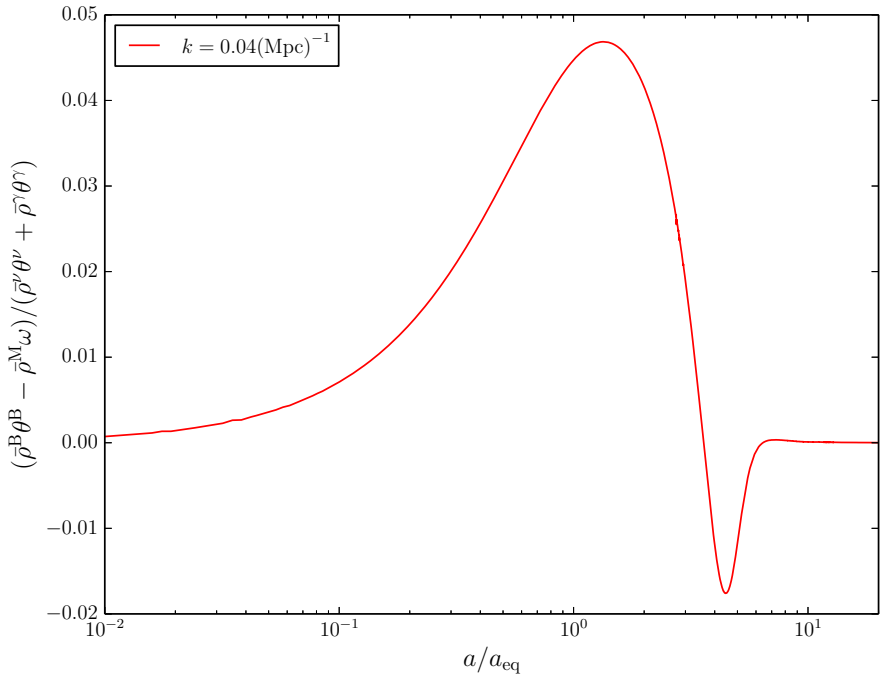

Figure 4.1. Effects of non-radiation modifying terms compared to the effects of radiation, at $k = 0.04$ Mpc^{-1} (see Eq. (4.29)). This shows that the non-radiation terms are smaller by more than a factor of 20.

stant number through time and for every scale.

The final test of the modified `CAMB` code is at the perturbation level when the GA parameter, G_{RN}, is not set to zero and GA is fully effective. Based on the discussion in the preceding paragraphs the code should produce the same C_ℓs for the following two models: $\mathcal{P}1 := \{G_{\mathrm{RN}} = 1/3G_{\mathrm{N}}, \mathcal{N}_{\mathrm{eff}} = 3.04, T_0^4 = (2.7255)^4\}$ and $\mathcal{P}2 := \{\text{GR with } \mathcal{N}_{\mathrm{eff}} = 4/3 \times 3.04,\ T_0^4 = 4/3 \times (2.7255)^4\}$, when the non-radiation terms, i.e., terms in $\Delta\omega$ are ignored. We use the value of the present CMB temperature, T_0, from Ref. [124]. However, one needs to be careful while performing this test, since T_0 appears in many parts of the code that are totally irrelevant to gravity (see Ref. [125] for a related discussion), e.g., the sound speed of the plasma before last scattering depends on the photon-to-baryon density ratio and hence on T_0. Figs. 4.2 and 4.3 show these tests of our calculations for GGA. The

right panel of these figures tests the code at the perturbation level, while the left panels show the effect of non-radiation fluids on the CMB anisotropies and matter power spectra. Ignoring the effect of non-radiation fluids, is crucial in reducing the GA Eqs. (4.1–4.3), to Eq. (4.8) at the perturbation level, and hence the $G_{\rm RN}$–ζ_4 correspondence.

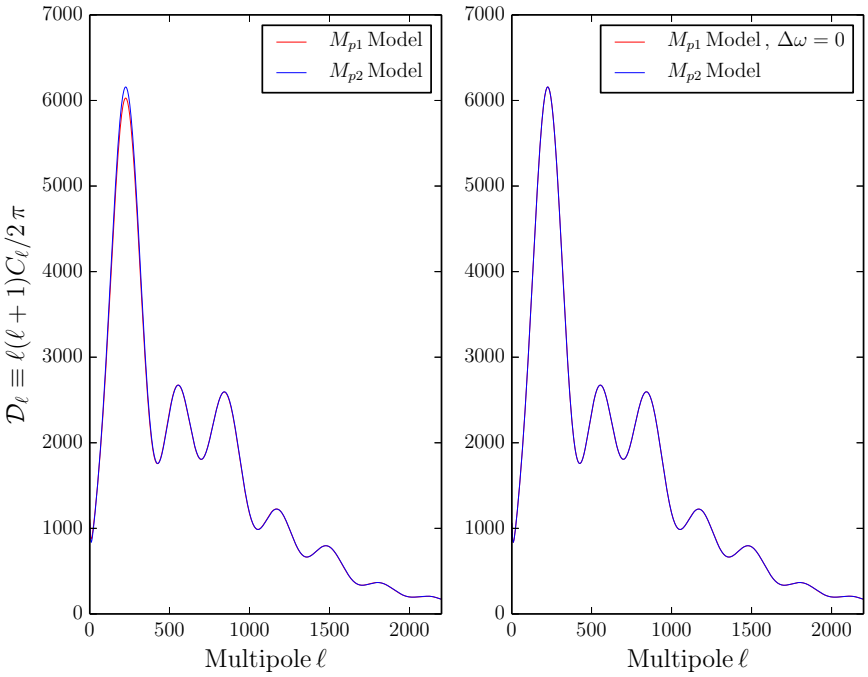

Figure 4.2. Checking the code at the perturbation level by comparing the CMB anisotropies power spectra for the models $\mathcal{P}1 := \{G_{\rm RN} = 1/3G_{\rm N}, \mathcal{N}_{\rm eff} = 3.04, T_0^4 = (2.7255)^4\}$ and $\mathcal{P}2 := \{\text{GR with } \mathcal{N}_{\rm eff} = 4/3 \times 3.04,\ T_0^4 = 4/3 \times (2.7255)^4\}$ (left panel). There is a small difference between the two at around the first peak. This can be explained by considering the effects of a non-zero ω (divergence of the aether four-velocity). The two models completely coincide with each other by setting $\Delta\omega$ to zero in the $\mathcal{P}1$ model (right panel).

Figure 4.4 shows the CMB anisotropy power spectrum predictions from GR and GA (with other GGA models interpolating between the two). The input parameters of the left panel are the same for both theories and are taken from Ref. [1]. We see on the left panel that the positions of the peaks are consistently shifted towards smaller scales, i.e., higher

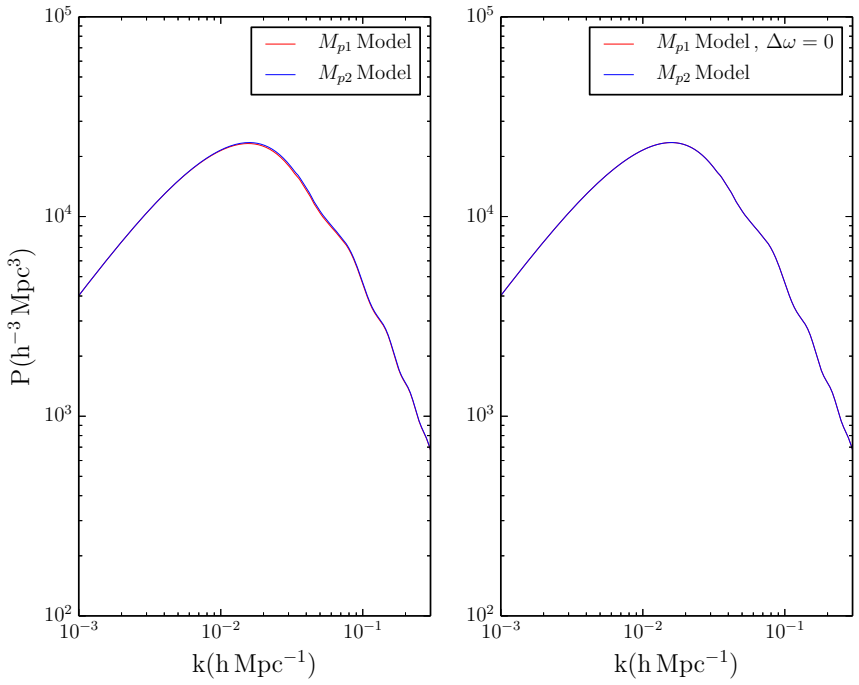

Figure 4.3. Checking the code at the perturbation level by comparing the the models $\mathcal{P}1 := \{G_{\rm RN} = 1/3G_{\rm N}, \mathcal{N}_{\rm eff} = 3.04, T_0^4 = (2.7255)^4\}$ and $\mathcal{P}2 := \{\text{GR with } \mathcal{N}_{\rm eff} = 4/3 \times 3.04,\ T_0^4 = 4/3 \times (2.7255)^4\}$ (left panel). The small difference between the two can be explained by considering the effects of a non-zero ω. The two models completely coincide with each other by setting $\Delta\omega$ to zero in the $\mathcal{P}1$ model (right panel).

ℓs. This is because the Universe is younger at recombination in the GA theory, which in turn is due to having effectively more radiation at the background level of the GA theory compared to GR. There is also an enhanced early ISW effect [126] in the GA theory due the presence of the the two modifying functions, B and D, as was explained in chapter 3. This can be understood more intuitively using the fact that GA is effectively degenerate at the background and perturbation level with a GR model with one third more radiation. Since the ISW effect is proportional to $e^{-\tau}$ (where τ is the optical depth), and the time derivative of the metric potentials (that are non-zero only during the matter radiation transition and at very late times), then having more radiation in the Universe will delay the radiation to matter transition to later times with smaller τ and enhance the ISW effect.

In order for the GA model to match GR and hence fit the data, since there is a very good match between data and GR predictions, one needs to change the matter to radiation density ratio to get the right position for the peaks. This can be done by either deducting from the radiation density, or adding more matter to the GA model. The first option is highly restricted from the CMB temperature data [124]. The second option can be done either through adding baryons or cold dark matter, or both. Since the density of baryons is constrained through helium abundance ratio (see e.g. [127]), the only remaining option is to add cold dark matter to the theory. This is also limited by the ratio of even to odd peaks in the CMB power spectra, but is the last resort! The best fit value for the cold dark matter density in the GA theory, using CMB data only, is: $\Omega_{\rm DM}h^2 = 0.147 \pm 0.004$.

After fixing the position of the peaks, one needs to get the right amplitude for the spectra. The relative amplitude of the high-ℓ to low-ℓ multi-poles is highly affected by the early ISW effect that was explained before and is evident in the left panel of Fig. 4.4 by comparing the ratio of the power of the two curves in $\ell \sim 250$, and $\ell \sim 2000$. This relative mismatch in the amplitude can be fixed by choosing higher values of the spectral index, n_s. The best fit value of this parameter in the GA theory is: $n_s = 1.042 \pm 0.008$.

The best-fit predictions of the two theories are compared in the right panel of Fig. 4.4. We see that the best fit GA theory predicts less power at high ℓs compared to GR. The best-fit predictions of the two theories are compared with *Planck* and SPT data in Fig. 4.5.

4.3.2 Cosmological constraints

We now turn to deriving precision constraints on GGA from cosmological observations. We assume that $G_{\rm N}$ is equal to the Newtonian gravitational constant measured in Cavendish-type experiments (see e.g. Ref. [128]) using sources with negligible pressure. Then `CosmoMC` can be used for sampling $G_{\rm R}$ using different combinations of the following cosmological data.

1. The first data release of the all-sky CMB temperature anisotropy power spectrum,

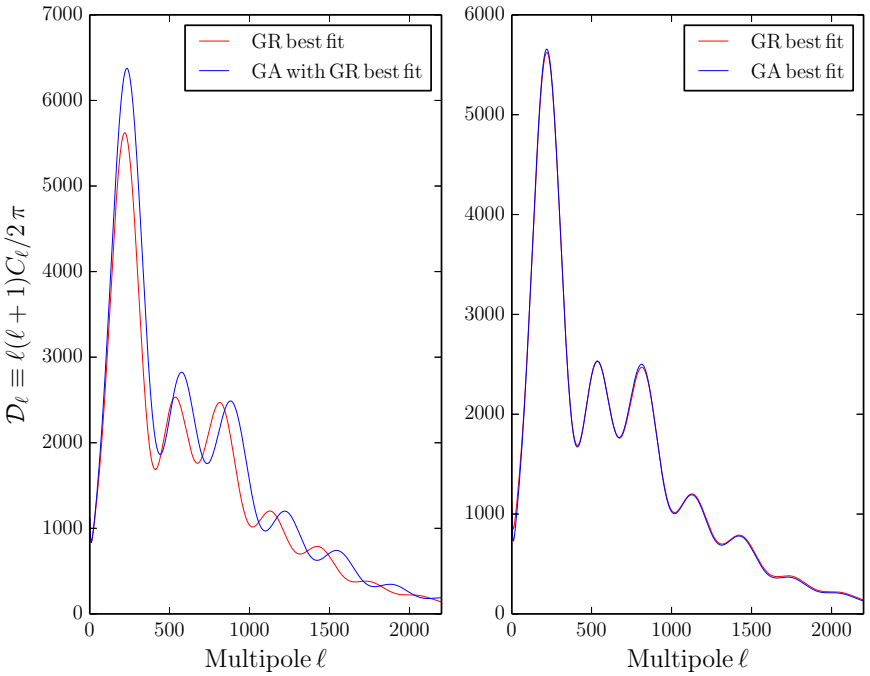

Figure 4.4. Comparing general relativity versus gravitational aether predictions for the CMB power spectrum. The values of the input parameters for the left panel are taken from the *Planck* analysis [1]. The right panel compares the best-fit predictions of the two theories with all cosmological parameters also allowed to vary. GA predicts less power at higher ℓs, as one can see from the right panel (this difference is more evident in the residual plot in Fig. 4.5).

measured by the *Planck* [129] satellite.[12]

2. The 9-year (and final) data release of the *WMAP* satellite CMB temperature and polarization anisotropy power spectra, which we denote as *WMAP*-9 [119] (with "WP" indicating the large angle polarization data only).

3. Three seasons of high resolution CMB temperature anisotropy measurements from the ACT experiment [121].

4. 790 $\deg^2$ of high resolution CMB temperature anisotropy measurements from the

[12] http://pla.esac.esa.int/pla/aio/planckProducts.html

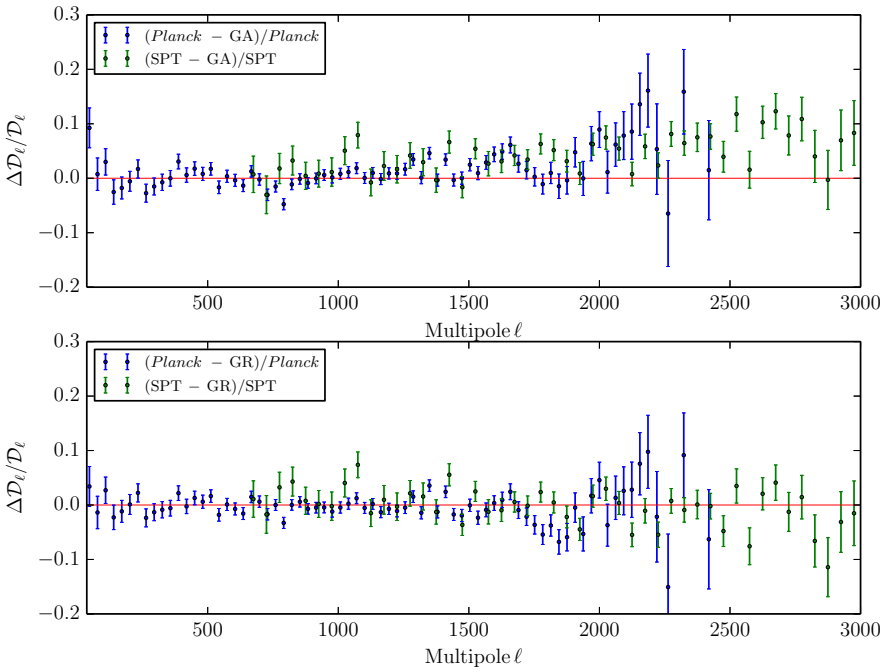

Figure 4.5. Comparing general relativity (bottom panel) and gravitational aether (top panel) predictions for the CMB power spectrum with *Planck* and SPT data sets. Here we plot $\mathcal{D}_\ell \equiv \ell(\ell+1)C_\ell 1/2\pi$ residuals, along with $\pm 1\,\sigma$ error bars, from Refs. [1] and [5]. While the two theories can both fit the lower-ℓ observations, GR fits the data points significantly better than GA for $\ell \gtrsim 1000$, at the $> 4\,\sigma$ level.

SPT experiment [5].

5. Sloan Digital Sky Survey (SDSS) [130] and other estimates of the BAO length scale [131–133].

6. The first claimed detection of the amplitude of primordial gravitational waves, based on B-mode polarization anisotropy band-powers detected by the BICEP2 experiment at degree scales [134].

There are two special cases of particular interest, which are $G_{\rm R} = G_{\rm N}$ (standard General Relativity; $\zeta_4 = 0$) and $G_{\rm R} = \frac{4}{3}G_{\rm N}$ (Gravitational Aether theory; $\zeta_4 = \frac{1}{3}$). If the data are consistent with the $G_{\rm R}/G_{\rm N} = 4/3$ case, or favour this theory over GR, then that would be

Parameter	*WMAP*-9	WP + *Planck*	WP+*Planck*+HighL	WP+*Planck*+BAO
$\Omega_b h^2$	0.0226 ± 0.0005	0.0227 ± 0.0005	0.0225 ± 0.0004	0.0223 ± 0.0003
$\Omega_{DM} h^2$	0.14 ± 0.03	0.128 ± 0.006	0.124 ± 0.005	0.125 ± 0.005
$100\,\theta$	1.038 ± 0.003	1.0421 ± 0.0008	1.0418 ± 0.0007	1.0415 ± 0.0006
τ	0.088 ± 0.014	0.097 ± 0.015	0.096 ± 0.015	0.090 ± 0.013
$\log(10^{10} A_s)$	3.10 ± 0.04	3.11 ± 0.03	3.10 ± 0.03	3.10 ± 0.03
n_s	0.979 ± 0.019	0.987 ± 0.017	0.975 ± 0.014	0.970 ± 0.009
G_N/G_R	0.86 ± 0.18	0.913 ± 0.048	0.951 ± 0.043	0.959 ± 0.035

Table 4.1. Mean likelihood values together with the 68% confidence intervals for the usual six cosmological parameters (see Ref. [1]), together with the GGA parameter G_N/G_R. "WP" refers to *WMAP*-9 polarization, which has been used to constrain the optical depth, τ. "HighL" refers to the higher multipole data sets, ACT and SPT. The PPN parameter, ζ_4 can be obtained through $\zeta_4 = G_R/G_N - 1$.

Parameter	WP+*Planck*+BICEP2	WP+*Planck*+HighL+BICEP2	WP+*Planck*+BAO+BICEP
$\Omega_b h^2$	0.0229 ± 0.0005	0.0228 ± 0.0004	0.0223 ± 0.0003
$\Omega_{DM} h^2$	0.132 ± 0.006	0.128 ± 0.005	0.127 ± 0.005
$100\,\theta$	1.0425 ± 0.0008	1.0422 ± 0.0007	1.0416 ± 0.0006
τ	0.101 ± 0.015	0.101 ± 0.015	0.090 ± 0.013
$\log(10^{10} A_s)$	3.11 ± 0.03	3.11 ± 0.03	3.10 ± 0.03
n_s	1.001 ± 0.016	0.991 ± 0.015	0.976 ± 0.009
r	0.18 ± 0.04	0.18 ± 0.04	0.16 ± 0.03
G_N/G_R	0.871 ± 0.045	0.905 ± 0.040	0.938 ± 0.034

Table 4.2. Mean likelihood values together with the 68% confidence intervals for the usual six cosmological parameters, plus r (the tensor-to-scalar ratio), together with the GGA parameter G_N/G_R. The data are as in Table 4.1, but now including BICEP2 measurements of the B-mode CMB polarization. GR is still favoured over GA if we include HighL CMB or BAO measurements. However, even the conventional seven parameter GR model (that includes r), is disfavoured at around the $3\,\sigma$ level when one considers BICEP2, as well as *Planck*, and HighL data. The PPN parameter, ζ_4 can be obtained through $\zeta_4 = G_R/G_N - 1$.

evidence that GA theory provides a better description of the cosmological data.

From a broader perspective, *any* unequal values for G_N and G_R would be interesting, because this is a way of parameterizing general deviations from the matter-radiation equivalence principle. The MCMC constraints on GGA, excluding the recent BICEP2 data release, are summarized in Table 4.1. It is important to allow the usual cosmological parameters to vary while constraining G_N/G_R. This is because there could be (and indeed are)

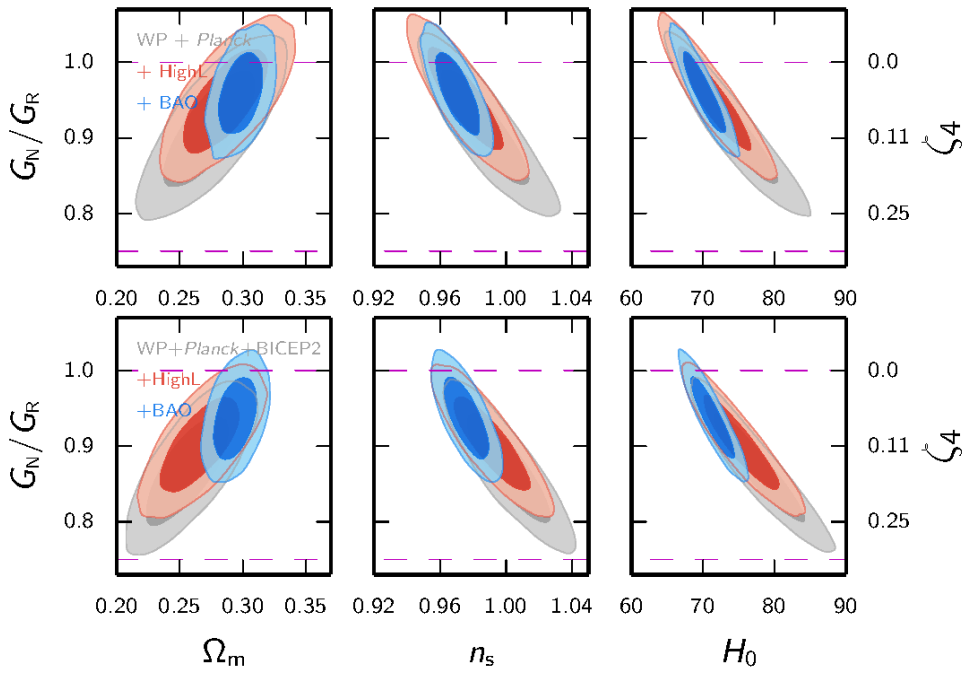

Figure 4.6. Confidence intervals (68% and 95%) for the GGA parameter and the cosmological parameters it is most degenerate with. The ratio G_N/G_R is plotted on the left axes and ζ_4 on the right axes. The horizontal dashed lines indicate the GR (top line) and GA (bottom line) predictions.

degeneracies in the new 7-parameter (or 8-parameter when the tensor-to-scalar ratio r is included) space. Some of these degeneracies between the GGA parameter, G_N/G_R, and the conventional parameters of cosmology are shown in Fig. 4.6.

In fact, we find that if one omits the BICEP2 data, then $G_N/G_R = 1$ provides a good fit and the cosmological parameters hardly shift from their best-fit GR values. On the other hand, adding BICEP2 data shifts the results towards GA by about 1 σ. This may be pointing to some tension in data, or a mild inconsistency between GR and the existing data sets. Of course the most exciting possibility that any such tension is due to missing physics rather than systematic effects. Table 4.2 shows these constraints, while Fig. 4.7 presents a pictorial comparison of constraints on G_N/G_R using different data sets.

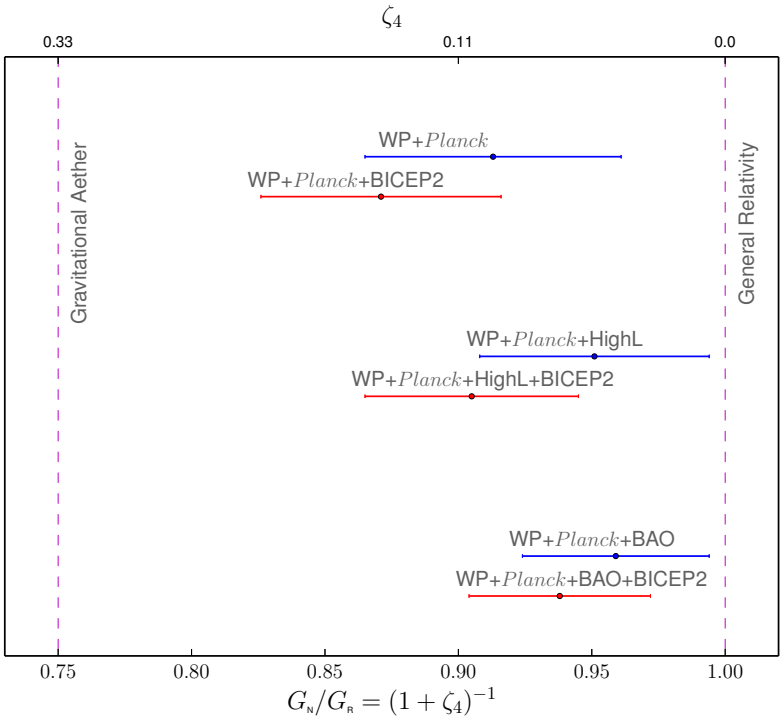

Figure 4.7. A pictorial comparison of marginalized $G_{\rm N}/G_{\rm R} = (1+\zeta_4)^{-1}$ measurements. We have plotted the central values and $\pm 1\,\sigma$ error bars using different data sets. The GR and GA predictions are shown as vertical dashed lines.

4.4 Discussion

As we can see in Fig. 4.7, although GR is generally preferred over GA, different combinations of data sets appear to give constraints for the GGA parameter (or anomalous pressure coupling), which are discrepant by as much as $2\,\sigma$. Perhaps most intriguingly, the combination of *Planck* temperature anisotropies and polarization from *WMAP*-9 and BICEP2 (which represents the state of the art for CMB anisotropy measurements above 0.1°), lies about mid-way between the GA and GR predictions (with a preference for GA, but only at the level of $\Delta\chi^2 \simeq 1$). Nevertheless, the best fit for $G_{\rm N}/G_{\rm R}$ is inconsistent with both GA and GR at 2.7 and $2.9\,\sigma$, respectively. The latter is a manifestation of the well-known tension between the *Planck* upper limit on tensor modes, and the reported detection by BICEP2 (at

least for standard ΛCDM cosmology with a power-law primordial power spectrum).

Let us now try to qualitatively understand what might be responsible for the different trends that we observe when fitting different data sets, as we turn up the GGA parameter. The first step is to obtain the gross structure of the CMB $C_\ell^{\rm TT}$ power spectrum peaks by fixing θ, the ratio of the sound horizon at last scattering, to the distance to the last-scattering surface. For any value of $G_{\rm N}/G_{\rm R}$, this can be done by picking appropriate values of Ω_m and h, which explains the degeneracy directions in Fig. 4.7 for these parameters.

The next step is to recognize the effect of free steaming on the damping tail of the CMB power spectrum. Similar to the effect of free streaming of additional neutrinos, boosting the gravitational effect of neutrinos leads to additional suppression of power at small scales, or high ℓ, in the CMB power spectrum, as we can see in Fig. 4.5. This can be partially compensated for by increasing the spectral index of the scalar perturbations, leading to a bluer primordial spectrum. In fact, we see that combinations of data sets that prefer larger $G_{\rm R}$ (in Tables 4.1–4.2) prefer a near scale-invariant power spectrum, $n_{\rm s} \simeq 1$ (which is up from the value $n_{\rm s} \simeq 0.96$ in GR+ΛCDM).

Finally, a bluer scalar spectral index tends to suppress scalar power for $\ell \lesssim 100$, which then relaxes the upper bound on tensors from the *Planck* temperature power spectrum. This allows a higher value of r than the limit ($r < 0.11$ [1]) found from the temperature anisotropies in ΛCDM.

Of course, none of these degeneracies are perfect. In particular, the additional damping due to free-streaming is much steeper than a power law, which is why even the best-fit GA model underpredicts CMB power for $\ell \gtrsim 1000$ in Fig. 4.5. This is also why adding higher resolution CMB observations (from ACT and SPT), pushes the best fit away from GA. It is possible that adding a positive running for the spectral index might be able to partially cancel the effect, at least for the observable range of multipoles. However, a significant positive running would be hard to justify in simple models of inflation, and may also exacerbate the observational tensions with structure formation on small scales in ΛCDM.

A more stringent constraint on GA (and thus anomalous pressure coupling) comes from

the degeneracy with the Hubble constant, which can also be seen in Fig. 4.6. Additional gravitational coupling to pressure, of the sort required in GA, requires $H_0 > 80\,\mathrm{km\,s^{-1}\,Mpc^{-1}}$, which is larger than even the highest measurements in the current literature (see e.g., figure 16 in Ref. [1]). In particular, BAO geometric constraints place tight bounds of $H_0 \simeq 68$–$72\,\mathrm{km\,s^{-1}\,Mpc^{-1}}$, which is why the inclusion of these data substantially cuts off the smaller values of $G_\mathrm{N}/G_\mathrm{R}$. However, we should note that this inference is based on a simple cosmological constant model for dark energy at low redshifts; more complex descriptions of dark energy, as suggested by some recent BAO [135] or Supernovae Ia [136] studies, could relax these H_0 constraints.

There are certainly hints of possible systematics among the different data sets that could explain some of these tensions. For example, the power spectrum of *WMAP*-9 appears to be about 2.5% higher than *Planck* [1, 137], independent of scale. Additionally, the first 30 or so multipoles appear low (in both *WMAP* and *Planck* data), which, coupled with calibration, can affect the best fit in the damping tail. A perhaps related issue is that the best-fit lensing amplitude in *Planck* and *Planck*+HighL spectra, appears to be around 20% higher than expected in the ΛCDM model [1, 138]. Since lensing moves power from small ℓs to high ℓs, this could also have an indirect effect on the shape of the high-ℓ power spectrum.

Finally, there are legitimate questions about whether BICEP2 analysis [134] has underestimated the effect of instrumental systematics or Galactic foregrounds (e.g., [139]). Decreasing the primordial amplitude of B-modes would reduce the tension with *Planck*, and thus relax the need for anomalous pressure coupling (i.e., $G_\mathrm{N} < G_\mathrm{R}$).

On balance it seems premature to claim that $\zeta_4 > 0$ is required by the current cosmological data. The simple GA theory (with $\zeta_4 = 1/3$) certainly appears disfavoured by the data. However, as the quality of the data continue to improve, it is worth bearing in mind that the GGA picture provides a particular degree of freedom. This should be considered in future fits, particularly with the upcoming release of the *Planck* polarization data.

4.5 Conclusions, and open questions

In this paper, we have closely examined the question of anomalous pressure coupling to gravity in cosmology. This was done in the context of the Generalized Gravitational Aether framework, which allows for an anomalous sourcing of gravity by pressure (ζ_4 in the PPN framework), while not affecting other precision tests of gravity. The idea would mean that the gravitational constant during the radiation era, when $p = \frac{1}{3}\rho$, is boosted to $G_{\rm R} = (1 + \zeta_4)G_{\rm N}$, compared to the gravitational constant for non-relativistic matter $G_{\rm N}$. In particular, the case with $\zeta_4 = 1/3$ or $G_{\rm R} = 4G_{\rm N}/3$, can be used to decouple vacuum energy from gravity, and thus solve the (old) cosmological constant problem.

We have implemented cosmological linear perturbations for this theory into the code `CAMB`, and explored the models that best fit different combinations of cosmological data. The effects are qualitatively similar to introducing additional neutrinos ($N_{\rm eff}$), or dark radiation. Our constraints are summarized in Tables 4.1–4.2 and Figs. 4.6–4.7.

There is clearly some mild tension between different data combinations, but $\zeta_4 = 1/3$ is inconsistent with current observations at around the 2.6-−5 σ level, depending on the combination used. CMB B-mode observations (from BICEP2) push for larger ζ_4, while high resolution CMB or baryonic acoustic oscillations, go in the opposite direction. The best fit is in the range $0.04 \lesssim \zeta_4 \lesssim 0.15$, or $0.87 \lesssim G_{\rm N}/G_{\rm R} \lesssim 0.96$, with statistical errors of a half to third of this range. It may be interesting to notice that even GR ($\zeta_4 = 0$) is disfavoured at 3 σ when we combine lower resolution CMB observations.

To bring some statistical perspective, we should note that even if the gravitational aether solution to the cosmological constant problem is ruled out at 5 σ, the standard GR+ΛCDM paradigm, *with no fine-tuning*, is ruled out at $> 10^{60}\,\sigma$! Therefore, while the first attempt at solving the problem might not have been entirely successful (compared to a model that takes the liberty of fine-tuning the vacuum energy), we argue, that it may be a step in the right direction. So, other than working to improve the quality and consistency of observational data, what can we do to tackle this problem, that quantum fluctuations appear not to gravitate?

From the theoretical standpoint, there are several clear avenues that we have already alluded to:

1. As we discussed in the Introduction, gravitational aether is a classical theory for an effective low energy description of gravity. Therefore, like all effective theories, it has an energy cut-off above which it will not be valid. In fact, the length-scale λ_c (inverse energy scale) associated with this cut-off should be $\lambda_c \sim 0.1$ mm, since a smaller λ_c would not fully solve the cosmological constant problem, while larger λ_c could have been seen in torsion balance tests of gravity (although it is not entirely clear what the signature would be). It is worth noting that the number density of baryons at CMB last scattering is $0.33\,\mathrm{mm}^{-3}$, implying that to calculate T^α_α in Eq. (4.1), it might be necessary to use a microscopic description of atoms interacting with aether, as opposed to the usual mean fluid density picture.[13] If this is the case, then each microscopic particle would carry an aether halo of size about $\sim \lambda_c$; this would appear like a renormalization of particle mass for all macroscopic gravitational effects, but otherwise (like for other vacuum tests of gravity), the theory would be indistinguishable from GR. Nevertheless, in lieu of a quantum theory of gravitational aether, it is not clear how much progress can be made in this direction.

2. Another possibility is to modify the simple ansatz in Eq. (4.2) for the energy-momentum tensor of the gravitational aether, e.g., by introducing a density, ρ'. This might be a reasonable approach if one is also attempting to connect gravitational aether to dark energy (which does have both density and pressure at late times). However, Eq. (4.3) will no longer be sufficient to predict the evolution of the aether, and thus we would need another equation to fix the aether equation of state.

3. In solving for the evolution of aether with respect to dark matter, ω, we have assumed that the two substances were originally comoving, i.e., $\omega = 0$ at early times. However, depending on the process that generates primordial scalar fluctuations in this picture,

[13] The density of dark matter particles is much more model dependent, but is expected to be even less than this baryon value for conventional WIMP models

ω could have also been sourced in the early Universe. So, even though its amplitude decays as a^{-1} on super-horizon scales, depending on its amplitude and spectrum, it can impact CMB observations. This would be akin to introducing isocurvature modes, but for aether perturbations. Although, since ω decays exponentially on sub-horizon scales, this could only affect the CMB at $\ell \lesssim 100$.

4. Finally, we have not included the effect of neutrino mass in our GGA treatment. Massive neutrinos will be qualitatively different from other components, as they start as radiation, which does not couple to aether, but then gradually start sourcing aether as they become non-relativistic. However, this happens relatively late in cosmic history, long after CMB last-scattering, and when neutrinos make up only a small fraction of cosmic density. Therefore, although this would be a useful direction to pursue, we do not expect a significant change from the analyses presented here.

In contrast to unfalsifiable approaches for solving the cosmological constant problem, such as landscape/multiverse ideas with anthropic arguments, the gravitational aether concept has the very distinct advantage of being predictive and hence it can be falsified. Here, we have demonstrated this explicitly, since the basic picture does not appear to fit the current cosmological data. However, like elsewhere in physics, the logical next step would be to learn from this process and propose better physical models (rather than relying on metaphysics). We believe that the GGA approach yields a useful parameterization of a particular degree of freedom in models of modified gravity, and that this idea is worth pursuing further.

Chapter 5

Planck 2015 Results. XIV. Dark Energy and Modified Gravity

5.1 Introduction

The cosmic microwave background (CMB) is a key probe of our cosmological model [2], providing information on the primordial Universe and its physics, including inflationary models [71] and constraints on primordial non-Gaussianities [140]. In this chapter we use the 2015 data release from *Planck*[14] [42] to perform an analysis of $f(R)$ theories and effective field theory approaches to modified gravity.

Observations have long shown that only a small fraction of the total energy density in the Universe (around 5 %) is in the form of baryonic matter, with the dark matter needed for structure formation accounting for about another 26 %. In one scenario the dominant component, generically referred to as dark energy (hereafter DE), brings the total close to the critical density and is responsible for the recent phase of accelerated expansion. In another scenario the accelerated expansion arises, partly or fully, due to a modification of the theory of gravity on cosmological scales. Elucidating the nature of this DE and testing General Relativity (GR) on cosmological scales are major challenges for contemporary cosmology, both on the theoretical and experimental sides [e.g., 141–145].

In preparation for future experimental investigations of DE and modified gravity (here-

[14] Planck (http://www.esa.int/Planck) is a project of the European Space Agency (ESA) with instruments provided by two scientific consortia funded by ESA member states and led by Principal Investigators from France and Italy, telescope reflectors provided through a collaboration between ESA and a scientific consortium led and funded by Denmark, and additional contributions from NASA (USA).

after MG), it is important to determine what we already know about these models at different epochs in redshift and different length scales. CMB anisotropies fix the cosmology at early times, while additional cosmological data sets further constrain on how DE or MG evolve at lower redshifts.

The simplest model for DE is a cosmological constant, Λ, first introduced by Einstein [146] in order to keep the Universe static, but soon dismissed when the Universe was found to be expanding [147, 148]. This constant has been reintroduced several times over the years in attempts to explain several astrophysical phenomena, including most recently the flat spatial geometry implied by the CMB and supernova observations of a recent phase of accelerated expansion [149, 150]. A cosmological constant is described by a single parameter, the inclusion of which brings the model (ΛCDM) into excellent agreement with the data. ΛCDM still represents a good fit to a wide range of observations, more than 20 years after it was introduced. Nonetheless, theoretical estimates for the vacuum density are many orders of magnitude larger than its observed value, as is more thoroughly discussed in Chapter. 4. In addition, Ω_Λ and Ω_m are of the same order of magnitude only at present, which marks our epoch as a special time in the evolution of the Universe (sometimes referred to as the "coincidence problem"). This lack of a clear theoretical understanding has motivated the development of a wide variety of alternative models. Those models which are close to ΛCDM are in broad agreement with current constraints on the background cosmology, but the perturbations may still evolve differently, and hence it is important to test their predictions against CMB data.

There are at least three difficulties in studying modified gravity models. First, there appears to be a vast array of possibilities in the literature and no agreement yet in the scientific community on a comprehensive framework for discussing the landscape of models. A second complication is that robust constraints come from a combination of different data sets working in concert. Hence we have to be careful in the choice of the data sets so that we do not find apparent hints for non-standard models that are in fact due to systematic errors. A third area of concern is the fact that numerical codes available at present for DE and MG are

not as well tested in these scenarios as for ΛCDM, especially given the accuracy reached by the data. Furthermore, in some cases, we need to rely on stability routines that deserve further investigation to assure that they are not excluding more models than required.

Among all the possible options, we consider the effective field theory (EFT) for MG [e.g. 151], which has a clear theoretical motivation, since it includes all theories derived when accounting for all symmetry operators in the Lagrangian, written in unitary gauge, i.e. in terms of metric perturbations only. This is a very general classification that has the advantage of providing a broad overview of (at least) all universally coupled DE models. One advantage of the currently available EFT numerical codes is the theoretical prior it puts on the MG models, as we will discuss further later in this chapter. However, these stability routines are not fully tested and may discard more models than necessary. Another clear disadvantage of this framework is that the number of free parameters is large and the constraints are consequently weak.

As a complementary approach, we focus on $f(R)$ models, since they have already been thoroughly discussed in the literature and are better understood theoretically. This part of the study can partly be considered as applications of the previous case where the CMB constraints are more informative, because there is less freedom in any particular theory than in a generic parameterization.

The CMB is the cleanest probe of large scales, which are of particular interest for modifications to gravity. We will investigate the constraints coming from Planck data in combination with other data sets, addressing strengths and potential weaknesses of different analyses. Before describing in detail the models and data sets that correspond to our requirements, in Sect. 5.2 we first address the main question that motivates this chapter, discussing why CMB is relevant for DE. We then present the specific model parameterizations in Sect. 5.3. We present results in Sect. 5.6 and discuss conclusions in Sect. 5.7.

5.2 Why is the CMB relevant for modified gravity?

The CMB anisotropies are largely generated at the last-scattering epoch, and hence can be used to pin down the theory at early times. In fact many forecasts of future DE or MG experiments are for new data *plus* constraints from Planck. However, there are also several effects that DE and MG models can have on the CMB, some of which are to:

1. change the expansion history and hence distance to the last scattering surface, with a shift in the peaks, sometimes referred to as a geometrical projection effect [152];

2. cause the decay of gravitational potentials at late times, affecting the low-multipole CMB anisotropies through the integrated Sachs-Wolfe (or ISW) effect [153, 154];

3. enhance the cross-correlation between the CMB and large-scale structure, through the ISW effect [155];

4. change the lensing potential, through additional DE perturbations or modifications of GR [156, 157];

5. change the growth of structure [158, 159] leading to a mismatch between the CMB-inferred amplitude of the fluctuations A_s and late-time measurements of σ_8 [160, 161];

6. impact small scales, modifying the damping tail in C_ℓ^{TT}, giving a measurement of the abundance of DE at different redshifts [162, 163];

7. affect the ratio between odd and even peaks if modifications of gravity treat baryons and cold dark matter differently [164];

8. modify the lensing B-mode contribution, through changes in the lensing potential [165];

9. modify the primordial B-mode amplitude and scale dependence, by changing the sound speed of gravitational waves [165, 166].

In this chapter we restrict our analysis to scalar perturbations. The dominant effects on the temperature power spectrum are then due to lensing and the ISW effect, as was discussed in length in chapter 3.

5.3 Models and parameterizations

We now provide an overview of the models addressed in this chapter. Details on the specific parameterization will be discussed in Sect. 5.6, where we also present the results for each specific choice of parameters.

We start by noticing that one can generally follow two different approaches: (1) given a theoretical set up, one can specify the action (or Lagrangian) of the theory and derive background and perturbation equations in that framework; or (2) more phenomenologically, one can construct functions that map closely onto cosmological observables, probing the geometry of spacetime and the growth of perturbations. We discussed this latter option in chapter 3, and will consider the first option in here.

Assuming spatial flatness for simplicity, the geometry is given by the expansion rate H and perturbations to the metric. If we consider only scalar-type components the metric perturbations can be written in terms of the gravitational potentials Φ and Ψ (or equivalently by any two independent combinations of these potentials). Cosmological observations thus constrain one "background" function of time $H(a)$ and two "perturbation" functions of scale and time $\Phi(k, a)$ and $\Psi(k, a)$ (as was discussed earlier and also e.g. in [167]). These functions fix the metric, and thus the Einstein tensor $G_{\mu\nu}$. Einstein's equations link this tensor to the energy-momentum tensor $T_{\mu\nu}$, which in turn can be related to DE or MG properties.

Throughout this chapter we will adopt the metric given by the line element

$$ds^2 = a^2 \left[-(1 + 2\Psi) d\tau^2 + (1 - 2\Phi) dx^2 \right] . \tag{5.1}$$

The gauge invariant potentials Φ and Ψ are related to the Bardeen [36] potentials Φ_A and Φ_H and to the Kodama and Sasaki [35] potentials Ψ_{KS} and Φ_{KS} in the following way:

$\Psi = \Phi_A = \Psi_{KS}$ and $\Phi = -\Phi_H = -\Phi_{KS}$. We use a metric signature $(-,+++)$ and follow the notation of Ma and Bertschinger [168]; the speed of light is set to $c = 1$, except where explicitly stated otherwise.

We define the equation of state $\bar{p}(a) = w(a)\bar{\rho}(a)$, where $\bar{p}$ and $\bar{\rho}$ are the average pressure and energy density. The sound speed c_s is defined in the fluid rest frame in terms of pressure and density perturbations as $\delta p(k,a) = c_s^2(k,a)\delta\rho(k,a)$. The anisotropic stress $\sigma(k,a)$ is the scalar part of the off-diagonal space-space stress energy tensor perturbation. The set of functions $\{H, \Phi, \Psi\}$ describing the metric is formally equivalent to the set of functions $\{w, c_s^2, \sigma\}$ [169].

Specific theories typically cover only subsets of this function space and thus make specific predictions for their form. In the following sections we will discuss the particular theories that we consider in this chapter.

5.4 Modified gravity and effective field theory

Modified gravity models (in which gravity is modified with respect to GR) in general affect both the background and the perturbation equations. In this section we lay out the foundations of the EFT theory approach to modified gravity.

This approach starts from a Lagrangian, derived from an effective field theory (EFT) expansion [170], discussed in [151] in the context of MG. Specifically, EFT describes the space of (universally coupled) scalar field theories, with a Lagrangian written in unitary gauge that preserves isotropy and homogeneity at the background level, assumes the weak equivalence principle, and has only one extra dynamical field besides the matter fields con-

ventionally considered in cosmology. The action reads:

$$
\begin{aligned}
S \quad = \quad & \int d^4x\sqrt{-g}\left\{\frac{m_0^2}{2}\left[1+\Omega(\tau)\right]R+\Lambda(\tau)-a^2c(\tau)\delta g^{00}+\frac{M_2^4(\tau)}{2}\left(a^2\delta g^{00}\right)^2\right. \\
& -\bar{M}_1^3(\tau)2a^2\delta g^{00}\delta K_\mu^\mu-\frac{\bar{M}_2^2(\tau)}{2}\left(\delta K_\mu^\mu\right)^2-\frac{\bar{M}_3^2(\tau)}{2}\delta K_\nu^\mu\delta K_\mu^\nu+\frac{a^2\hat{M}^2(\tau)}{2}\delta g^{00}\delta R^{(3)} \\
& \left.+m_2^2(\tau)\left(g^{\mu\nu}+n^\mu n^\nu\right)\partial_\mu\left(a^2g^{00}\right)\partial_\nu\left(a^2g^{00}\right)\right\}+S_{\rm m}[\chi_i,g_{\mu\nu}]. \qquad (5.2)
\end{aligned}
$$

Here R is the Ricci scalar, $\delta R^{(3)}$ is its spatial perturbation, K_ν^μ is the extrinsic curvature, and m_0 is the bare (reduced) Planck mass. The matter part of the action, $S_{\rm m}$, includes all fluid components except dark energy, i.e., baryons, cold dark matter, radiation, and neutrinos. The action in Eq. (5.2) depends on nine time-dependent functions [171], here $\{\Omega, c, \Lambda, \bar{M}_1^3, \bar{M}_2^4, \bar{M}_3^2, M_2^4, \hat{M}^2, m_2^2\}$, whose choice specifies the theory. In this way, EFT provides a direct link to any scalar field theory. A particular subset of EFT theories are the Horndeski [68] models, which include (almost) all stable scalar-tensor theories, universally coupled to gravity, with second-order equations of motion in the fields, and depend on five functions of time [172, 173].

Although the EFT approach has the advantage of being very versatile, in practice it is necessary to choose suitable parameterizations for the free functions listed above, in order to compare the action with the data. We will describe our specific choices, together with results for each of them, in the next section.

5.5 Data

We now discuss the data sets we use, both from *Planck* and in combination with other experiments. We should notice that if we combine many different data sets (not all of which will be equally reliable) and take them all at face value, we risk attributing systematic problems between data sets to genuine physical effects in modified gravity models. On the other hand, we need to avoid bias in confirming ΛCDM, and remain open to the possibility that some tensions may be providing hints that point towards a genuine deviation from the

model. While discussing results in Sect. 5.6, we will try to assess the impact of additional data sets, separating them from the *Planck* baseline choice, keeping in mind caveats that might appear when considering some of them.

5.5.1 *Planck* data sets

Planck low-ℓ data

This data set consists of the foreground-cleaned *Planck* LFI 70 GHz polarization maps which are processed together with the temperature map. This likelihood is pixel-based, extends up to multipoles $\ell = 29$ and masks the polarization maps with a specific polarization mask, which uses 46 % of the sky. Use of this likelihood is denoted as "lowP" hereafter.

Planck high-ℓ data

Following [174], the high-ℓ part of the likelihood ($30 < \ell < 2500$) uses a Gaussian approximation,

$$-\log\mathcal{L}(\hat{C}|C(\theta)) = \frac{1}{2}(\hat{C} - C(\theta))^{\mathrm{T}} \cdot \mathbf{C}^{-1} \cdot (\hat{C} - C(\theta)) + \text{const.}\,, \tag{5.3}$$

with $\hat{C}$ the data vector, $C(\theta)$ the model with parameters θ and $\mathbf{C}$ the covariance matrix. The data vector consists of the temperature power spectra of the best CMB frequencies of the HFI instrument. Specifically, as discussed in [175], we use 100 GHz, 143 GHz and 217 GHz half-mission cross-spectra, measured on the cleanest part of the sky, avoiding the Galactic plane.

Planck CMB lensing

Gravitational lensing by large-scale structure introduces dependencies in CMB observables on the late-time geometry and clustering, which otherwise would be degenerate in the primary anisotropies [176, 177]. This provides some sensitivity to dark energy and late-time modifications of gravity from the CMB alone. The source plane for CMB lensing is the

last-scattering surface, so the peak sensitivity is to lenses at $z \approx 2$ (i.e., half-way to the last-scattering surface) with typical sizes of order 10^2 Mpc. Although this peak lensing redshift is rather high for constraining simple late-time dark energy models, CMB lensing deflections at angular multipoles $\ell \lesssim 60$ have sources extending to low enough redshift that DE becomes dynamically important (e.g., Pan et al. 178).

The main observable effects of CMB lensing are a smoothing of the acoustic peaks and troughs in the temperature and polarization power spectra, the generation of significant non-Gaussianity in the form of a non-zero connected 4-point function, and the conversion of E-mode to B-mode polarization. The smoothing effect on the power spectra is included routinely in all results in this paper. We additionally include measurements of the power spectrum $C_\ell^{\phi\phi}$ of the CMB lensing potential ϕ, which are extracted from the *Planck* temperature and polarization 4-point functions, as presented in Planck Collaboration XV [179].

The construction of the CMB lensing likelihood we use in this chapter is described fully in Planck Collaboration XV [179]; see also Planck Collaboration XIII [2]. It is a simple Gaussian approximation in the estimated $C_\ell^{\phi\phi}$ bandpowers, covering the multipole range $40 \leq \ell \leq 400$. The $C_\ell^{\phi\phi}$ are estimated from the full-mission temperature and polarization 4-point functions, using the the component-separated maps [180] over approximately 70 % of the sky.

Planck CMB polarization

The TE and EE likelihood follows the same principle as the TT likelihood described in Sect. 5.5.1. The data vector is extended to contain the TE and EE cross-half-mission power spectra of the same 100 GHz, 143 GHz, and 217 GHz frequency maps. Following [181], the regions where the dust intensity is important are masked, and 70 %, 50 %, and 41 % of the sky is retained for the three frequencies.

5.5.2 Background data combination

We identify a first basic combination of data sets that we mostly rely on, for which we have a high confidence that systematics are under control. Throughout this paper, we indicate for simplicity with "BSH" the combination BAO + SN-Ia + H_0, which we now discuss in detail.

Baryon acoustic oscillations

The BAO data can be used to measure both the angular diameter distance $D_{\rm A}(z)$, and the expansion rate of the Universe $H(z)$ either separately or through the combination

$$D_{\rm V}(z) = \left[(1+z)^2 D_{\rm A}^2(z)\frac{cz}{H(z)}\right]^{1/3}. \tag{5.4}$$

In this chapter we use the SDSS Main Galaxy Sample at $z_{\rm eff} = 0.15$ [182]; the Baryon Oscillation Spectroscopic Survey (BOSS) "LOWZ" sample at $z_{\rm eff} = 0.32$ [183]; the BOSS CMASS (i.e. "constant mass" sample) at $z_{\rm eff} = 0.57$ of Anderson et al. [183]; and the six-degree-Field Galaxy survey (6dFGS) at $z_{\rm eff} = 0.106$ [184]. The first two measurements are based on peculiar velocity field reconstructions to sharpen the BAO feature and reduce the errors on the quantity $D_{\rm V}/r_{\rm s}$; the analysis in Anderson et al. [183] provides constraints on both $D_A(z_{\rm eff})$ and $H(z_{\rm eff})$. In all cases considered here the BAO observations are modelled as distance ratios, and therefore provide no direct measurement of H_0. However, they provide a link between the expansion rate at low redshift and the constraints placed by *Planck* at $z \approx 1100$.

Supernovae

Type-Ia supernovae (SNe) are among the most important probes of expansion and historically led to the general acceptance that a DE component is needed [150, 185]. Supernovae are considered as "standardizable candles" and so provide a measurement of the luminosity distance as a function of redshift. However, the absolute luminosity of SNe is considered

uncertain and is marginalized out, which also removes any constraints on H_0.

Consistently with [2], we use here the analysis by Betoule et al. [186] of the "Joint Light-curve Analysis" (JLA) sample. JLA is constructed from the SNLS and SDSS SNe data, together with several samples of low redshift SNe. Cosmological constraints from the JLA sample are discussed by Betoule et al. [187], and as mentioned in [2] the constraints are consistent with the 2013 and 2104 *Planck* values for standard ΛCDM.

The Hubble constant

The CMB measures mostly physics at the epoch of recombination, and so provides only weak direct constraints about low-redshift quantities through the integrated Sachs-Wolfe effect and CMB lensing. The CMB-inferred constraints on the local expansion rate H_0 are model dependent, and this makes the comparison to direct measurements interesting, since any mismatch could be evidence of new physics.

Here, we rely on the re-analysis of the Riess et al. [22] Cepheid data made by Efstathiou [23]. By using a revised geometric maser distance to NGC 4258 from Humphreys et al. [188], Ref. [23] obtains the following value for the Hubble constant:

$$H_0 = (70.6 \pm 3.3)\,\mathrm{km\,s^{-1}\,Mpc^{-1}}, \tag{5.5}$$

which is within $1\,\sigma$ of the *Planck* TT+lowP estimate.

5.5.3 Perturbation data sets

The additional freedom present in MG models can be calibrated using external data that test perturbations in particular. In the following we describe other available data sets that we included in the grid of runs for this chapter.

Redshift space distortions (RSD)

Observations of the anisotropic clustering of galaxies in redshift space permit the measurement of their peculiar velocities, which are related to the Newtonian potential Ψ via the Euler equation. This, in turn, allows us to break a degeneracy with gravitational lensing that is sensitive to the combination $\Phi + \Psi$. Galaxy redshift surveys now provide very precise constraints on redshift-space clustering. The difficulty in using these data is that much of the signal currently comes from scales where nonlinear effects and galaxy bias are significant and must be accurately modelled [see, e.g., the discussions in 189, 190].

In linear theory, anisotropic clustering along the line of sight and in the transverse directions measures the combination $f(z)\sigma_8(z)$, where the growth rate is defined by

$$f(z) = \frac{\mathrm{d}\ln\sigma_8}{\mathrm{d}\ln a}\,. \tag{5.6}$$

Anisotropic clustering also contains geometric information from the Alcock-Paczynski effect [191], which is sensitive to

$$F_{\mathrm{AP}}(z) = (1+z)D_{\mathrm{A}}(z)H(z)\,. \tag{5.7}$$

In addition, fits which constrain RSD frequently also measure the BAO scale, $D_V(z)/r_{\mathrm{s}}$, where r_{s} is the comoving sound horizon at the drag epoch, and D_V is given in Eq. (5.4).

The Baryon Oscillation Spectroscopic Survey (BOSS) collaboration have measured the power spectrum of their CMASS galaxy sample [192] in the range $k = 0.01$–$0.20\,\mathrm{h\,Mpc^{-1}}$. Samushia et al. [51] have estimated the multipole moments of the redshift-space correlation function of CMASS galaxies on scales $> 25\,\mathrm{h^{-1}Mpc}$. Both papers provide tight constraints on the quantity $f\sigma_8$, and the constraints are consistent. The Samushia et al. [51] result was shown to behave marginally better in terms of small-scale bias compared to mock simulations, so we choose to adopt this as our baseline result.

Galaxy weak lensing

The distortion of the shapes of distant galaxies by large-scale structure along the line of sight (weak gravitational lensing or cosmic shear) is particularly important for constraining DE and MG, due to its dependence on the growth of fluctuations and the two scalar metric potentials.

Currently the largest weak lensing (WL) survey is the Canada France Hawaii Telescope Lensing Survey (CFHTLenS), and we make use of this data set in our analysis.

5.6 Results

We now proceed by illustrating in more detail the model and parameterization described in Sect. 5.3, through presenting results for a specific subset of them. In Sect. 5.6.1 we study the constraints on the presence of non-negligible dark energy perturbations, in the context of general modified gravity models described through effective field theories. The last part, Sect. 5.6.3, illustrates results for a range of particular examples often considered in the literature.

5.6.1 Perturbation parameterizations

General modifications of gravity change both the background and the perturbation equations, allowing for contribution to clustering and anisotropic stress. Here we discuss results for EFT cosmologies, with a "top-down" approach that starts from the most general action allowed by symmetry and then selects from there interesting classes belonging to the so-called "Horndeski models", which, as mentioned in Sect. 5.4, include almost all stable scalar-tensor theories, universally coupled, with second-order equations of motion in the fields.

The full background and perturbation equations of the action 5.2 have been derived in [193]. The implementation of the equations in the publicly available Boltzmann code

EFTCAMB is also discussed in [194][15]. We will briefly explain the role of the nine parameters that appear in action 5.2 in this section. From the set of the nine parameters, $\{\Omega, c, \Lambda, \bar{M}_1^3, \bar{M}_2^4, \bar{M}_3^2, M_2^4, \hat{M}^2, m_2^2\}$, three are in charge of the background evolution. Since the EFT Lagrangian preserves homogeneity and isotropy at the background level, the only extra physical degree of freedom at the background is the sound speed of an extra fluid. Therefore, from the three functions $\{\Omega, c, \Lambda\}$ that are in charge of the background evolution, only one is an independent function. Given an expansion history (which we fix to be ΛCDM, i.e., effectively $w = -1$) and an EFT function $\Omega(a)$, EFTCAMB computes c and Λ from the Friedmann equations and the assumption of spatial flatness [195]. In addition, EFTCAMB uses a set of stability criteria in order to specify whether a given model is stable and ghost-free, i.e. without negative energy density for the new degrees of freedom. This will automatically place a theoretical prior on the parameter space while performing the MCMC analysis.

The remaining six functions, $\bar{M}_1^3, \bar{M}_2^4, \bar{M}_3^2, M_2^4, \hat{M}^2, m_2^2$, are internally redefined in terms of the dimensionless parameters α_i with i running from 1 to 6:

$$\alpha_1^4 = \frac{M_2^4}{m_0^2 H_0^2}, \qquad \alpha_2^3 = \frac{\bar{M}_1^3}{m_0^2 H_0}, \qquad \alpha_3^2 = \frac{\bar{M}_2^2}{m_0^2},$$
$$\alpha_4^2 = \frac{\bar{M}_3^2}{m_0^2}, \qquad \alpha_5^2 = \frac{\hat{M}^2}{m_0^2}, \qquad \alpha_6^2 = \frac{m_2^2}{m_0^2}.$$

We should notice that unlike the PPF formalism discussed in chapter 3, all of these nine functions are 1-dimensional functions of the scale factor, as opposed to the 2-dimensional functions of PPF.

[15] http://www.lorentz.leidenuniv.nl/~hu/codes/, version 1.1, Oct. 2014.

5.6.2 Modified gravity: EFT and Horndeski models

We will always demand that

$$m_2^2 = 0 \text{ (or equivalently } \alpha_6^2 = 0), \tag{5.8}$$

$$\bar{M}_3^2 = -\bar{M}_2^2 \text{ (or equivalently } \alpha_4^2 = -\alpha_3^2), \tag{5.9}$$

which eliminates models containing higher-order spatial derivatives [172]. In this case the nine functions of time discussed above reduce to a minimal set of five functions of time that can be labelled $\{\alpha_{\rm M}, \alpha_{\rm K}, \alpha_{\rm B}, \alpha_{\rm T}, \alpha_{\rm H}\}$, in addition to the Planck mass M_*^2 (the evolution of which is determined by H and α_M), and an additional function of time describing the background evolution, e.g., $H(a)$. The former are related to the EFT functions via the following relations [172]:

$$M_*^2 = m_0^2\Omega + \bar{M}_2^2; \tag{5.10}$$

$$M_*^2 H \alpha_{\rm M} = m_0^2\dot{\Omega} + \dot{\bar{M}}_2^2; \tag{5.11}$$

$$M_*^2 H^2 \alpha_{\rm K} = 2c + 4M_2^4; \tag{5.12}$$

$$M_*^2 H \alpha_{\rm B} = -m_0^2\dot{\Omega} - \bar{M}_1^3; \tag{5.13}$$

$$M_*^2 \alpha_{\rm T} = -\bar{M}_2^2; \tag{5.14}$$

$$M_*^2 \alpha_{\rm H} = 2\hat{M}^2 - \bar{M}_2^2. \tag{5.15}$$

These five α functions are closer to a physical description of the theories under investigation. For example: α_T enters in the equation for gravitational waves, affecting their speed and the position of the primordial peak in B-mode polarization; α_M affects the lensing potential, but also the amplitude of the primordial polarization peak in B-modes [165, 166, 196]. It is then possible to relate the desired choice for the Horndeski variables

to an appropriate choice of the EFT functions,

$$\partial_\tau(M_*^2) = \mathcal{H}M_*^2\alpha_{\rm M}, \tag{5.16}$$

$$m_0^2(\Omega+1) = (1+\alpha_{\rm T})M_*^2, \tag{5.17}$$

$$\bar{M}_2^2 = -\alpha_{\rm T}M_*^2, \tag{5.18}$$

$$4M_2^4 = M_*^2\mathcal{H}^2\alpha_{\rm K} - 2c, \tag{5.19}$$

$$\bar{M}_1^3 = -M_*^2\mathcal{H}\alpha_{\rm B} + m_0^2\dot{\Omega}, \tag{5.20}$$

$$2\hat{M}^2 = M_*^2(\alpha_{\rm H} - \alpha_{\rm T}), \tag{5.21}$$

where $\mathcal{H}$ is the conformal Hubble function, m_0 the bare Planck mass and M_* the effective Plank mass. Fixing $\alpha_{\rm M}$ corresponds to fixing M_* through Eq. (5.16). Once $\alpha_{\rm T}$ has been chosen, Ω is obtained from Eq. (5.17). Finally, $\alpha_{\rm B}$ determines $\bar{M}_1^3$ via Eq. (5.20), while the choice of $\alpha_{\rm H}$ fixes $\hat{M}^2$ via Eq. (5.21). In this way, our choice of the EFT functions can be guided by the selection of different "physical" scenarios, corresponding to turning on different Horndeski functions.

To avoid possible consistency issues with higher derivatives, we set[16] $\bar{M}_3^2 = \bar{M}_2^2 = 0$ in order to satisfy Eq. (5.9). From Eq. (5.18) and Eq. (5.10) this implies $\alpha_{\rm T} = 0$, so that tensor waves move with the speed of light. In addition, we set $\alpha_{\rm H} = 0$ so as to remain in the original class of Horndeski theories, avoiding operators that may give rise to higher-order time derivatives [197]. As a consequence, $\hat{M}^2 = 0$ from Eq. (5.21) and $M_*^2 = m_0^2(1+\Omega)$ from Eq. (5.10). For simplicity we also turn off all other higher-order EFT operators and set $\bar{M}_1^3 = M_2^4 = 0$. Comparing Eq. (5.11) and Eq. (5.20), this implies $\alpha_{\rm B} = -\alpha_{\rm M}$.

In summary, in the following we consider Horndeski models in which $\alpha_{\rm M} = -\alpha_{\rm B}$, $\alpha_{\rm K}$ is fixed by Eq. (5.13), with $M_2 = 0$ as a function of c and $\alpha_{\rm T} = \alpha_{\rm H} = 0$.

The only free function in this case is $\alpha_{\rm M}$, which is linked to Ω through:

$$\alpha_M = \frac{a}{\Omega+1}\frac{{\rm d}\Omega}{{\rm d}a}\,. \tag{5.22}$$

[16] Because of the way `EFTCAMB` currently implements these equations internally, it is not possible to satisfy Eq. (5.9) otherwise.

By choosing a non-zero $\alpha_{\rm M}$ (and therefore a time evolving Ω) we introduce a non-minimal coupling in the action (see Eq. 5.2), which will lead to non-zero anisotropic stress and to modifications of the lensing potential, typical signatures of MG models. Here we will use a scaling ansatz, $\alpha_{\rm M} = \alpha_{\rm M0} a^{\beta}$, where $\alpha_{\rm M0}$ is the value of $\alpha_{\rm M}$ today, and $\beta > 0$ determines how quickly the modification of gravity decreases in the past.

Integrating Eq. (5.22) we obtain

$$\Omega(a) = \exp\left\{\frac{\alpha_{\rm M0}}{\beta} a^{\beta}\right\} - 1, \tag{5.23}$$

which coincides with the built-in exponential model of `EFTCAMB` for $\Omega_0 = \alpha_{\rm M0}/\beta$. The marginalized posterior distributions for the two parameters Ω_0 and β are plotted in Fig. 5.1 for different combinations of data. For $\alpha_{\rm M0} = 0$ we recover ΛCDM. For small values of Ω_0 and for $\beta = 1$, the exponential reduces to the built-in linear evolution in `EFTCAMB`,

$$\Omega(a) = \Omega_0\, a\,. \tag{5.24}$$

The results of the MCMC analysis are shown in Table 5.1. For both the exponential and the linear model we use a flat prior $\Omega_0 \in [0, 1]$. For the scaling exponent β of the exponential model we use a flat prior $\beta \in (0, 3]$. For $\beta \to 0$ the MG parameter α_M remains constant and does not go to zero in the early Universe, while for $\beta = 3$ the scaling would correspond to M functions in the action (5.2) which are of the same order as the relative energy density between DE and the dark matter background, similar to the suggestion in [172]. An important feature visible in Fig. 5.1 is the sharp cutoff at $\beta \approx 1.5$. This cutoff is due to "viability conditions" that are enforced by `EFTCAMB` and that reject models due to a set of theoretical criteria (see [195] for a full list of theoretical priors implemented in `EFTCAMB`). Disabling some of these conditions allows to extend the acceptable model space to larger β, and we find that the constraints on α_{M0} continue to weaken as β grows further, extending Fig. 5.1 in the obvious way. We prefer however to use here the current public `EFTCAMB` version without modifications. A better understanding of whether all stability conditions

implemented in the code are really necessary or exclude a larger region than necessary in parameter space will have to be addressed in the future. The posterior distribution of the linear evolution for Ω is shown in Fig. 5.2 and is compatible with ΛCDM. Finally, it is interesting to note that in both the exponential and the linear expansion, the inclusion of galaxy weak lensing (WL) data set weakens constraints with respect to Planck alone. This is due to the fact that in these EFT theories, WL and Planck are in tension with each other, WL preferring higher values of the expansion rate with respect to Planck.

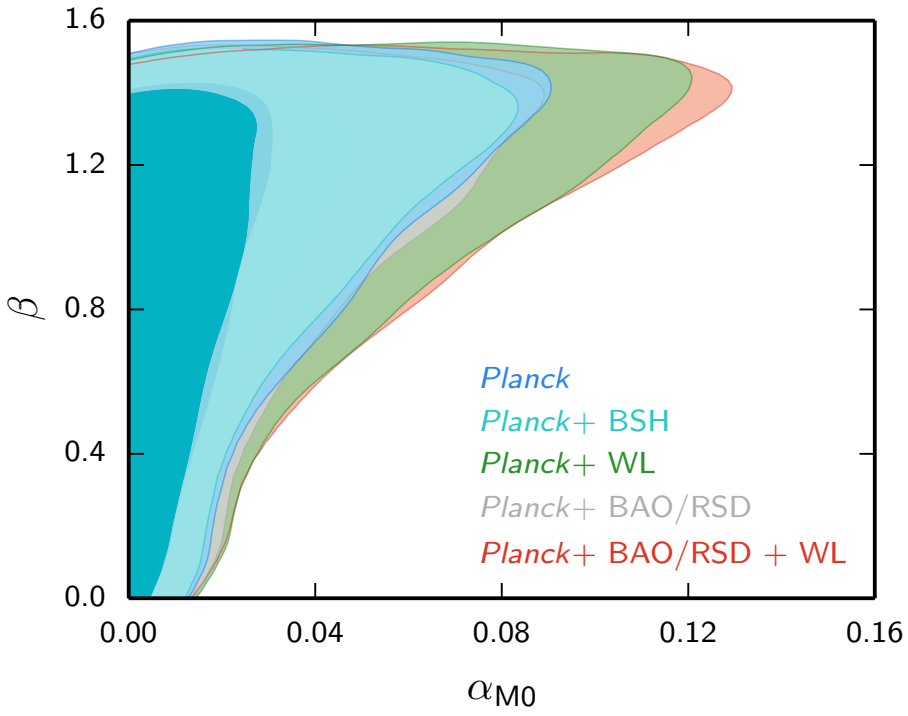

Figure 5.1. Marginalized posterior distributions at 68 % and 95 % C.L. for the two parameters $\alpha_{\rm M0}$ and β of the exponential evolution, $\Omega(a) = \exp(\Omega_0\, a^\beta) - 1.0$, see Sect. 5.6.2. Here $\alpha_{\rm M0}$ is defined as $\Omega_0\beta$ and the background is fixed to ΛCDM. $\alpha_{\rm M0} = 0$ corresponds to the ΛCDM model also at perturbation level. Note that Planck means *Planck* TT+lowP. Adding WL to the data sets results in broader contours, as a consequence of the slight tension between the Planck and WL data sets.

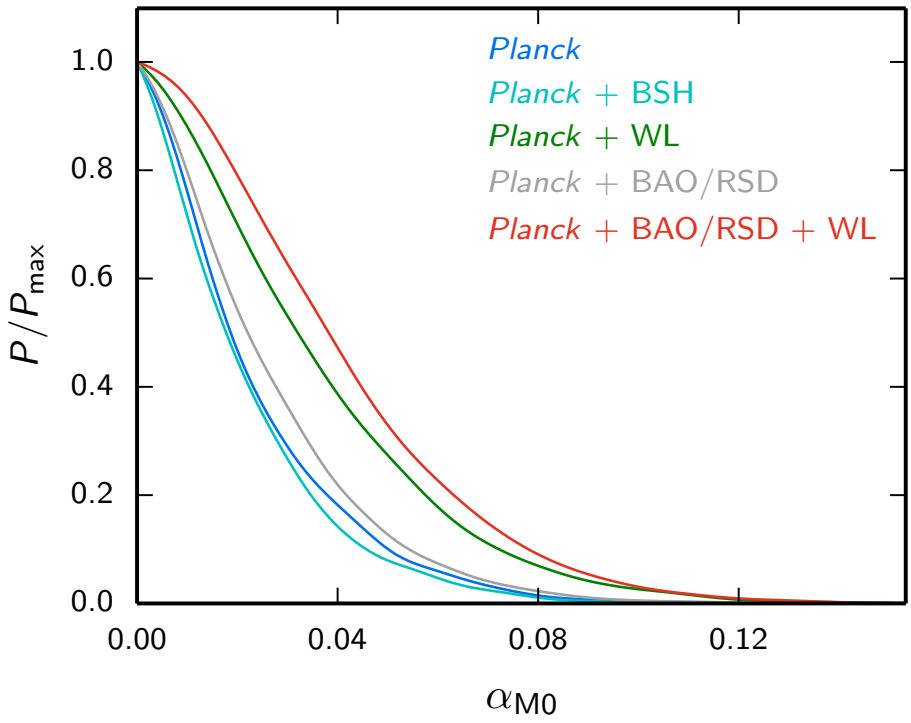

Figure 5.2. Marginalized posterior distribution of the linear EFT model background parameter, Ω, with Ω parameterized as a linear function of the scale factor, i.e., $\Omega(a) = \alpha_{\rm M0}\, a$, see Sect. 5.6.2. The equation of state parameter $w_{\rm de}$ is fixed to -1, and therefore, $\Omega_0 = 0$ will correspond to the ΛCDM model. Here Planck means *Planck* TT+lowP. Adding CMB lensing to the data sets does not change the results significantly; high-ℓ polarization tightens the constraints by a few percent, as shown in Tab. 5.1.

5.6.3 Further examples of particular models

Quite generally, DE and MG theories deal with at least one extra degree of freedom that can usually be associated with a scalar field. For 'standard' DE theories the scalar field couples minimally to gravity, while in MG theories the field can be seen as the mediator of a fifth force in addition to standard interactions. This happens in scalar-tensor theories (including $f(R)$ cosmologies), massive gravity, and all coupled DE models, both when matter is involved or when neutrino evolution is affected. Interactions and fifth forces are there-

Parameter	TT+lowP+BSH	TT+lowP+WL	TT+lowP+BAO/RSD	TT+lowP+BAO/RSD+WL	TT,TE,EE
Linear EFT					
α_{M0}	< 0.052(95 %CL)	< 0.072(95 %CL)	< 0.057(95 %CL)	< 0.074(95 %CL)	< 0.050(95 %CL)
H_0	67.69 ± 0.55	67.75 ± 0.95	67.63 ± 0.63	67.89 ± 0.62	67.17 ± 0.66
σ_8	0.826 ± 0.015	0.818 ± 0.014	0.822 ± 0.014	0.814 ± 0.014	0.830 ± 0.013
Exponential EFT					
α_{M0}	< 0.071(95 %CL)	< 0.098(95 %CL)	< 0.071(95 %CL)	< 0.094(95 %CL)	< 0.056(95 %CL)
β	$0.90^{+0.55}_{-0.25}$	$0.91^{+0.55}_{-0.25}$	$0.88^{+0.55}_{-0.27}$	$0.89^{+0.55}_{-0.27}$	$0.88^{+0.56}_{-0.27}$
H_0	67.70 ± 0.56	67.78 ± 0.96	67.60 ± 0.62	67.87 ± 0.63	67.15 ± 0.65
σ_8	0.826 ± 0.015	0.817 ± 0.014	0.821 ± 0.014	0.814 ± 0.014	0.830 ± 0.013

Table 5.1. Marginalized mean values and 68 % CL intervals for the EFT parameters, both in the linear model, α_{M0}, and in the exponential one, $\{\alpha_{M0}, \beta\}$ (see Sect. 5.6.2) Adding CMB lensing does not improve the constraints, while small-scale polarization can more strongly constraint α_{M0}.

fore a common characteristic of many proposed models, the difference being whether the interaction is universal (i.e., affecting all species with the same coupling, as in scalar-tensor theories) or is different for each species (as in coupled DE, [198, 199] or growing neutrino models, [200, 201]). In the following we will test one of the well known examples of these models, namely $f(R)$ theories.

Universal couplings: $f(R)$ cosmologies

A well-investigated class of MG models is constituted by the $f(R)$ theories that modify the Einstein-Hilbert action by substituting the Ricci scalar with a more general function of itself:

$$S = \frac{1}{2\kappa^2}\int d^4x\,\sqrt{-g}(R + f(R)) + \int d^4x\mathcal{L}_M(\chi_i, g_{\mu\nu}), \tag{5.25}$$

where $\kappa^2 = 8\pi G$. $f(R)$ cosmologies can be mapped to a subclass of scalar-tensor theories, where the coupling of the scalar field to the matter fields is universal.

For a fixed background, the Friedmann equation provides a second-order differential equation for $f(R(a))$ [see e.g., 202, 203]:

$$\mathcal{H}^2 - (\mathcal{H}\mathcal{H}')f_R + \frac{1}{6}f\,a^2 + \mathcal{H}^2 f_{RR}R' = \frac{8\,\pi\,G\rho\,a^2}{3}. \tag{5.26}$$

Here a prime denotes a derivative with respect to $\ln(a)$. One of the initial conditions is usually set by requiring

$$\lim_{R\to\infty} \frac{f(R)}{R} = 0, \tag{5.27}$$

and the other initial (or boundary condition), usually called B_0, is the present value of

$$B(z) = \frac{f_{RR}}{1 + f_R} \frac{H\dot{R}}{\dot{H} - H^2}. \tag{5.28}$$

Here, f_R and f_{RR} are the first and second derivatives of $f(R)$, and a dot means a derivative with respect to conformal time. $B(z) = 0$ corresponds to $f(R) \propto (R+ \textit{const.})$, i.e. GR plus a cosmological constant, after a rescaling of the gravitational constant. Higher values of B_0 hint towards a GR modification. They tend to suppress power at large scales in the CMB power spectrum, due to a modified ISW effect, and increase the amplitude of the CMB lensing potential, resulting in slightly smoother peaks at higher ℓs [204–207].

It is possible to restrict `EFTcamb` to describe $f(R)$-cosmologies. Given an evolution history for the scale factor and the value of B_0, `EFTcamb` effectively solves the Friedmann equation for $f(R)$. It then uses this function at the perturbation level to evolve the metric potentials and matter fields. The merit of `EFTcamb` over the other available similar codes is that it checks the model against some stability criteria and does not assume the quasi-static regime, where the scales of interest are still linear but smaller than the horizon and the time derivatives are ignored.

As shown in Fig. 5.3, there is a degeneracy between the optical depth, τ, and the $f(R)$ parameter, B_0. Adding any structure formation probe, such as WL, redshift space (RSD) or CMB lensing, breaks the degeneracy. Figure 5.4 shows the likelihood of the B_0 parameter using `EFTcamb`, where a ΛCDM background evolution is assumed, i.e., $w_{\rm DE} = -1$.

As the different data sets provide constraints on B_0 that vary by more than four orders of magnitude, we show plots for $\log_{10} B_0$; to make these figures we use a uniform prior in $\log_{10} B_0$ to avoid distorting the posterior due to prior effects. However, for the limits quoted in the tables we use B_0 (without log) as the fundamental quantity and quote 95 % limits

based on B_0. In this way the upper limit on B_0 is effectively given by the location of the drop in probability visible in the figures, but not influenced by the choice of a lower limit of $\log_{10} B_0$. Overall this appears to be the best compromise to present the constraints on the B_0 parameter. In the plots, the GR value ($B_0 = 0$) is reached by a plateau stretching towards minus infinity.

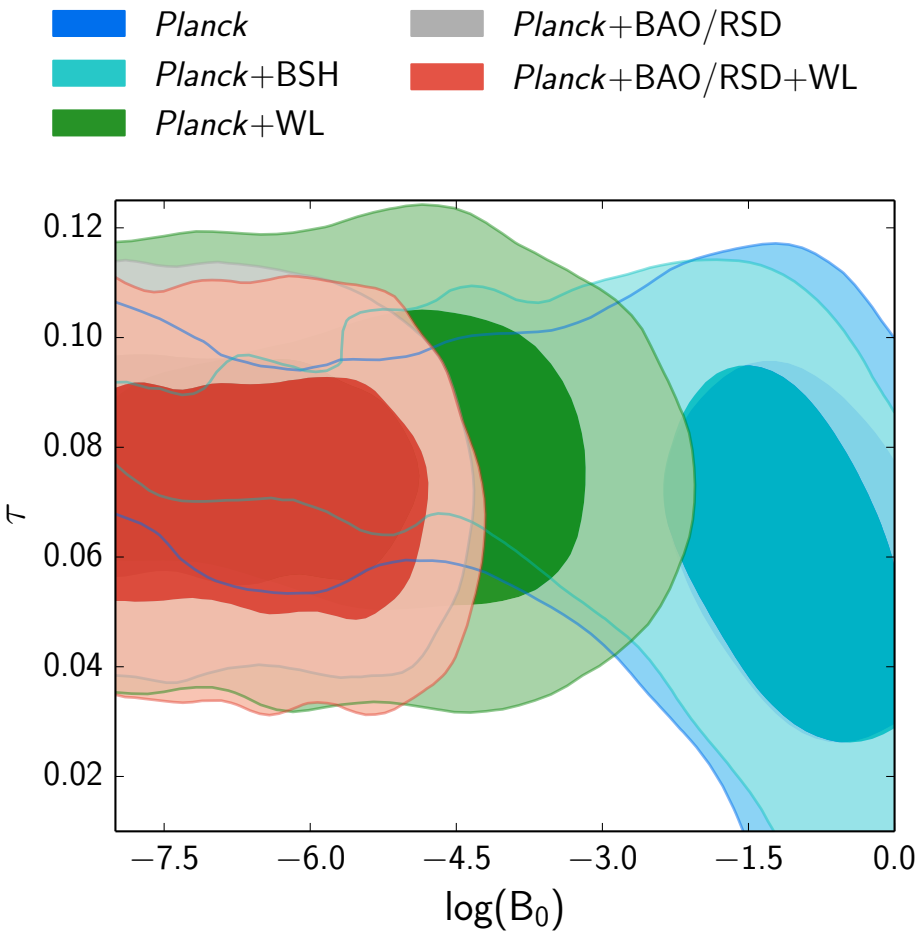

Figure 5.3. 68 % and 95 % contour plots for the two parameters, $\{\mathrm{Log}_{10}(\mathrm{B}_0), \tau\}$ (see Sect. 5.6.3). There is a degeneracy between the two parameters for *Planck* TT+lowP+BSH. Adding lensing will break the degeneracy between the two. Here Planck indicates *Planck* TT+lowP.

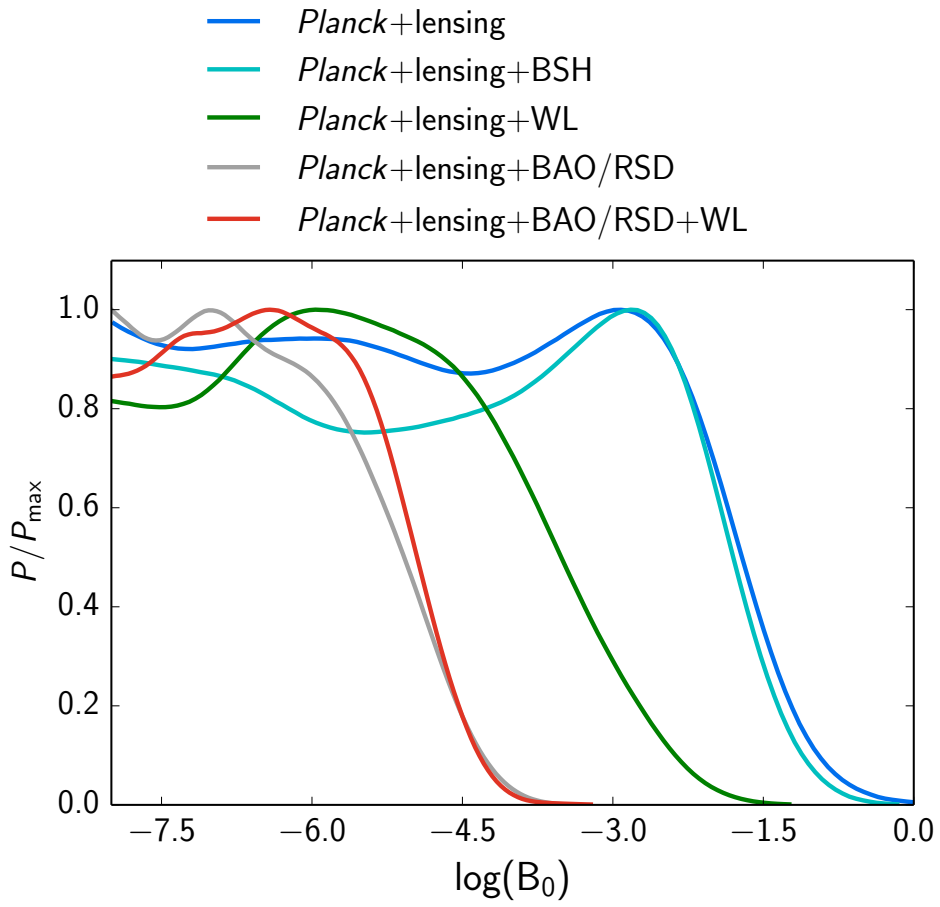

Figure 5.4. Likelihood plots of the $f(R)$ theory parameter, B_0 (see Sect. 5.6.3). CMB lensing breaks the degeneracy between B_0 and the optical depth, τ, resulting in lower upper bounds.

Finally, we note that $f(R)$ models can be studied also with the `MGcamb` parameterization, assuming the quasi-static limit. We find that for the allowed range of the B_0 parameter, the results with and without the quasi-static approximation are the same within the uncertainties. The 95 % confidence intervals are reported in Table 5.2. These values show an improvement over the WMAP analysis made with `MGcamb` ($B_0 < 1$ (95 % C.L.) in [202]) and are similar to the limits obtained in [208] with `MGcamb`.

$f(R)$ models	*Planck* TT+lowP	*Planck* TT+lowP +BSH	*Planck* TT+lowP +WL	*Planck* TT+lowP +BAO/RSD	*Planck* TT+lowP +WL+BAO/RSD
B_0	< 0.79 (95 % CL)	< 0.67 (95 % CL)	< 0.082 (95 % CL)	$< 0.88 \times 10^{-4}$ (95 % CL)	$< 0.10 \times 10^{-3}$ (95 % CL)
H_0	68.9 ± 1.0	68.37 ± 0.58	$69.1^{+1.0}_{-1.2}$	67.64 ± 0.65	67.92 ± 0.63
σ_8	$1.150^{+0.043}_{-0.031}$	$1.142^{+0.044}_{-0.030}$	$0.992^{+0.080}_{-0.056}$	$0.842^{+0.017}_{-0.020}$	$0.837^{+0.017}_{-0.019}$
B_0 (+lensing)	< 0.12 (95 % CL)	< 0.07 (95 % CL)	< 0.04 (95 % CL)	$< 0.95 \times 10^{-4}$ (95 % CL)	$< 0.83 \times 10^{-4}$(95 % CL)
H_0	69.0 ± 1.1	68.27 ± 0.57	69.1 ± 1.1	67.75 ± 0.61	67.91 ± 0.60
σ_8	$1.017^{+0.046}_{-0.030}$	$1.002^{+0.044}_{-0.028}$	0.959 ± 0.053	$0.836^{+0.014}_{-0.019}$	$0.833^{+0.014}_{-0.018}$

Table 5.2. 95 % CL intervals for the $f(R)$ parameter, B_0 (see Sect. 5.6.3). While the plots are produced for $\log_{10} B_0$, the numbers in this table are produced via an analysis on B_0 since the GR best fit value ($B_0 = 0$) lies out of the bounds in a $\log_{10} B_0$ analysis and its estimate would be prior dependent.

5.7 Conclusions

The quest for Dark Energy and Modified Gravity is far from over. A variety of different theoretical scenarios have been proposed in literature and need to be carefully compared with the data. This effort is still in its early stages, given the variety of theories and parameterizations that have been suggested, together with a lack of well tested numerical codes that allow us to make detailed predictions for the desired range of parameters. In this chapter, we considered a yet different approach to modified gravity in cosmology. Even though most of the weight in the *Planck* data lies at high redshift, *Planck* can still provide tight constraints on DE and MG, especially when used in combination with other probes. Our focus has been on the scales where linear theory is applicable, since these are the most theoretically robust. Overall, the constraints that we find are consistent with the simplest scenario, ΛCDM, with constraints on MG models (including effective field theory, and $f(R)$ models) that are significantly improved with respect to past analyses.

We discussed how to restrict EFT theories for MG, which include (almost) all universally coupled models in MG via nine generic functions of time, to Horndeski theories, described in terms of five free functions of time. Using the publicly available code `EFTcamb`, we have then varied three of these functions, in the limits allowed by the code, which correspond to a non-minimally coupled K-essence model (i.e. α_B, α_M, and α_K are varying

functions of the scale factor). We have found limits on the present value $\alpha_{\rm M0} < 0.052$ at 95% C.L. (in the linear EFT approximation), in agreement with ΛCDM. Constraints depend on the stability routines included in the code, which will need to be further tested in the future, together with allowing for a larger set of choices for the Horndeski functions, not available in the present version of the numerical code.

We also considered $f(R)$ models, written in terms of $B(z)$, conventionally related to the first and second derivatives of $f(R)$ with respect to R. The results of which show a remarkable agreement with GR.

Chapter 6

Conclusion

In this thesis, we discussed modified theories of gravity in general, and explored three different methods for studying these models in cosmology. We introduced a phenomenological method in chapter 3, studied a specific model of modified gravity (i.e. gravitational aether) in chapter 4, and considered approaches to modifying the Lagrangian in chapter 5. We discussed a variety of models, data sets, and numerical codes, but there are of course scenarios not included in this thesis that deserve future attention. Additional cosmologies within the EFT (and Horndeski) framework, massive gravity models (see [209] for a recent review), general violations of Lorentz invariance as a way to modify GR [210], and non-local gravity [211], have all been considered in recent years for a variety of different reasons, and cosmology can provide useful tests for them.

Cosmology has proven to be unique in testing gravity, thanks to its time-dependent background metric, and the diverse range of environmental conditions in the Universe since the big bang. The radiation-domination, matter-domination, and Λ-domination phases of cosmology provide unique tests for alternative models of gravity. Up to now, the tightest constraints have come from CMB temperature and polarization anisotropies, which explore early stages in the evolution of the Universe (together with BBN). However, there are other proposed and ongoing experiments that aim at studying the later epochs [212–215], and further promising constraints may come from a more precise measurement of the matter power spectrum, gravitational waves, and the reionization epoch. As of now, GR has passed all of the observational tests, and ΛCDM has proven to be the simplest model for describing the Universe. However, this is not considered desirable by many in theoretical physics. This situation can (and hopefully will) change in the future with access to more data from a

variety of different experiments. With access to all of these data sets, it may be temping to combine the results of all the different experiments and find the tightest constraints on the modified gravity parameters. However, we want to argue against this simplistic approach for the following two reasons.

The first reason deals with the issue of "false positives". We define false positives as signs of modified gravity that originate from inconsistencies between two data sets (given the ΛCDM model). These signs are considered "false", since the inconsistencies are either due to systematic noise, or cosmic variance fluctuations. Clearly, one needs to be careful to avoid being misled into claiming detection of a violation of GR that comes from systematic effects between data sets. Examples of this case have been discussed in Ref. [19].

The second reason is the "true negatives", i.e. real deviations from the standard model that are ignored due to compiling independent data sets. Let us explain this situation with a made-up example from the history of science. Let us imagine a case where the phenomenon of gravitational lensing was discovered prior to introducing GR (together with the already known empirical excess in precession of Mercury). The precession of Mercury can be explained in Newtonian mechanics by adding an A/r^2 term to the Newtonian gravitational potential. The amplitude A, is a free-parameter here, and lacking a more complete theory, is just a number that comes out of the fitting process. Fitting for this amplitude parameter would result in a non-zero value and hence would stand out as a hint for "modified gravity" (i.e. deviations from Newtonian gravity). On the other hand, gravitational lensing, which is also deviant from Newtonian gravity, does not prefer a $1/r^2$ term, but a gravitational constant that is twice as strong for photons. Combining the lensing experiment with the precession of Mercury, would therefore result in null results for deviations from Newtonian mechanics, even though these are both classical examples of such a deviation. One can keep combining more data (such as projectile trajectories, planetary orbits other than Mercury, gyroscope experiments, etc.) and increasing confidence on the $A = 0$ value by lowering the upper 95% confidence limit on A. We made up this example based of the fact that both the gravitational lensing, and the precession of Mercury are linear first order deviations

from Newtonian mechanics, while the underlying theory (i.e. GR) produces totally different correction terms for them. This means that if GR is not the ultimate theory of gravity, it is plausible to believe that a more complete (and fundamentally different) theory would result in totally different correction functions for different observables. Using the language of chapter 3 to parameterize deviations from GR via two functions of scale and time, A and B, this would mean that combining different data sets could result in constraints that are consistent with the GR value of these functions, i.e. $A = B = 0$, no matter if that is actually the case. It is therefore possible to ignore genuine GR deviations by combining enough independent data sets in the wrong theoretical framework.

Based on these observations, our suggestion for future experiments that are aimed at testing gravity is to keep an open mind and follow up any suggested (even statistically insignificant) deviations from GR in the existing data, using improved data sets. One such deviation is an oscillatory residual in *Planck* data at high multipoles in the temperature anisotropies [175]. This oscillatory residual is not statistically significant at the moment, due to the noise in data, and it is not clear whether it is an attribute of the Universe or is due to systematic noise (or just a statistical fluctuation). A future more precise experiment would be able to clear this up.

Besides detecting deviations from GR, there is also a need for building a theory that can explain the deviations. The above example also shows that a "reconstruction process" (i.e. using experimental data to build theories) could easily result in unnecessary complications if the new theory uses the same fundamentals as the existing theory. For example, one such approach might be a modified theory of Newtonian gravity where the gravitational constant smoothly becomes twice as strong when the mass of the particle goes to zero (with a parameter that controls this transition),[17] and a $1/r^2$ term is added to the potential such that it only couples with the angular momentum of an object in orbital motion. This is clearly not a desirable theory and this quote from E. F. Schumacher is probably the best conclusion for this discussion [216]: *"Any intelligent fool can make things bigger, more*

[17] One would also need to add a few "unseen" entities in order to save Newton's third law, as was mentioned in chapter 4.

complex, and more violent. It takes a touch of genius – and a lot of courage – to move in the opposite direction."

دو یار زیرک و از باده کهن دومنی فراغتی وکتابی و گوشه چمنی
من این مقام به دنیا و آخرت ندهم اگرچه در پی ام افتند هردم انجمنی
بیا که رونق این کارخانه کم نشود به زهد همچو تویی یا به فسق همچو منی

Two sweethearts and two bottles of old wine
A book, a scenic view, and a peace of mind
I won't give this up, for this world or the next
Even if prosecuted, time after time
O you, it shall not damage the prosperity of this world
Your devoted asceticism, or this fornication of mine
Iranian poet, Hafez, 14th century AD

Bibliography

[1] Planck Collaboration XVI. *A&A*, March 2013. arXiv:1303.5076.

[2] Planck Collaboration XIII. *Planck* 2015 results. XIII. Cosmological parameters. *AAP, submitted*, 2016.

[3] G. Hinshaw, D. Larson, and et. al. *ArXiv e-prints*, 2012. arXiv:1212.5226.

[4] K. T. Story, C. L. Reichardt, and et al. *ArXiv e-prints*, 2012. arXiv:1210.7231.

[5] R. Keisler, C. L. Reichardt, Aird, and et al. *APJ*, 743:28, 2011. doi: 10.1088/0004-637X/743/1/28. arXiv:1105.3182.

[6] J.L.E. Dreyer. *History of Planetary systems from Thales to Kepler*. Cambridge University Press, 1906.

[7] W. Turner. *History of Philosophy*. Forgotten Books, 2015.

[8] D. E. Hahm. The Fifth Element in Aristotle's De Philosophia: A Critical Re-Examination. *The Journal of Hellenic Studies*, 102:60–74, 1982.

[9] T. S. Kuhn. *The Structure of Scientific Revolutions*. University of Chicago Press, 1962.

[10] The Shapley - Curtis Debate in 1920. http://apod.nasa.gov/diamond_jubilee/debate_1920.html. [Online; accessed 12-April-2016].

[11] Albert Einstein. Die Grundlage der allgemeinen Relativit atstheorie. *Annalen der Physik*, 354:769–822, 1916.

[12] J. P. Zibin and A. Moss. Nowhere to hide: closing in on cosmological homogeneity. *ArXiv e-prints*, September 2014. arXiv:1409.3831.

[13] S. Weinberg. In *Gravitation and Cosmology*, 1976.

[14] H. P. Robertson. Kinematics and World-Structure. *APJ*, 82:284, November 1935. doi: 10.1086/143681.

[15] A. G. Walker. On Milnes theory of world-structure. *Proceedings of the London Mathematical Society*, 42:90, 1937. doi: 10.1112/plms/s2-42.1.90.

[16] A. Friedmann. Uber die Kr ummung des Raumes. *Zeitschrift fur Physik*, 10:377–386, 1922.

[17] G. R. Blumenthal, S. M. Faber, J. R. Primack, and M. J. Rees. Formation of galaxies and large-scale structure with cold dark matter. *NAT*, 311:517–525, October 1984. doi: 10.1038/311517a0.

[18] A. G. Riess, A. V. Filippenko, and et. al. Observational Evidence from Supernovae for an Accelerating Universe and a Cosmological Constant. *AJ*, 116:1009–1038, September 1998. doi: 10.1086/300499.

[19] Planck Collaboration XIV. *Planck* 2015 results. XIV. Dark energy and modified gravity. *AAP, submitted*, 2016.

[20] E. Hubble. A Relation between Distance and Radial Velocity among Extra-Galactic Nebulae. *Proceedings of the National Academy of Science*, 15:168–173, 1929.

[21] H. Kragh and R. W. Smith. Who Discovered the Expanding Universe? *History of Science*, 41:141–162, 2003.

[22] A. G. Riess, L. Macri, S. Casertano, H. Lampeitl, H. C. Ferguson, A. V. Filippenko, S. W. Jha, W. Li, and R. Chornock. A 3% Solution: Determination of the Hubble Constant with the Hubble Space Telescope and Wide Field Camera 3. *APJ*, 730:119, April 2011. doi: 10.1088/0004-637X/730/2/119. arXiv:1103.2976.

[23] G. Efstathiou. H_0 revisited. *MNRAS*, 440:1138–1152, May 2014. doi: 10.1093/mnras/stu278. arXiv:1311.3461.

[24] E. J. Copeland, M. Sami, and S. Tsujikawa. Dynamics of Dark Energy. *International Journal of Modern Physics D*, 15:1753–1935, 2006. doi: 10.1142/S021827180600942X.

[25] R. A. Alpher, R. Herman, and G. A. Gamow. Thermonuclear Reactions in the Expanding Universe. *Physical Review*, 74:1198–1199, November 1948. doi: 10.1103/PhysRev.74.1198.2.

[26] D. Tytler, J. M. O'Meara, N. Suzuki, and D. Lubin. Review of Big Bang Nucleosynthesis and Primordial Abundances. *Physica Scripta Volume T*, 85:12, 2000. doi: 10.1238/Physica.Topical.085a00012. arXiv:astro-ph/0001318.

[27] R. H. Cyburt, B. D. Fields, K. A. Olive, and T.-H. Yeh. Big Bang Nucleosynthesis: 2015. *ArXiv e-prints*, May 2015.

[28] P. J. E. Peebles, L. A. Page, and R. B. Partridge. *Finding the Big Bang*. Cambridge University Press, 2009.

[29] A. A. Penzias and R. W. Wilson. A Measurement of Excess Antenna Temperature at 4080 Mc/s. *APJ*, 142:419–421, July 1965. doi: 10.1086/148307.

[30] D. J. Fixsen. The Temperature of the Cosmic Microwave Background. *APJ*, 707:916–920, December 2009. doi: 10.1088/0004-637X/707/2/916. arXiv:0911.1955.

[31] D. H. Weinberg, M. J. Mortonson, and et. al. Observational probes of cosmic acceleration. , 530:87–255, September 2013. doi: 10.1016/j.physrep.2013.05.001.

[32] Alexei A. Starobinsky. A New Type of Isotropic Cosmological Models Without Singularity. *Phys.Lett.*, B91:99–102, 1980. doi: 10.1016/0370-2693(80)90670-X.

[33] A. H. Guth. Inflationary universe: A possible solution to the horizon and flatness problems. *PRD*, 23:347–356, January 1981. doi: 10.1103/PhysRevD.23.347.

[34] D. Baumann. TASI Lectures on Inflation. *ArXiv e-prints*, July 2009. arXiv:0907.5424.

[35] Hideo Kodama and Misao Sasaki. Cosmological Perturbation Theory. *Prog. Theor. Phys. Suppl.*, 78:1–166, 1984. doi: 10.1143/PTPS.78.1.

[36] James Bardeen. Gauge-invariant cosmological perturbations. *Phys. Rev. D*, 22:1882–1905, Oct 1980. doi: 10.1103/PhysRevD.22.1882. URL http://link.aps.org/doi/10.1103/PhysRevD.22.1882.

[37] C.-P. Ma and E. Bertschinger. *APJ*, 455:7, 1995. doi: 10.1086/176550. arXiv:astro-ph/9506072.

[38] W. Hu and N. Sugiyama. Anisotropies in the cosmic microwave background: an analytic approach. *APJ*, 444:489–506, May 1995. doi: 10.1086/175624.

[39] S. Dodelson. *Modern Cosmology*. American Press, 2003.

[40] Antony Lewis, Anthony Challinor, and Anthony Lasenby. Efficient computation of CMB anisotropies in closed FRW models. *Astrophys.J.*, 538:473–476, 2000. doi: 10.1086/309179. arXiv:astro-ph/9911177.

[41] J. C. Mather, E. S. Cheng, D. A. Cottingham, R. E. Eplee, Jr., D. J. Fixsen, T. Hewagama, R. B. Isaacman, K. A. Jensen, S. S. Meyer, P. D. Noerdlinger, S. M. Read, L. P. Rosen, R. A. Shafer, E. L. Wright, C. L. Bennett, N. W. Boggess, M. G. Hauser, T. Kelsall, S. H. Moseley, Jr., R. F. Silverberg, G. F. Smoot, R. Weiss, and D. T. Wilkinson. Measurement of the cosmic microwave background spectrum by the COBE FIRAS instrument. *APJ*, 420:439–444, January 1994. doi: 10.1086/173574.

[42] Planck Collaboration I. *Planck* 2015 results. I. Overview of products and results. *AAP, submitted*, 2016.

[43] D. Eisenstein. Large-Scale Structure and Future Surveys. *ArXiv Astrophysics e-prints*, January 2003. arXiv:astro-ph/0301623.

[44] C. Blake and K. Glazebrook. Probing Dark Energy Using Baryonic Oscillations in the Galaxy Power Spectrum as a Cosmological Ruler. *APJ*, 594:665–673, September 2003. doi: 10.1086/376983. arXiv:astro-ph/0301632.

[45] W. Hu and Z. Haiman. Redshifting rings of power. *PRD*, 68(6):063004, September 2003. doi: 10.1103/PhysRevD.68.063004. arXiv:astro-ph/0306053.

[46] A. Meiksin, M. White, and J. A. Peacock. Baryonic signatures in large-scale structure. *MNRAS*, 304:851–864, April 1999. doi: 10.1046/j.1365-8711.1999.02369.x.

[47] S. Cole, W. J. Percival, J. A. Peacock, P. Norberg, C. M. Baugh, C. S. Frenk, I. Baldry, J. Bland-Hawthorn, T. Bridges, R. Cannon, M. Colless, C. Collins, W. Couch, N. J. G. Cross, G. Dalton, V. R. Eke, R. De Propris, S. P. Driver, G. Efstathiou, R. S. Ellis, K. Glazebrook, C. Jackson, A. Jenkins, O. Lahav, I. Lewis, S. Lumsden, S. Maddox, D. Madgwick, B. A. Peterson, W. Sutherland, and K. Taylor. The 2dF Galaxy Redshift Survey: power-spectrum analysis of the final data set and cosmological implications. *MNRAS*, 362:505–534, September 2005. doi: 10.1111/j.1365-2966.2005.09318.x. arXiv:astro-ph/0501174.

[48] D. J. Eisenstein, I. Zehavi, D. W. Hogg, R. Scoccimarro, M. R. Blanton, R. C. Nichol, R. Scranton, H.-J. Seo, M. Tegmark, Z. Zheng, S. F. Anderson, J. Annis, N. Bahcall, J. Brinkmann, S. Burles, F. J. Castander, A. Connolly, I. Csabai, M. Doi, M. Fukugita, J. A. Frieman, K. Glazebrook, J. E. Gunn, J. S. Hendry, G. Hennessy, Z. Ivezić, S. Kent, G. R. Knapp, H. Lin, Y.-S. Loh, R. H. Lupton, B. Margon, T. A. McKay, A. Meiksin, J. A. Munn, A. Pope, M. W. Richmond, D. Schlegel, D. P. Schneider, K. Shimasaku, C. Stoughton, M. A. Strauss, M. SubbaRao, A. S. Szalay, I. Szapudi, D. L. Tucker, B. Yanny, and D. G. York. Detection of the Baryon Acoustic Peak in the Large-Scale Correlation Function of SDSS Luminous Red Galaxies. *APJ*, 633: 560–574, November 2005. doi: 10.1086/466512. arXiv:astro-ph/0501171.

[49] M. Kilbinger, L. Fu, C. Heymans, F. Simpson, J. Benjamin, T. Erben, J. Harnois-Déraps, H. Hoekstra, H. Hildebrandt, T. D. Kitching, Y. Mellier, L. Miller, L. Van

Waerbeke, K. Benabed, C. Bonnett, J. Coupon, M. J. Hudson, K. Kuijken, B. Rowe, T. Schrabback, E. Semboloni, S. Vafaei, and M. Velander. CFHTLenS: combined probe cosmological model comparison using 2D weak gravitational lensing. *MNRAS*, 430:2200–2220, April 2013. doi: 10.1093/mnras/stt041. arXiv:1212.3338.

[50] C. Heymans, E. Grocutt, A. Heavens, M. Kilbinger, T. D. Kitching, F. Simpson, J. Benjamin, T. Erben, H. Hildebrandt, H. Hoekstra, Y. Mellier, L. Miller, L. Van Waerbeke, M. L. Brown, J. Coupon, L. Fu, J. Harnois-Déraps, M. J. Hudson, K. Kuijken, B. Rowe, T. Schrabback, E. Semboloni, S. Vafaei, and M. Velander. CFHTLenS tomographic weak lensing cosmological parameter constraints: Mitigating the impact of intrinsic galaxy alignments. *MNRAS*, 432:2433–2453, July 2013. doi: 10.1093/mnras/stt601. arXiv:1303.1808.

[51] L. Samushia, B. A. Reid, M. White, W. J. Percival, A. J. Cuesta, G.-B. Zhao, A. J. Ross, M. Manera, É. Aubourg, F. Beutler, J. Brinkmann, J. R. Brownstein, K. S. Dawson, D. J. Eisenstein, S. Ho, K. Honscheid, C. Maraston, F. Montesano, R. C. Nichol, N. A. Roe, N. P. Ross, A. G. Sánchez, D. J. Schlegel, D. P. Schneider, A. Streblyanska, D. Thomas, J. L. Tinker, D. A. Wake, B. A. Weaver, and I. Zehavi. The clustering of galaxies in the SDSS-III Baryon Oscillation Spectroscopic Survey: measuring growth rate and geometry with anisotropic clustering. *MNRAS*, 439:3504–3519, April 2014. doi: 10.1093/mnras/stu197. arXiv:1312.4899.

[52] A. Einstein. ber das Relativittsprinzip und die aus demselben gezogenen Folgerungen. *Jahrbuch der Radioaktivitt und Elektronik 4*, pages 411–462, 1907. doi: 10.1103/PhysRevLett.13.789.

[53] A. Einstein. Näherungsweise Integration der Feldgleichungen der Gravitation. *Sitzungsberichte der Königlich Preußischen Akademie der Wissenschaften (Berlin), Seite 688-696.*, 1916.

[54] A. Ashtekar and J. Lewandowski. TOPICAL REVIEW: Background independent

quantum gravity: a status report. *Classical and Quantum Gravity*, 21:R53–R152, August 2004. doi: 10.1088/0264-9381/21/15/R01.

[55] O. Aharony, S. S. Gubser, J. Maldacena, H. Ooguri, and Y. Oz. Large N field theories, string theory and gravity. , 323:183–386, January 2000. doi: 10.1016/S0370-1573(99)00083-6.

[56] T. Clifton, P. G. Ferreira, A. Padilla, and C. Skordis. *Physics Reports*, 513:1–189, 2012. doi: 10.1016/j.physrep.2012.01.001. arXiv:1106.2476.

[57] S. Tsujikawa. Modified Gravity Models of Dark Energy. In G. Wolschin, editor, *Lecture Notes in Physics, Berlin Springer Verlag*, volume 800 of *Lecture Notes in Physics, Berlin Springer Verlag*, pages 99–145, March 2010. doi: 10.1007/978-3-642-10598-2_3.

[58] D. Lovelock. The Einstein tensor and its generalizations. *J. Math. Phys.*, 12:498–501, 1971. doi: 10.1063/1.1665613.

[59] C. H. Brans and H. Dicke, R. *Physical Review*, 124:925935, 1961. doi: 10.1103/PhysRev.125.388.

[60] E. Mach. The Science of Mechanics; a Critical and Historical Account of its Development. 1906.

[61] B. Bertotti, L. Iess, and P. Tortora. A test of general relativity using radio links with the Cassini spacecraft. *NAT*, 425:374–376, September 2003. doi: 10.1038/nature01997.

[62] P. Bergmann. Comments on the scalar-tensor theory. *International Journal of theoretical Physics*, 1:25–36, May 1968.

[63] K. Nordtvedt, Jr. Post-Newtonian Metric for a General Class of Scalar-Tensor Gravitational Theories and Observational Consequences. *APJ*, 161:1059, September 1970. doi: 10.1086/150607.

[64] V. Faraoni and E. Gunzig. Einstein frame or Jordan frame ? *ArXiv Astrophysics e-prints*, October 1999.

[65] V. Faraoni, E. Gunzig, and P. Nardone. Conformal transformations in classical gravitational theories and in cosmology. *FCP*, 20:121–175, June 1999.

[66] R. Catena, M. Pietroni, and L. Scarabello. Einstein and Jordan frames reconciled: A frame-invariant approach to scalar-tensor cosmology. *PRD*, 76(8):084039, October 2007. doi: 10.1103/PhysRevD.76.084039.

[67] A. Narimani, A. Moss, and D. Scott. Dimensionless cosmology. *APSS*, 341:617–629, October 2012. doi: 10.1007/s10509-012-1113-7.

[68] Gregory Walter Horndeski. Second-order scalar-tensor field equations in a four-dimensional space. *Int.J.Theor.Phys.*, 10:363–384, 1974. doi: 10.1007/BF01807638.

[69] C. Charmousis, E. J. Copeland, A. Padilla, and P. M. Saffin. General Second-Order Scalar-Tensor Theory and Self-Tuning. *Physical Review Letters*, 108(5):051101, February 2012. doi: 10.1103/PhysRevLett.108.051101.

[70] A. A. Starobinsky. The Perturbation Spectrum Evolving from a Nonsingular Initially De-Sitter Cosmology and the Microwave Background Anisotropy. *Sov. Astron. Lett.*, 9:302, 1983.

[71] Planck Collaboration XX. *Planck* 2015 results. XX. Constraints on inflation. *AAP, submitted*, 2016.

[72] D. Leverington. *A History of Astronomy: from 1890 to the Present*. Springer, 2012.

[73] F. W. Dyson, A. S. Eddington, and C. Davidson. *Royal Society of London Philosophical Transactions Series A*, 220:291–333, 1920. doi: 10.1098/rsta.1920.0009.

[74] I. I. Shapiro. *PRL*, 13:789–791, 1964. doi: 10.1103/PhysRevLett.13.789.

[75] R. P. Kerr. In *Quasi-Stellar Sources and Gravitational Collapse*, 1965.

[76] S. W. Hawking and R. Penrose. *Royal Society of London Proceedings Series A*, 314: 529–548, 1970. doi: 10.1098/rspa.1970.0021.

[77] S. W. Hawking. In D. J. Hegyi, editor, *Sixth Texas Symposium on Relativistic Astrophysics*, volume 224 of *Annals of the New York Academy of Sciences*, 1973. doi: 10.1111/j.1749-6632.1973.tb41462.x.

[78] R. A. Hulse and J. H. Taylor. *Astrophysical Journal Letters*, 195:L51–L53, 1975. doi: 10.1086/181708.

[79] C. S. Frenk and S. D. M. White. *Annalen der Physik*, 524:507–534, 2012. doi: 10.1002/andp.201200212. arXiv:1210.0544.

[80] S. Perlmutter, G. Aldering, and et al. *APJ*, 517:565–586, 1999. arXiv:astro-ph/9812133.

[81] A. H. Guth. *ArXiv e-prints*, 2004. arXiv:astro-ph/0404546.

[82] K. Nordtvedt. *APJ*, 161:1059, 1970. doi: 10.1086/150607.

[83] S. Nojiri and S. D. Odintsov. *PRD*, 74(8):086005, 2006. doi: 10.1103/PhysRevD.74.086005. arXiv:hep-th/0608008.

[84] T. P. Sotiriou and V. Faraoni. *Reviews of Modern Physics*, 82:451–497, 2010. doi: 10.1103/RevModPhys.82.451. arXiv:0805.1726.

[85] P. Hořava. *PRD*, 79(8):084008, 2009. doi: 10.1103/PhysRevD.79.084008. arXiv:0901.3775.

[86] E. W. Kolb, D. Lindley, and D. Seckel. *PRD*, 30:1205–1213, 1984. doi: 10.1103/PhysRevD.30.1205.

[87] H. Kodama, A. Ishibashi, and O. Seto. *PRD*, 62(6):064022, 2000. doi: 10.1103/PhysRevD.62.064022. arXiv:hep-th/0004160.

[88] Planck Collaboration, P. A. R. Ade, N. Aghanim, Arnaud, and et al. *ArXiv e-prints*, 536:A1, 2011. arXiv:1101.2022.

[89] D. Parkinson, S. Riemer-Sørensen, Blake, and et al. *ArXiv e-prints*, 2012. arXiv:1210.2130.

[90] K. S. Dawson, D. J. Schlegel, C. P. Ahn, and et al. *ArXiv e-prints*, 2012. arXiv:1208.0022.

[91] T. Baker, P. G. Ferreira, and C. Skordis. *PRD*, 87(2):024015, 2013. doi: 10.1103/PhysRevD.87.024015. arXiv:1209.2117.

[92] A. Lewis and S. Bridle. *PRD*, 66(10):103511, 2002. doi: 10.1103/PhysRevD.66.103511. arXiv:astro-ph/0205436.

[93] C. P. Burgess. *Living Reviews in Relativity*, 7:5, 2004. arXiv:gr-qc/0311082.

[94] K. A. Malik and D. Wands. *ArXiv General Relativity and Quantum Cosmology e-prints*, 1998. arXiv:gr-qc/9804046.

[95] I. Ferreras, N. E. Mavromatos, M. Sakellariadou, and M. F. Yusaf. *PRD*, 80(10):103506, 2009. doi: 10.1103/PhysRevD.80.103506. arXiv:0907.1463.

[96] A. Hojjati, L. Pogosian, and G.-B. Zhao. *Journal of Cosmology and Astroparticle Physics*, 8:005, 2011. doi: 10.1088/1475-7516/2011/08/005. arXiv:1106.4543.

[97] L. Pogosian, A. Silvestri, and et.al. *PRD*, 81(10):104023, 2010. doi: 10.1103/PhysRevD.81.104023. arXiv:1002.2382.

[98] A. Silvestri, L. Pogosian, and R. V. Buniy. *PRD*, 87(10):104015, 2013. doi: 10.1103/PhysRevD.87.104015. arXiv:1302.1193.

[99] T. Baker, P. G. Ferreira, C. Skordis, and J. Zuntz. *PRD*, 84(12):124018, 2011. doi: 10.1103/PhysRevD.84.124018. arXiv:1107.0491.

[100] J. Zuntz, T. Baker, P. G. Ferreira, and C. Skordis. *Journal of Cosmology and Astroparticle Physics*, 6:032, 2012. doi: 10.1088/1475-7516/2012/06/032. arXiv:1110.3830.

[101] R. K. Sachs and A. M. Wolfe. *APJ*, 147:73, 1967. doi: 10.1086/148982.

[102] D. Hanson, A. Challinor, and et al. *PRD*, 83(4):043005, 2011. doi: 10.1103/PhysRevD.83.043005. arXiv:1008.4403.

[103] A. Barreira, B. Li, and et al. *PRD*, 87(10):103511, 2013. doi: 10.1103/PhysRevD.87.103511. arXiv:1302.6241.

[104] S. Weinberg. *Reviews of Modern Physics*, 61:1–23, January 1989. doi: 10.1103/RevModPhys.61.1.

[105] N. Straumann. The history of the cosmological constant problem. In *XVIIIth IAP Colloquium: Observational and theoretical results on the accelerating universe*, August 2003. arXiv:gr-qc/0208027.

[106] A. G. Riess, A. V. Filippenko, and et. al. *Astronomy Journal*, 116:1009–1038, September 1998. doi: 10.1086/300499. arXiv:astro-ph/9805201.

[107] S. Perlmutter, G. Aldering, and et. al. *APJ*, 517:565–586, June 1999. doi: 10.1086/307221. arXiv:astro-ph/9812133.

[108] N. Afshordi. July 2008. arXiv:0807.2639.

[109] S. Aslanbeigi, G. Robbers, and et. al. *PRD*, 84(10):103522, November 2011. doi: 10.1103/PhysRevD.84.103522. arXiv:1106.3955.

[110] Y. B. Zel'dovich. *Soviet Physics Uspekhi*, 11:381–393, March 1968. doi: 10.1070/PU1968v011n03ABEH003927.

[111] E. C. Thomas, F. R. Urban, and A. R. Zhitnitsky. *Journal of High Energy Physics*, 8:043, August 2009. doi: 10.1088/1126-6708/2009/08/043. arXiv:0904.3779.

[112] C. Prescod-Weinstein, N. Afshordi, and M. L. Balogh. *PRD*, 80(4):043513, August 2009. doi: 10.1103/PhysRevD.80.043513. arXiv:0905.3551.

[113] C. M. Will. March 2014. arXiv:1403.7377.

[114] C. M. Will. *APJ*, 204:224–234, February 1976. doi: 10.1086/154164.

[115] D. J. Kapner, T. S. Cook, and et. al. *Physical Review Letters*, 98(2):021101, January 2007. doi: 10.1103/PhysRevLett.98.021101. arXiv:hep-ph/0611184.

[116] J. Schwab, S. A. Hughes, and S. Rappaport. The Self-Gravity of Pressure in Neutron Stars. *ArXiv e-prints*, June 2008. arXiv:0806.0798.

[117] F. Kamiab and N. Afshordi. *PRD*, 84(6):063011, September 2011. doi: 10.1103/PhysRevD.84.063011. arXiv:1104.5704.

[118] S. Rappaport, J. Schwab, S. Burles, and G. Steigman. Big bang nucleosynthesis constraints on the self-gravity of pressure. *PRD*, 77(2):023515, January 2008. doi: 10.1103/PhysRevD.77.023515. arXiv:0710.5300.

[119] G. Hinshaw, D. Larson, and et. al. *ApJS*, 208:19, October 2013. doi: 10.1088/0067-0049/208/2/19. arXiv:1212.5226.

[120] Planck Collaboration, P. A. R. Ade, N. Aghanim, M. Arnaud, M. Ashdown, J. Aumont, C. Baccigalupi, M. Baker, A. Balbi, A. J. Banday, and et al. Planck early results. I. The Planck mission. *A&A*, 536:A1, December 2011. doi: 10.1051/0004-6361/201116464. arXiv:1101.2022.

[121] S. Das, T. Louis, and et. al. *JCAP*, 4:014, April 2014. doi: 10.1088/1475-7516/2014/04/014. arXiv:1301.1037.

[122] A. Narimani and D. Scott. *PRD*, 88(8):083513, October 2013. doi: 10.1103/PhysRevD.88.083513. arXiv:1303.3197.

[123] R. K. Sachs and A. M. Wolfe. *APJ*, 147:73, January 1967. doi: 10.1086/148982.

[124] D. J. Fixsen. The Temperature of the Cosmic Microwave Background. *APJ*, 707: 916–920, December 2009. doi: 10.1088/0004-637X/707/2/916. arXiv:0911.1955.

[125] A. Narimani, A. Moss, and D. Scott. *Astrophysics and Space Science*, 341:617–629, October 2012. doi: 10.1007/s10509-012-1113-7. arXiv:1109.0492.

[126] W. Hu and N. Sugiyama. *PRD*, 50:627–631, July 1994. doi: 10.1103/PhysRevD.50.627. arXiv:astro-ph/9310046.

[127] E. Aver, K. A. Olive, and E. D. Skillman. *JCAP*, 5:003, May 2010. doi: 10.1088/1475-7516/2010/05/003. arXiv:1001.5218.

[128] C. M. Will. *Theory and Experiment in Gravitational Physics*. Cambridge University Press, March 1993.

[129] Planck Collaboration I. *A&A*, March 2013. arXiv:1303.5062.

[130] D. J. Eisenstein, D. H. Weinberg, and et al. *Astrophysical Journal*, 142:72, September 2011. doi: 10.1088/0004-6256/142/3/72. arXiv:1101.1529.

[131] N. Padmanabhan, X. Xu, and et al. *MNRAS*, 427:2132–2145, December 2012. doi: 10.1111/j.1365-2966.2012.21888.x. arXiv:1202.0090.

[132] L. Anderson, E. Aubourg, and et al. *MNRAS*, 427:3435–3467, December 2012. doi: 10.1111/j.1365-2966.2012.22066.x. arXiv:1203.6594.

[133] F. Beutler, C. Blake, and et al. *MNRAS*, 416:3017–3032, October 2011. doi: 10.1111/j.1365-2966.2011.19250.x. arXiv:1106.3366.

[134] BICEP2 Collaboration. March 2014. arXiv:1403.3985.

[135] T. Delubac, J. E. Bautista, and et. al. April 2014. arXiv:1404.1801.

[136] A. Rest, D. Scolnic, and et. al. October 2013. arXiv:1310.3828.

[137] A. Kovács, J. Carron, and I. Szapudi. *MNRAS*, 436:1422–1429, December 2013. doi: 10.1093/mnras/stt1661. arXiv:1307.1111.

[138] F. Beutler, S. Saito, and et. al. March 2014. arXiv:1403.4599.

[139] H. Liu, P. Mertsch, and S. Sarkar. April 2014. arXiv:1404.1899.

[140] Planck Collaboration XVII. *Planck* 2015 results. XVII. Constraints on primordial non-Gaussianity. *AAP, submitted*, 2016.

[141] LSST Science Collaboration, P. A. Abell, J. Allison, S. F. Anderson, J. R. Andrew, J. R. P. Angel, L. Armus, D. Arnett, S. J. Asztalos, T. S. Axelrod, and et al. LSST Science Book, Version 2.0. *ArXiv e-prints*, December 2009. arXiv:0912.0201.

[142] L. Amendola, S. Appleby, D. Bacon, T. Baker, M. Baldi, N. Bartolo, A. Blanchard, C. Bonvin, S. Borgani, E. Branchini, C. Burrage, S. Camera, C. Carbone, L. Casarini, M. Cropper, C. deRham, C. di Porto, A. Ealet, P. G. Ferreira, F. Finelli, J. Garcia-Bellido, T. Giannantonio, L. Guzzo, A. Heavens, L. Heisenberg, C. Heymans, H. Hoekstra, L. Hollenstein, R. Holmes, O. Horst, K. Jahnke, T. D. Kitching, T. Koivisto, M. Kunz, G. La Vacca, M. March, E. Majerotto, K. Markovic, D. Marsh, F. Marulli, R. Massey, Y. Mellier, D. F. Mota, N. Nunes, W. Percival, V. Pettorino, C. Porciani, C. Quercellini, J. Read, M. Rinaldi, D. Sapone, R. Scaramella, C. Skordis, F. Simpson, A. Taylor, S. Thomas, R. Trotta, L. Verde, F. Vernizzi, A. Vollmer, Y. Wang, J. Weller, and T. Zlosnik. Cosmology and fundamental physics with the Euclid satellite. *ArXiv e-prints*, June 2012. arXiv:1206.1225.

[143] Timothy Clifton, Pedro G. Ferreira, Antonio Padilla, and Constantinos Skordis. Modified Gravity and Cosmology. *Phys.Rept.*, 513:1–189, 2012. doi: 10.1016/j.physrep.2012.01.001. arXiv:1106.2476.

[144] A. Joyce, B. Jain, J. Khoury, and M. Trodden. Beyond the Cosmological Standard Model. *ArXiv e-prints*, June 2014. arXiv:1407.0059.

[145] D. Huterer, D. Kirkby, R. Bean, A. Connolly, K. Dawson, S. Dodelson, A. Evrard, B. Jain, M. Jarvis, E. Linder, R. Mandelbaum, M. May, A. Raccanelli, B. Reid, E. Rozo, F. Schmidt, N. Sehgal, A. Slosar, A. van Engelen, H.-Y. Wu, and G. Zhao. Growth of cosmic structure: Probing dark energy beyond expansion. *Astroparticle Physics*, 63:23–41, March 2015. doi: 10.1016/j.astropartphys.2014.07.004.

[146] A. Einstein. Kosmologische Betrachtungen zur allgemeinen Relativitätstheorie. *Sitzungsberichte der Königlich Preußischen Akademie der Wissenschaften (Berlin), Seite 142-152.*, pages 142–152, 1917.

[147] G. Lemaître. Un Univers homogène de masse constante et de rayon croissant rendant compte de la vitesse radiale des nébuleuses extra-galactiques. *Annales de la Société Scientifique de Bruxelles*, 47:49–59, 1927.

[148] Edwin Hubble. A relation between distance and radial velocity among extra-galactic nebulae. *Proc.Nat.Acad.Sci.*, 15:168–173, 1929. doi: 10.1073/pnas.15.3.168.

[149] Adam G. Riess, Alexei V. Filippenko, Peter Challis, Alejandro Clocchiatti, Alan Diercks, Peter M. Garnavich, Ron L. Gilliland, Craig J. Hogan, Saurabh Jha, Robert P. Kirshner, B. Leibundgut, M. M. Phillips, David Reiss, Brian P. Schmidt, Robert a. Schommer, R. Chris Smith, J. Spyromilio, Christopher Stubbs, Nicholas B. Suntzeff, and John Tonry. Observational Evidence from Supernovae for an Accelerating Universe and a Cosmological Constant. *The Astronomical Journal*, 116(3): 1009–1038, September 1998. doi: 10.1086/300499. arXiv:9805201v1.

[150] S. Perlmutter, G. Aldering, G. Goldhaber, R. A. Knop, P. Nugent, P. G. Castro, S. Deustua, S. Fabbro, A. Goobar, D. E. Groom, I. M. Hook, A. G. Kim, M. Y. Kim, J. C. Lee, N. J. Nunes, R. Pain, C. R. Pennypacker, R. Quimby, C. Lidman, R. S. Ellis, M. Irwin, R. G. McMahon, P. Ruiz-Lapuente, N. Walton, B. Schaefer, B. J. Boyle, A. V. Filippenko, T. Matheson, A. S. Fruchter, N. Panagia, H. J. M. Newberg, W. J. Couch, and T. S. C. Project. Measurements of Ω and Λ from 42

High-Redshift Supernovae. *APJ*, 517:565–586, June 1999. doi: 10.1086/307221. arXiv:astro-ph/9812133.

[151] Giulia Gubitosi, Federico Piazza, and Filippo Vernizzi. The Effective Field Theory of Dark Energy. *JCAP*, 1302:032, 2013. doi: 10.1088/1475-7516/2013/02/032. arXiv:1210.0201.

[152] W. Hu and M. White. Acoustic Signatures in the Cosmic Microwave Background. *APJ*, 471:30, November 1996. doi: 10.1086/177951. arXiv:arXiv:astro-ph/9602019.

[153] R. K. Sachs and A. M. Wolfe. Perturbations of a Cosmological Model and Angular Variations of the Microwave Background. *APJ*, 147:73, January 1967. doi: 10.1086/148982.

[154] L. A. Kofman and A. A. Starobinskii. Effect of the Cosmological Constant on Largescale Anisotropies in the Microwave Background. *Soviet Astronomy Letters*, 11:271–274, September 1985.

[155] Tommaso Giannantonio et al. Combined analysis of the integrated Sachs-Wolfe effect and cosmological implications. *Phys. Rev.*, D77:123520, 2008. doi: 10.1103/PhysRevD.77.123520. arXiv:0801.4380.

[156] V. Acquaviva and C. Baccigalupi. Dark energy records in lensed cosmic microwave background. *PRD*, 74(10):103510, November 2006. doi: 10.1103/PhysRevD.74.103510. arXiv:astro-ph/0507644.

[157] C. Carbone, M. Baldi, V. Pettorino, and C. Baccigalupi. Maps of CMB lensing deflection from N-body simulations in Coupled Dark Energy Cosmologies. *JCAP*, 9:004, September 2013. doi: 10.1088/1475-7516/2013/09/004. arXiv:1305.0829.

[158] P. J. E. Peebles. Tests of cosmological models constrained by inflation. *APJ*, 284:439–444, September 1984. doi: 10.1086/162425.

[159] J. D. Barrow and P. Saich. Growth of large-scale structure with a cosmological constant. *MNRAS*, 262:717–725, June 1993.

[160] Martin Kunz, Pier-Stefano Corasaniti, David Parkinson, and Edmund J. Copeland. Model-independent dark energy test with sigma(8) using results from the Wilkinson microwave anisotropy probe. *Phys.Rev.*, D70:041301, 2004. doi: 10.1103/PhysRevD.70.041301. arXiv:astro-ph/0307346.

[161] Marco Baldi and Valeria Pettorino. High-z massive clusters as a test for dynamical coupled dark energy. *Mon.Not.Roy.Astron.Soc.*, 412:L1, 2011. doi: 10.1111/j.1745-3933.2010.00975.x. arXiv:1006.3761.

[162] E. Calabrese, D. Huterer, E. V. Linder, A. Melchiorri, and L. Pagano. Limits on dark radiation, early dark energy, and relativistic degrees of freedom. *PRD*, 83(12):123504, June 2011. doi: 10.1103/PhysRevD.83.123504. arXiv:1103.4132.

[163] C. L. Reichardt, R. de Putter, O. Zahn, and Z. Hou. New Limits on Early Dark Energy from the South Pole Telescope. *APJL*, 749:L9, April 2012. doi: 10.1088/2041-8205/749/1/L9. arXiv:1110.5328.

[164] L. Amendola, V. Pettorino, C. Quercellini, and A. Vollmer. Testing coupled dark energy with next-generation large-scale observations. *PRD*, 85(10):103008, May 2012. doi: 10.1103/PhysRevD.85.103008. arXiv:1111.1404.

[165] Luca Amendola, Guillermo Ballesteros, and Valeria Pettorino. Effects of modified gravity on B-mode polarization. *Phys.Rev.*, D90:043009, 2014. doi: 10.1103/PhysRevD.90.043009. arXiv:1405.7004.

[166] M. Raveri, C. Baccigalupi, A. Silvestri, and S.-Y. Zhou. Measuring the speed of cosmological gravitational waves. *ArXiv e-prints*, May 2014. arXiv:1405.7974.

[167] Martin Kunz. The phenomenological approach to modeling the dark energy. *Comptes Rendus Physique*, 13:539–565, 2012. doi: 10.1016/j.crhy.2012.04.007. arXiv:1204.5482.

[168] Chung-Pei Ma and Edmund Bertschinger. Cosmological perturbation theory in the synchronous and conformal Newtonian gauges. *Astrophys.J.*, 455:7–25, 1995. doi: 10.1086/176550. arXiv:astro-ph/9506072.

[169] Guillermo Ballesteros, Lukas Hollenstein, Rajeev Kumar Jain, and Martin Kunz. Nonlinear cosmological consistency relations and effective matter stresses. *JCAP*, 1205:038, 2012. doi: 10.1088/1475-7516/2012/05/038. arXiv:1112.4837.

[170] C. Cheung, A. L. Fitzpatrick, J. Kaplan, L. Senatore, and P. Creminelli. The effective field theory of inflation. *Journal of High Energy Physics*, 3:014, March 2008. doi: 10.1088/1126-6708/2008/03/014. arXiv:0709.0293.

[171] J. Bloomfield, É. É. Flanagan, M. Park, and S. Watson. Dark energy or modified gravity? An effective field theory approach. *JCAP*, 8:010, August 2013. doi: 10.1088/1475-7516/2013/08/010. arXiv:1211.7054.

[172] E. Bellini and I. Sawicki. Maximal freedom at minimum cost: linear large-scale structure in general modifications of gravity. *JCAP*, 7:050, July 2014. doi: 10.1088/1475-7516/2014/07/050. arXiv:1404.3713.

[173] F. Piazza, H. Steigerwald, and C. Marinoni. Phenomenology of dark energy: exploring the space of theories with future redshift surveys. *JCAP*, 5:043, May 2014. doi: 10.1088/1475-7516/2014/05/043. arXiv:1312.6111.

[174] Planck Collaboration XV. *Planck* 2013 results. XV. CMB power spectra and likelihood. *AAP*, 571:A15, 2014. doi: 10.1051/0004-6361/201321573.

[175] Planck Collaboration XI. *Planck* 2015 results. XI. CMB power spectra, likelihoods, and robustness of parameters. *AAP, submitted*, 2016.

[176] W. Hu. Dark synergy: Gravitational lensing and the CMB. *PRD*, 65(2):023003, January 2002. doi: 10.1103/PhysRevD.65.023003. arXiv:astro-ph/0108090.

[177] A. Lewis and A. Challinor. Weak gravitational lensing of the CMB. *Physics Reports*, 429:1–65, June 2006. doi: 10.1016/j.physrep.2006.03.002. arXiv:arXiv:astro-ph/0601594.

[178] Z. Pan, L. Knox, and M. White. Dependence of the cosmic microwave background lensing power spectrum on the matter density. *MNRAS*, 445:2941–2945, December 2014. doi: 10.1093/mnras/stu1971. arXiv:1406.5459.

[179] Planck Collaboration XV. *Planck* 2015 results. XV. Gravitational lensing. *AAP, submitted*, 2016.

[180] Planck Collaboration IX. *Planck* 2015 results. IX. Diffuse component separation: CMB maps. *AAP, submitted*, 2016.

[181] Planck Collaboration Int. XXX. *Planck* intermediate results. XXX. The angular power spectrum of polarized dust emission at intermediate and high Galactic latitudes. *AAP*, 586:A133, 2016. doi: 10.1051/0004-6361/201425034.

[182] A. J. Ross, L. Samushia, C. Howlett, W. J. Percival, A. Burden, and M. Manera. The Clustering of the SDSS DR7 Main Galaxy Sample I: A 4 per cent Distance Measure at z=0.15. *ArXiv e-prints*, September 2014. arXiv:1409.3242.

[183] L. Anderson, É. Aubourg, S. Bailey, F. Beutler, V. Bhardwaj, M. Blanton, A. S. Bolton, J. Brinkmann, J. R. Brownstein, A. Burden, C.-H. Chuang, A. J. Cuesta, K. S. Dawson, D. J. Eisenstein, S. Escoffier, J. E. Gunn, H. Guo, S. Ho, K. Honscheid, C. Howlett, D. Kirkby, R. H. Lupton, M. Manera, C. Maraston, C. K. McBride, O. Mena, F. Montesano, R. C. Nichol, S. E. Nuza, M. D. Olmstead, N. Padmanabhan, N. Palanque-Delabrouille, J. Parejko, W. J. Percival, P. Petitjean, F. Prada, A. M. Price-Whelan, B. Reid, N. A. Roe, A. J. Ross, N. P. Ross, C. G. Sabiu, S. Saito, L. Samushia, A. G. Sánchez, D. J. Schlegel, D. P. Schneider, C. G. Scoccola, H.-J. Seo, R. A. Skibba, M. A. Strauss, M. E. C. Swanson, D. Thomas, J. L. Tinker, R. Tojeiro, M. V. Magaña, L. Verde, D. A. Wake, B. A. Weaver, D. H. Weinberg,

M. White, X. Xu, C. Yèche, I. Zehavi, and G.-B. Zhao. The clustering of galaxies in the SDSS-III Baryon Oscillation Spectroscopic Survey: baryon acoustic oscillations in the Data Releases 10 and 11 Galaxy samples. *MNRAS*, 441:24–62, June 2014. doi: 10.1093/mnras/stu523. arXiv:1312.4877.

[184] F. Beutler, C. Blake, M. Colless, D. H. Jones, L. Staveley-Smith, L. Campbell, Q. Parker, W. Saunders, and F. Watson. The 6dF Galaxy Survey: baryon acoustic oscillations and the local Hubble constant. *MNRAS*, 416:3017–3032, October 2011. doi: 10.1111/j.1365-2966.2011.19250.x. arXiv:1106.3366.

[185] A. G. Riess, A. V. Filippenko, P. Challis, A. Clocchiatti, A. Diercks, P. M. Garnavich, R. L. Gilliland, C. J. Hogan, S. Jha, R. P. Kirshner, B. Leibundgut, M. M. Phillips, D. Reiss, B. P. Schmidt, R. A. Schommer, R. C. Smith, J. Spyromilio, C. Stubbs, N. B. Suntzeff, and J. Tonry. Observational Evidence from Supernovae for an Accelerating Universe and a Cosmological Constant. *AJ*, 116:1009–1038, September 1998. doi: 10.1086/300499. arXiv:astro-ph/9805201.

[186] M. Betoule, J. Marriner, N. Regnault, J.-C. Cuillandre, P. Astier, J. Guy, C. Balland, P. El Hage, D. Hardin, R. Kessler, L. Le Guillou, J. Mosher, R. Pain, P.-F. Rocci, M. Sako, and K. Schahmaneche. Improved photometric calibration of the SNLS and the SDSS supernova surveys. *AAP*, 552:A124, April 2013. doi: 10.1051/0004-6361/201220610. arXiv:1212.4864.

[187] M. Betoule, R. Kessler, J. Guy, J. Mosher, D. Hardin, R. Biswas, P. Astier, P. El-Hage, M. Konig, S. Kuhlmann, J. Marriner, R. Pain, N. Regnault, C. Balland, B. A. Bassett, P. J. Brown, H. Campbell, R. G. Carlberg, F. Cellier-Holzem, D. Cinabro, A. Conley, C. B. D'Andrea, D. L. DePoy, M. Doi, R. S. Ellis, S. Fabbro, A. V. Filippenko, R. J. Foley, J. A. Frieman, D. Fouchez, L. Galbany, A. Goobar, R. R. Gupta, G. J. Hill, R. Hlozek, C. J. Hogan, I. M. Hook, D. A. Howell, S. W. Jha, L. Le Guillou, G. Leloudas, C. Lidman, J. L. Marshall, A. Möller, A. M. Mourão, J. Neveu, R. Nichol, M. D. Olmstead, N. Palanque-Delabrouille, S. Perlmutter, J. L.

Prieto, C. J. Pritchet, M. Richmond, A. G. Riess, V. Ruhlmann-Kleider, M. Sako, K. Schahmaneche, D. P. Schneider, M. Smith, J. Sollerman, M. Sullivan, N. A. Walton, and C. J. Wheeler. Improved cosmological constraints from a joint analysis of the SDSS-II and SNLS supernova samples. *AAP*, 568:A22, August 2014. doi: 10.1051/0004-6361/201423413. arXiv:1401.4064.

[188] L. Humphreys, M. Reid, J. Moran, L. Greenhill, and A. Argon. Toward a New Geometric Distance to the Active Galaxy NGC 4258. III. Final Results and the Hubble Constant. *ArXiv e-prints*, July 2013. arXiv:1307.6031.

[189] D. Bianchi, L. Guzzo, E. Branchini, E. Majerotto, S. de la Torre, F. Marulli, L. Moscardini, and R. E. Angulo. Statistical and systematic errors in redshift-space distortion measurements from large surveys. *MNRAS*, 427:2420–2436, December 2012. doi: 10.1111/j.1365-2966.2012.22110.x. arXiv:1203.1545.

[190] H. Gil-Marín, C. Wagner, L. Verde, C. Porciani, and R. Jimenez. Perturbation theory approach for the power spectrum: from dark matter in real space to massive haloes in redshift space. *JCAP*, 11:029, November 2012. doi: 10.1088/1475-7516/2012/11/029. arXiv:1209.3771.

[191] C. Alcock and B. Paczynski. An evolution free test for non-zero cosmological constant. *NAT*, 281:358, October 1979. doi: 10.1038/281358a0.

[192] F. Beutler, S. Saito, H.-J. Seo, J. Brinkmann, K. S. Dawson, D. J. Eisenstein, A. Font-Ribera, S. Ho, C. K. McBride, F. Montesano, W. J. Percival, A. J. Ross, N. P. Ross, L. Samushia, D. J. Schlegel, A. G. Sánchez, J. L. Tinker, and B. A. Weaver. The clustering of galaxies in the SDSS-III Baryon Oscillation Spectroscopic Survey: testing gravity with redshift space distortions using the power spectrum multipoles. *MNRAS*, 443:1065–1089, September 2014. doi: 10.1093/mnras/stu1051. arXiv:1312.4611.

[193] Marco Raveri, Bin Hu, Noemi Frusciante, and Alessandra Silvestri. Effective Field

Theory of Cosmic Acceleration: constraining dark energy with CMB data. 2014. arXiv:1405.1022.

[194] B. Hu, M. Raveri, A. Silvestri, and N. Frusciante. EFTCAMB/EFTCosmoMC: massive neutrinos in dark cosmologies. *ArXiv e-prints*, October 2014. arXiv:1410.5807.

[195] B. Hu, M. Raveri, N. Frusciante, and A. Silvestri. EFTCAMB/EFTCosmoMC: Numerical Notes v1.0. *ArXiv e-prints*, May 2014. arXiv:1405.3590.

[196] V. Pettorino and L. Amendola. Friction in Gravitational Waves: a test for early-time modified gravity. *ArXiv e-prints*, August 2014. arXiv:1408.2224.

[197] J. Gleyzes, D. Langlois, F. Piazza, and F. Vernizzi. Exploring gravitational theories beyond Horndeski. *ArXiv e-prints*, August 2014. arXiv:1408.1952.

[198] Christof Wetterich. The Cosmon model for an asymptotically vanishing time dependent cosmological 'constant'. *Astron. Astrophys.*, 301:321–328, 1995. arXiv:hep-th/9408025.

[199] Luca Amendola. Coupled quintessence. *Phys. Rev.*, D62:043511, 2000. doi: 10.1103/PhysRevD.62.043511. arXiv:astro-ph/9908023.

[200] Rob Fardon, Ann E. Nelson, and Neal Weiner. Dark Energy from Mass Varying Neutrinos. *JCAP*, 0410:005, 2004. doi: 10.1088/1475-7516/2004/10/005. arXiv:astro-ph/0309800.

[201] Luca Amendola, Marco Baldi, and Christofn Wetterich. Growing Matter. *Phys. Rev.*, D78:023015, 2008. doi: 10.1103/PhysRevD.78.023015. arXiv:0706.3064.

[202] Y.-S. Song, W. Hu, and I. Sawicki. Large scale structure of f(R) gravity. *PRD*, 75(4):044004, February 2007. doi: 10.1103/PhysRevD.75.044004. arXiv:astro-ph/0610532.

[203] L. Pogosian and A. Silvestri. Pattern of growth in viable f(R) cosmologies. *PRD*, 77 (2):023503, January 2008. doi: 10.1103/PhysRevD.77.023503. arXiv:0709.0296.

[204] Y.-S. Song, H. Peiris, and W. Hu. Cosmological constraints on f(R) acceleration models. *PRD*, 76(6):063517, September 2007. doi: 10.1103/PhysRevD.76.063517. arXiv:0706.2399.

[205] F. Schmidt. Weak lensing probes of modified gravity. *PRD*, 78(4):043002, August 2008. doi: 10.1103/PhysRevD.78.043002. arXiv:0805.4812.

[206] E. Bertschinger and P. Zukin. Distinguishing modified gravity from dark energy. *PRD*, 78(2):024015, July 2008. doi: 10.1103/PhysRevD.78.024015. arXiv:0801.2431.

[207] Andrea Marchini, Alessandro Melchiorri, Valentina Salvatelli, and Luca Pagano. Constraints on modified gravity from the Atacama Cosmology Telescope and the South Pole Telescope. *Phys.Rev.*, D87(8):083527, 2013. doi: 10.1103/PhysRevD.87.083527. arXiv:1302.2593.

[208] Andrea Marchini and Valentina Salvatelli. Updated constraints from the PLANCK experiment on modified gravity. *Phys.Rev.*, D88(2):027502, 2013. doi: 10.1103/PhysRevD.88.027502. arXiv:1307.2002.

[209] C. de Rham. Massive Gravity. *Living Reviews in Relativity*, 17:7, August 2014. doi: 10.12942/lrr-2014-7. arXiv:1401.4173.

[210] B. Audren, D. Blas, M.M. Ivanov, J. Lesgourgues, and S. Sibiryakov. Cosmological constraints on deviations from Lorentz invariance in gravity and dark matter. 2014. arXiv:1410.6514.

[211] Y. Dirian, S. Foffa, M. Kunz, M. Maggiore, and V. Pettorino. Non-local gravity and comparison with observational datasets. *ArXiv e-prints*, November 2014. arXiv:1411.7692.

[212] eLISA: The Mission. https://www.elisascience.org/articles/elisa-mission/elisa-mission-gravitational-universe. [Online; accessed 20-April-2016].

[213] L. Amendola, S. Appleby, and et. al. Cosmology and Fundamental Physics with the Euclid Satellite. *Living Reviews in Relativity*, 16, September 2013. doi: 10.12942/lrr-2013-6.

[214] K. Bandura, G. E. Addison, and et. al. Canadian Hydrogen Intensity Mapping Experiment (CHIME) pathfinder. In *Ground-based and Airborne Telescopes V*, volume 9145 of , page 914522, July 2014. doi: 10.1117/12.2054950.

[215] LEDA — Large-Aperture Experiment to Detect the Dark Ages. http://www.tauceti.caltech.edu/leda/. [Online; accessed 20-April-2016].

[216] E. F. Schumacher. *Small is Beautirful: a study of economics as if people mattered*. Blond and Briggs, 1973.